HIDRAULICA

HYDRAULICS-PNEUMATICS-TRIBOLOGY-ECOLOGY-SENSORICS-MECHATRONICS

2024
March
No. 1

ISSN 1453 - 7303
ISSN-L 1453 - 7303

https://hidraulica.fluidas.ro

CONTENTS

BOARD

Published by:
Hydraulics and Pneumatics Research Institute, Bucharest-Romania
Address: 14 Cuţitul de Argint, district 4, Bucharest, 040558, Romania
Phone: +40 21 336 39 91; Fax: +40 21 337 30 40; e-Mail: ihp@fluidas.ro; Web: www.ihp.ro
with support from:
National Professional Association of Hydraulics and Pneumatics in Romania - FLUIDAS
e-Mail: fluidas@fluidas.ro; Web: www.fluidas.ro

HIDRAULICA Magazine is indexed by international databases

ISSN 1453 – 7303; ISSN – L 1453 – 7303

EDITORIAL

Importanța acționărilor hidraulice și pneumatice în contextul industrial actual

Dr. Ing. Gabriela Matache
REDACTOR ȘEF

Acționările hidraulice și pneumatice ("*Fluid Power*"), știința și tehnologia fluidelor sub presiune cu scopul a genera, controla și transmite putere, are o importanță uriașă în peisajul contemporan al industriei. Într-o epocă marcată de progrese tehnologice rapide și de cerințe tot mai ridicate de eficiență, fiabilitate și durabilitate, sistemele *fluid power* au devenit instrumente indispensabile în diverse sectoare.

Unul dintre motivele principale ale importanței domeniului *Fluid Power* constă în versatilitatea acestora. Acționările hidraulice și pneumatice își găsesc aplicabilitate într-o gamă variată de industrii, incluzând industria manufacturieră, construcții, agricultură, robotică, industriile aerospațială și auto, printre altele. Fie că este vorba despre ridicarea unor încărcături mari într-o fabrică, acționarea excavatoarelor hidraulice pe un șantier de construcții sau controlul trenului de aterizare al aeronavei, sistemele *fluid power* joacă un rol central în facilitarea funcțiilor esențiale în toate industriile.

Eficiența este un alt aspect critic care determină relevanța acționărilor hidraulice și pneumatice în industria modernă. Sistemele *fluid power* sunt cunoscute pentru densitatea lor mare de putere, permițându-le să furnizeze o forță sau un cuplu semnificativ în structuri compacte. Acest atribut este deosebit de valoros în situațiile în care spațiul este limitat, cum ar fi echipamentele mobile sau aplicațiile robotizate. Mai mult decât atât, progresele în tehnologiile bazate pe acționări hidraulice și pneumatice contribuie la îmbunătățirea eficienței generale a sistemului, reducând astfel consumul de energie și costurile.

În plus, sistemele *fluid power* oferă o precizie și un control de neegalat, crucial pentru obținerea performanțelor optime în diferite procese industriale. Fie că este vorba de reglarea vitezei unei benzi transportoare, de poziționarea componentelor pe o linie de producție sau de controlul mișcării brațelor robotizate, acționările hidraulice și pneumatice permit controlul precis al mișcării cu timp rapid de răspuns, rezultând o productivitate și o calitate sporită a rezultatelor. Sistemele *fluid power* pot fi integrate în rețele industriale inteligente, permițând monitorizarea în timp real a performanței echipamentelor. Acest lucru facilitează implementarea practicilor de mentenanță predictivă și optimizarea operațiunilor industriale.

În contextul Industriei 4.0 și al accentului din ce în ce mai mare pe automatizare și sistemele interconectate, acționările hidraulice și pneumatice joacă un rol vital în a permite integrarea și interoperabilitatea fără întreruperi. Folosind tehnologii precum senzori, actuatoare și sisteme de control inteligente, sistemele *fluid power* pot fi integrate în rețele industriale sofisticate, permițând monitorizarea în timp real, analiza datelor și mentenanță predictivă. Acest lucru nu numai că îmbunătățește eficiența operațională, dar facilitează și tranziția către procese de producție mai agile și adaptabile. Sistemele *fluid power* pot fi proiectate pentru a fi foarte eficiente din punct de vedere energetic, contribuind astfel la reducerea consumului de energie și la optimizarea performanței sistemelor industriale. Utilizarea corectă a tehnologiilor *fluid power* poate ajuta la reducerea amprentei de carbon în industrie.

Mai mult, într-o epocă în care sustenabilitatea mediului este o preocupare presantă, sistemele *fluid power* oferă avantaje inerente în ceea ce privește eficiența energetică și impactul asupra mediului. Sistemele hidraulice și pneumatice pot fi proiectate să funcționeze pe surse de energie regenerabilă sau fluide alternative, cu amprente mai reduse asupra mediului, reducând astfel dependența de combustibilii fosili și minimizând emisiile de carbon. Sistemele *fluid power* pot fi proiectate pentru a fi foarte eficiente din punct de vedere energetic, contribuind astfel la reducerea consumului de energie; utilizarea adecvată a tehnologiilor *fluid power* poate ajuta la reducerea amprentei de carbon a operațiunilor industriale.

În concluzie, acționările hidraulice și pneumatice pot juca un rol semnificativ în revoluționarea Industriei 4.0, contribuind la creșterea eficienței, flexibilității și durabilității în procesele industriale moderne. Utilizarea corectă a tehnologiilor *fluid power* poate ajuta la transformarea industriei și la crearea unui mediu de producție mai inteligent și mai eficient. De la activarea aplicațiilor versatile până la îmbunătățirea eficienței, preciziei și durabilității, sistemele *fluid power* continuă să stimuleze inovația și progresul într-o gamă largă de industrii. Pe măsură ce tehnologia continuă să evolueze, acționările hidraulice și pneumatice rămân o piatră de temelie a operațiunilor industriale moderne, permițând organizațiilor să facă față provocărilor pieței dinamice de mâine.

EDITORIAL

The Importance of Fluid Power in the Current Industrial Context

Ph.D.Eng. Gabriela Matache
EDITOR-IN-CHIEF

Fluid power, the science and technology of fluids under pressure to generate, control, and transmit power, holds immense significance in the contemporary landscape of industry. In an era marked by rapid technological advancements and increasing demands for efficiency, reliability, and sustainability, fluid power systems have emerged as indispensable tools across various sectors.

One of the primary reasons for the importance of fluid power lies in its versatility. Fluid power finds application in a diverse array of industries, including manufacturing, construction, agriculture, robotics, aerospace, and automotive, among others. Whether it's lifting heavy loads in a factory, powering hydraulic excavators at a construction site, or controlling aircraft landing gear, fluid power systems play a pivotal role in facilitating essential functions across industries.

Efficiency is another critical aspect driving the relevance of fluid power in modern industry. Hydraulic and pneumatic systems are known for their high power density, enabling them to deliver significant force or torque in compact designs. This attribute is particularly valuable in situations where space is limited, such as in mobile equipment or robotic applications. Moreover, advancements in fluid power technologies contribute to enhancing overall system efficiency, thereby reducing energy consumption and operational costs.

Furthermore, fluid power systems offer unparalleled precision and control, which is crucial for achieving optimal performance in various industrial processes. Whether it's regulating the speed of a conveyor belt, positioning components on a production line, or controlling the motion of robotic arms, fluid power enables precise motion control with quick response times, resulting in enhanced productivity and quality of output. Fluid power systems can be integrated into smart industrial networks, allowing real-time monitoring of equipment performance. This facilitates the implementation of predictive maintenance practices and optimization of industrial operations.

In the context of Industry 4.0 and the growing emphasis on automation and interconnected systems, fluid power plays a vital role in enabling seamless integration and interoperability. By leveraging technologies such as sensors, actuators, and intelligent control systems, fluid power systems can be integrated into sophisticated industrial networks, enabling real-time monitoring, data analytics, and predictive maintenance. This not only enhances operational efficiency but also facilitates the transition towards more agile and adaptive manufacturing processes. Fluid power systems can be designed to be highly energy-efficient, thus contributing to reducing energy consumption and optimizing the performance of industrial systems. Proper use of fluid power technologies can help reduce the carbon footprint of industrial operations.

Moreover, in an era where environmental sustainability is a pressing concern, fluid power systems offer inherent advantages in terms of energy efficiency and environmental impact. Hydraulic and pneumatic systems can be designed to operate on renewable energy sources or alternative fluids with lower environmental footprints, thereby reducing reliance on fossil fuels and minimizing carbon emissions. Fluid power systems can be designed to be highly energy-efficient, thus contributing to reducing energy consumption; proper use of fluid power technologies can help reduce the carbon footprint of industrial operations.

In conclusion, fluid power can play a significant role in revolutionizing Industry 4.0, contributing to increased efficiency, flexibility, and sustainability in modern industrial processes. Proper use of fluid power technologies can help transform the industry and create a smarter and more efficient production environment. From enabling versatile applications to enhancing efficiency, precision, and sustainability, fluid power systems continue to drive innovation and progress across a wide range of industries. As technology continues to evolve, fluid power is poised to remain a cornerstone of modern industrial operations, enabling organizations to meet the challenges of tomorrow's dynamic marketplace.

Constructive Design Elements of Large Dimensions Cyclones

Professor Emeritus Ph. D. Eng. **Radu I. IATAN[1,*]**,
Ph. D. Candidate **Melania (MITUCĂ) CORLECIUC[2]**,
Lecturer Ph. D. Eng. **Gheorghiţa TOMESCU[1]**,
Assoc. Prof. Ph. D. Eng. **Anca Mădălina DUMITRESCU[1]**,
Lecturer Ph. D. Eng. **Luminiţa Georgiana ENĂCHESCU[1]**,
Assist. Prof. Ph. D. Eng. **Gheorghe-Cosmin CIOCOIU[1]**

[1] National University of Sciences and Technology Polytechnic Bucharest – Romania

[2] National Agency for Environmental Protection – Romania

* iatan.radu@gmail.com

Abstract: *The article addresses the issues specific to the constructive design of large cyclones, with tangential supply of the dust impurified gas. In this sense, the expressions for the stresses developed in the separation sections of the vortex finder tube and the flat sheet are established. The radial size of the plate, fixed also to the side body of the cyclone, is considered large. In this sense, the deformation states and stresses in the edges are accepted as not influencing each other.*

Keywords: *Large size cyclones, deformation states and stress*

1. Introduction

Over time, industrial production has been constantly developed, many technological processes being producers of dust-impure gases. As a result, it became increasingly important to protect the external environment against harmful effects. Cyclones are among the simplest systems used for dedusting dry gases in various industrial sectors. Among these, those with tangential supply of impurity gas stood out.
The technological design of the cyclones takes into account their geometry, the impurified gas flow and the number of revolutions/rotations in the downward movement. The theory developed by **Leith D**. and **Licht W**. (1972) [1] proved useful in the practical design of cyclones. In this context, it is taken into account that the velocity profile in a cyclone does not strictly coincide with the ideal, uniform shape.
Any technological design variant is based on theories that depend on the accuracy of the evaluation of the collection efficiency and the pressure drop in the cyclones [2 - 4]. The two characteristics represent two major criteria regarding the performance of a cyclone. Both are dependent on the dimensions of the cyclone, the height and width of the inlet ($a \cdot b$ – fig.1), the diameter of the gas outlet D_e, the length of the exhaust pipe S, the height of the cylindrical area h, the height of the cyclone H and the outlet diameter of the settled dust B.
Several simplified models and empirical correlations have been proposed, in the sense of the above.
Relying on the performance of a cyclone considered "benchmark" ultimately leads to a faulty design, considering that each cyclone has a specific behavior due to the unique physics of the impurity air flow [6]. The computational fluid dynamics (CFD) method has become a powerful aid in the design and evaluation of cyclones with the rapid advances in computer technology. Using this technique, there is a great potential to predict the characteristics of the fluid flow, the trajectory of the particles (adequate turbulence model) and the pressure drop in the cyclone [7]. Now, thanks to the increased processing performance of computers, at a relatively low cost, it has become possible to simulate cyclones with greater precision [8, 9].
The capacity of a cyclone is determined by the value of the cross section area of the supply pipe ($a \cdot b$, fig. 1) and the inlet velocity of the gas to be cleaned. This is in agreement, mainly, with the connection between the main dimensions of the cyclone and its pressure drop.
In the present paper, an appropriate methodology for the constructive design of a cyclone with

larger geometric dimensions, established as a result of the functional analysis, is used. As a study hypothesis, the joint between the cleaned gas exhaust tube and the large plate is considered. In this case, it is assumed that the stresses developed at the edges of the plate do not influence each other.

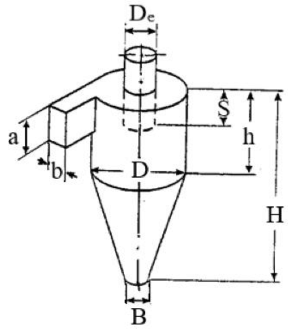

Fig. 1. Cyclone construction and characteristics [5]

2. Study hypotheses

As can be seen in figure 2. a, a practical way of fixing the exhaust tube of the cleaned gas discharged from the cyclone is that of a flat plate, fixed by welding to the outer cylindrical body of the cyclone.

In order to be able to evaluate the stress states in the areas with discontinuities of the structure analyzed in the present case, some appropriate study hypotheses are considered. Thus:

a) The constructive elements are made of homogeneous metallic material, joined by welding (the values of the longitudinal elasticity modules can be considered different or equal: $E_1 = E_2 = E_3 = E$; the values of the transverse contraction coefficients can be considered different or equal: $\mu_1 = \mu_2 = \mu_3 = \mu$).

b) The stress is considered in the elastic domain.

c) The working temperatures are considered to be different, within the calculation relationships. If it is estimated that the differences are insignificant, during the calculation the values of the thermal gradients are easily equalized ($\Delta T_1 = \Delta T_2 = \Delta T_3 = \Delta T$). In this vein, thermal deformation factors can be taken into account $\alpha_1 = \alpha_2 = \alpha_3 = \alpha_4$, with different values for construction materials or for special thermal regimes.

d) Constructive elements 1 and 3 are considered to be longer than the values of the half-wave $h_1 < \ell_{sc1} \approx 1,77 \cdot \sqrt{D_{m1} \cdot \delta_1}$; $h_3 < \ell_{sc3} \approx 1,77 \cdot \sqrt{D_{m3} \cdot \delta_3}$; $h_1, h_3 -$ lengths/heights of constructive elements 1 and 3; $l_{sc1}, l_{sc3} -$ the half-wave lengths of the two cylindrical portions 1 and 3; $D_{m1}, D_{m3} -$ the average diameters of elements 1 and 3; ($D_{m1} = D_{i1} + \delta_1$; $D_{m3} = D_{i3} + \delta_1$; $D_{i1} = D_{i3} -$ (inner diameters of tubes 1 and 3; $\delta_1, \delta_3 -$ thicknesses of tubes 1 and 3 (in general, $\delta_1 = \delta_3$,since only one tube is used). Having the same geometry of constructive elements 1 and 3 (fig. 2), the cylindrical stiffnesses are equal $\Re_1 = \Re_3$.

2) It is considered that the flat plate 2 (fig. 2) has a thickness greater than the wall thickness of the purified gas exhaust tube.

3. Continuity equations of deformations. Connection loads

Notations

Q_{01}, Q_{02} – unitary bond shear forces (fig. 2); M_{01}, M_{02} – radial bending moments, unitary (fig. 2); $R_{m1} = 0,5 \cdot \left(D_{i1} + \delta_1 \right) = R_{m3}$; $\overline{P}_1, \overline{P}_2 -$ unitary axial forces distributed along the median circumferences of the dust exhaust tube; p_1, p_2 – pressure distributed inside the dust exhaust tube, respectively on the outer surface, located inside the cyclone; $R_{m4} = 0,5 \cdot \left(D_{i4} + \delta_4 \right)$ – the average radius of the cylindrical element 4; D_{i4}, δ_4 – the inner diameter of the outer body of the cyclone, respectively the thickness of its wall; $k_j, \Re_j$ – factors for mitigating the intensity of the connection loads along the corresponding cylindrical ferrules, respectively the cylindrical stiffnesses of the mentioned ferrules (usually $k_1 = k_3$; $\Re_1 = \Re_3$).

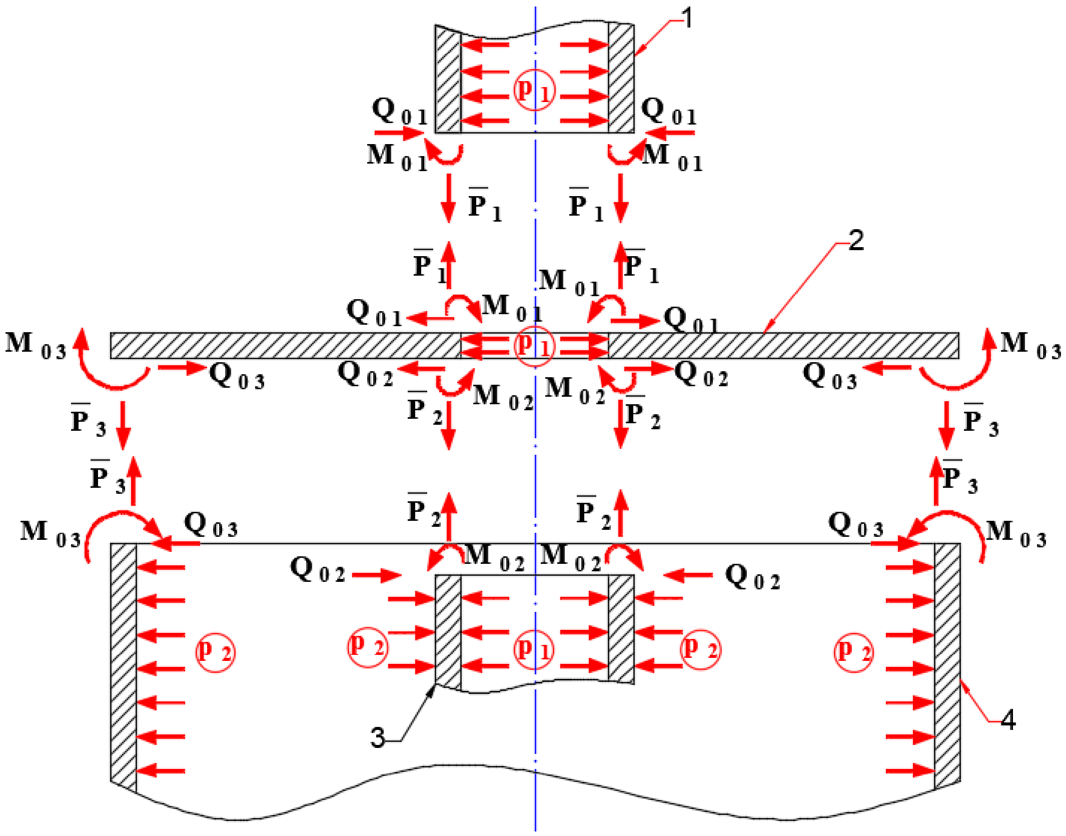

Fig. 2. The joint of the exhaust tube of the purified gas from the cyclone with the cover of the outer body
1- the upper (outer) part of the gas exhaust tube; 2 – flat tube fixing plate; 3 – the inner part of the cleaned gas exhaust tube; 4- the outer cylindrical body of the cyclone

Writing the continuity equations of radial deformations and rotations for elements 1 and 2, respectively 2 and 3, results the algebraic system written in the form:

$$[A] \cdot \{ S_l \} = \{ T_l \}, \qquad (1)$$

where the determinant of ***influencing factors*** has the form:

$$[A] = \begin{bmatrix} a_{11} & a_{12} & a_{13} & a_{14} \\ a_{21} & a_{22} & a_{23} & a_{24} \\ a_{31} & a_{32} & a_{33} & a_{34} \\ a_{41} & a_{42} & a_{43} & a_{44} \end{bmatrix}; \qquad (2)$$

vector (transposed) of connection loads: $a_{ij}\,(i=1,\,...\,4;\;\; j=1,\,...\,4\,)$:

$$\left\{S_l\right\}=\left\{Q_{01}\;\; M_{01}\;\; Q_{02}\;\; M_{02}\right\}^T; \tag{3}$$

vector (transposed) ***of free terms***: $b_j\;(\,j=1,...\,4\,)$:

$$\left\{T_l\right\}=\left\{b_1\;\; b_2\;\; b_3\;\; b_4\right\}^T. \tag{4}$$

From the equation (1), the values of the connection loads are inferred, in the form:

$$\left\{S_l\right\}=\left[A\right]^{-1}\cdot\left\{T_l\right\}, \tag{5}$$

where $\lfloor A \rfloor^{-1}$ represents the inverse of the determinant of the influencing factors (the value of the determinant is not null).
Expressions of influencing factors are presented as:

$$a_{11}=\frac{1}{2\cdot k_1^3\cdot\Re_1}+\frac{1}{4}\cdot\delta_2^2\cdot f_{jMR_{m1}}-\frac{1}{\delta_2}\cdot R_{m1}\cdot c_{1p_r};\;\; a_{12}=-\frac{1}{2\cdot k_1^2\cdot\Re_1}-\frac{1}{2}\cdot\delta_2\cdot f_{jMR_{m1}};$$

$$a_{13}=-\frac{1}{4}\cdot\delta_2^2\cdot f_{jMR_{m1}}-\frac{1}{\delta_2}\cdot R_{m1}\cdot c_{1p_r};\;\; a_{14}=\frac{1}{2}\cdot\delta_2\cdot f_{jMR_{m1}};\; a_{21}=\frac{1}{2\cdot k_1^2\cdot\Re_1}-\frac{1}{2}\cdot\delta_2\cdot f_{jMR_{m1}};$$

$$a_{22}=-\frac{1}{k_1\cdot\Re_1}+f_{jMR_{m1}};\; a_{23}=\frac{1}{2}\cdot\delta_2\cdot f_{jMR_{m1}};$$

$$a_{24}=-f_{jMRm1};\;\; a_{31}=\frac{1}{4}\cdot\delta_2^2\cdot f_{jMR_{m1}}+\frac{1}{\delta_2}\cdot c_{1p_r}\cdot R_{m1};\; a_{32}=-\frac{1}{2}\cdot\delta_2\cdot f_{jMR_{m1}}; \tag{6}$$

$$a_{33}=-\frac{1}{2\cdot k_1^3\cdot\Re_1}-\frac{1}{4}\cdot\delta_2^2\cdot f_{jMR_{m1}}+\frac{1}{\delta_2}\cdot R_{m1}\cdot c_{1p_r};\; a_{34}=\frac{1}{2\cdot k_1^2\cdot\Re_1}+\frac{1}{2}\cdot\delta_2\cdot f_{jMR_{m1}};$$

$$a_{41}=\frac{1}{2}\cdot\delta_2\cdot f_{jMR_{m1}};\; a_{42}=-f_{jMR_{m1}};\; a_{43}=-\frac{1}{2}\cdot\delta_2\cdot f_{jMR_{m1}}-\frac{1}{2\cdot k_1^2\cdot\Re_1};$$

$$a_{44}=f_{jMR_{m1}}+\frac{1}{k_1\cdot\Re_1}.$$

The expressions of the free terms (radial displacements: b_1, b_3 ; rotations: b_2, b_4):

$$b_1=\frac{(4-\mu_1)\cdot p_1}{16\cdot k_1^4\cdot\Re_1}+\frac{E_1\cdot\alpha_1\cdot\delta_1}{4\cdot k_1^4\cdot\Re_1\cdot R_{m1}}\cdot\Delta T_1+\frac{1}{2}\cdot\delta_2\cdot F_i(p_1,p_2)-\frac{1}{2}\cdot\delta_2\cdot c_{kp_2}\cdot p_2+$$

$$+\left(c_{1p_r}\cdot p_1-c_{2p_r}\cdot p_2\right)\cdot R_{m1}-C^{\bullet}_{1T}\cdot R_{m1}-\frac{C^{\bullet}_{2T}}{R_{m1}}; \tag{7}$$

$$b_2=-F_i\,(p_1,p_2)+c_{kp_2}\cdot p_2; \tag{8}$$

$$b_3=\frac{(4-\mu_2)}{16\cdot k_1^4\cdot\Re_1}\cdot(p_2-p_1)-\frac{E_3\cdot\alpha_3\cdot\delta_3}{16\cdot k_3^4\cdot\Re_3\cdot R_{m3}}\cdot\Delta T_3+\frac{1}{2}\cdot\delta_3\cdot F_i(p_1,p_2)-\frac{1}{2}\cdot\delta_3\cdot c_{kp_2}\cdot p_2-$$

$$-\left(c_{1p_r}\cdot p_1 - c_{2p_r}\cdot p_2\right)\cdot R_{m3} - \frac{1}{R_{m1}}\cdot c_{5p_r} + C^{\bullet}_{1T}\cdot R_{m1} + \frac{C^{\bullet}_{2T}}{R_{m1}}; \tag{9}$$

$$b_4 = F_i\left(p_1, p_2\right) - c_{kp_2}\cdot p_2 . \tag{10}$$

In the previous expressions, auxiliary quantities are used:

$$A_{11} = -\frac{R^2_{m1}}{2\cdot\Re_2}\cdot\left(\frac{1-\mu_2}{1+\mu_2} - \frac{2\cdot R^2_{m1}}{R^2_{m4}-R^2_{m1}}\cdot ln\frac{R_{m1}}{R_{m4}}\right); \tag{11}$$

$$A_{12} = \frac{R^2_{m1}}{4\cdot\Re_2}\cdot\left(\frac{1-\mu_2}{1+\mu_2} - \frac{2\cdot R^2_{m1}}{R^2_{m4}-R^2_{m1}}\cdot ln\frac{R_{m1}}{R_{m4}}\right); \tag{12}$$

$$A_{21} = \frac{1}{2\cdot\Re_2}\frac{1+\mu_2}{1-\mu_2}\cdot\frac{R^4_{m1}\cdot R^2_{m4}}{R^2_{m4}-R^2_{m1}}\cdot ln\frac{R_{m1}}{R_{m4}}; \tag{13}$$

$$A_{22} = -\frac{1}{4\cdot\Re_2}\frac{1+\mu_2}{1-\mu_2}\cdot\frac{R^4_{m1}\cdot R^2_{m4}}{R^2_{m4}-R^2_{m1}}\cdot ln\frac{R_{m1}}{R_{m4}}; \tag{14}$$

$$F_{1p} = B_1\left(R_{m1}\right) - \frac{1}{2}\cdot R_{m1}\cdot A_{11} - \frac{1}{R_{m1}}\cdot A_{21};\ F_{2p} = B_2\left(R_{m1}\right) - \frac{1}{2}\cdot R_{m1}\cdot A_{12} - \frac{1}{R_{m1}}\cdot A_{22}; \tag{15}$$

$$B_1\left(R_{m1}\right) = -\frac{R^3_{m1}}{4\cdot\Re_2}\cdot\left(ln\frac{R_{m1}}{R_{m4}} - \frac{1}{2}\right);\quad B_2\left(R_{m1}\right) = \frac{R^3_{m1}}{4\cdot\Re_2}\cdot\left(ln\frac{R_{m1}}{R_{m4}} - \frac{1}{2}\right); \tag{16}$$

$$K_1 = -\frac{R_{m1}\cdot R^2_{m4}}{4\cdot\Re_2}\cdot\left[\frac{\left(1+\mu_2\right)\cdot ln\,\beta_2}{\left(1-\mu_2\right)\cdot\left(\beta^2_2-1\right)} + \left(\frac{1}{1+\mu_2} + \frac{\beta^2_2\cdot ln\,\beta_2}{\beta^2_2-1}\right)\cdot\frac{1}{\beta^2_2}\right];\quad \beta_2 = \frac{R_{m4}}{R_{m1}}; \tag{17}$$

$$K_2 = \frac{R_{m1}\cdot R^2_{m4}}{4\cdot\Re_2}\cdot\left[\frac{\left(1+\mu_2\right)\cdot ln\,\beta_2}{\left(1-\mu_2\right)\cdot\left(\beta^2_2-1\right)} + \left(\frac{1}{1+\mu_2} + \frac{\beta^2_2\cdot ln\,\beta_2}{\beta^2_2-1}\right)\cdot\frac{1}{\beta^2_2}\right]; \tag{18}$$

$$C_{31}\left(R_{m1}\right) = -\frac{R^2_{m1}\cdot R^2_{m4}}{8\cdot\Re_2}\cdot\left[-\frac{2\cdot R^2_{m4}}{R^3_{m1}}\cdot\left(\frac{3+\mu_2}{1+\mu_2} - \frac{2\cdot R^2_{m1}}{R^2_{m4}-R^2_{m1}}\right) - 4\cdot\frac{1+\mu_2}{1+\mu_2}\cdot\frac{2\cdot R_{m1}}{R^2_{m4}-R^2_{m1}} - \right.$$

$$\left. -\frac{R^2_{m4}}{R^3_{m1}}\cdot\left(2\cdot ln\,\frac{R_{m4}}{R_{m1}} + 1\right)\right];\qquad C_{32}\left(R_{m1}\right) = \frac{1}{2}\cdot C_{31}\left(R_{m1}\right); \tag{19}$$

$$c_{1p_2n} = \frac{R^4_{m4}}{16\cdot\Re_2\cdot R_{m1}}\cdot\left[\frac{3}{\beta^4_2} - \frac{3+\mu_2}{1+\mu_2}\cdot\frac{\beta^2_2+1}{\beta^4_2} - \frac{3+\mu_2}{\left(1-\mu_2\right)\cdot\beta^2_2} + 2\cdot\frac{1-\mu_2}{\left(1+\mu_2\right)\cdot\beta^4_2} - \right.$$

$$\left. -\frac{8\cdot\mu_2\cdot ln\,\beta_2}{\beta^2_2\cdot\left(\beta^2_2-1\right)\cdot\left(1-\mu_2\right)}\right]; \tag{20}$$

$$c_{3p_2n} = \frac{R_{m4}^2}{16 \cdot \Re_2} \cdot \left[\frac{1}{1+\mu_2} \cdot \left(3+\mu_2 - \frac{4}{\beta_2^2} + k \right) \cdot \frac{1}{\beta_2} - \frac{1}{\beta_2^2} + \right.$$

$$\left. + \frac{k}{1-\mu_2} \cdot \beta_2 + \frac{4}{\beta_2^3} \cdot ln\,\beta_2 \right]; \; k = \frac{1}{\beta_2^2} \cdot \left[3+\mu_2 - 4 \cdot (1+\mu_2) \cdot \frac{ln\,\beta_2}{\beta_2^2 - 1} \right]; \tag{21}$$

$$f_{1MR_{m1}} = \frac{R_{m4}^2}{\left(\beta_2^2 - 1\right) \cdot \Re_2 \cdot R_{m1}} \cdot \left[\frac{1}{(1+\mu_2) \cdot \beta_2^2} + \frac{1}{1-\mu_2} \right]; \tag{22}$$

$$f_{2MR_{m1}} = \frac{R_{m4}}{\left(\beta_2^2 - 1\right) \cdot (1+\mu_2) \cdot \Re_2} \cdot \left(\frac{R_{m1}}{R_{m4}} + \frac{1+\mu_2}{1-\mu_2} \cdot \frac{R_{m4}}{R_{m1}} \right); \tag{23}$$

$$c_{1p_r} = -\frac{1-\mu_2}{E_2} \cdot \frac{R_{m1}^2}{R_{m4}^2 - R_{m1}^2}; \; c_{2p_r} = -c_{1p_r}; \; c_{3p_r} = \frac{1}{\delta_2} \cdot c_{1p_r}; \tag{24$_1$}$$

$$c_{4p_r} = -\frac{1-\mu_2}{E_2} \cdot \frac{R_{m4}^2}{\left(R_{m4}^2 - R_{m1}^2\right) \cdot \delta_2}; \; c_{5p_r} = -\frac{1+\mu_2}{E_2} \cdot \frac{R_{m4}^2 \cdot R_{m1}^2}{R_{m4}^2 - R_{m1}^2}. \tag{24$_2$}$$

$$C_{1T}^{\bullet} = \frac{1}{R_{m4}^2 - R_{m1}^2} \cdot \left(-R_{m1}^2 \cdot B_{1T} + R_{m4}^2 \cdot B_{2T} \right); \; C_{2T}^{\bullet} = \frac{R_{m1}^2 \cdot R_{m4}^2}{R_{m4}^2 - R_{m1}^2} \cdot \left(B_{1T} - B_{2T} \right); \tag{25}$$

$$B_{1T} = \frac{1}{4 \cdot k_1 \cdot \Re_1} \cdot \frac{E_1 \cdot \alpha_1 \cdot \delta_1}{R_{m1}^2} \cdot \Delta T_1; \tag{26}$$

$$B_{2T} = \frac{1}{2 \cdot R_{m4}^2} \cdot \left[(1+\mu_2) \cdot \left(R_{m4}^2 - R_{m1}^2 \right) \cdot \alpha_2 \cdot \Delta T_2 \right] + \frac{E_4 \cdot \alpha_4 \cdot \delta_4}{2 \cdot k_4 \cdot \Re_4} \cdot \Delta T_4; \tag{27}$$

$$\overline{P}_1 = \frac{D_{i1}^2}{4 \cdot D_{m1}} \cdot p_1; \; \overline{P}_2 = \frac{D_{i3}^2}{4 \cdot D_{m3}} \cdot p_2 = \frac{D_{i1}^2}{4 \cdot D_{m1}} \cdot p_2; \tag{28}$$

$$k_j = \sqrt[4]{3 \cdot \left(1-\mu_j^2\right)} \Big/ \sqrt{R_{mj} \cdot \delta_j}; \; \Re_j = \frac{E_j \cdot \delta_j^3}{12 \cdot \left(1-\mu_j^2\right)}; \; j = 1, 3, 4. \tag{29}$$

Note: The following bibliographic sources and the expressions specified above were used for writing the radial deformations and rotations:

a. 1 - *the effect of unitary axial forces,* $\overline{P}_1, \overline{P}_2$ uniformly distributed on the inner contour of plate 2 (fig. 4. 5) is introduced by means of the expression:

$F_i(p_1, p_2)$, choosing $F_{i1}(p_1, p_2)$ or $F_{i2}(p_1, p_2)$ or $F_{i3}(p_1, p_2)$,

where:

$F_{i1}(p_1, p_2) = F_{1p} \cdot p_1 + F_{2p} \cdot p_2 -$ variant I [1, 44, 47, 48];

$F_{i2}(p_1, p_2) = K_1 \cdot p_1 + K_2 \cdot p_2 -$variant II [44, 49, 50];

$F_{i3}(p_1, p_2) = C_{31}(R_{m1}) \cdot p_1 + C_{32}(R_{m1}) \cdot p_2$ - variant III [44, 51];

b. 1 - *the effect of the uniformly distributed pressure on the lower surface of the plate 2, at the level of the inner circumference*, is appreciated by means of the quantity:

$$c_k(p_2)\text{, choosing } c_1(p_2) \text{ or } c_2(p_2),$$

where:

$c_1(p_2)=c_{1p_2n}$ - variant I [44, 49, 50, 52];

$c_2(p_2)=c_{3p_2n}$ - variant II [44, 51, 53, 54];

c. 1 - *the simultaneous effect of the unit radial moments developed by M_{01}, M_{02} and by the unit cutting forces* Q_{01}, Q_{02}, along the circumference of radius R_{m1}, is included by means of the quantities:

$$f_{jMR_{m1}}\text{, choosing } f_{1MR_{m1}} \text{ or } f_{2MR_{m1}},$$

where:

$f_{1MR_{m1}}$ - variant I **[44, 49, 50]**;

$f_{2MR_{m1}}$ - variant II **[44, 51, 53, 54]**;

d. 1 - *the simultaneous effect of the radial pressure developed on the inner surface of the plate 2 by the unitary pressures* p_1, p_2 and shearing forces Q_{01}, Q_{02} is included by means of the quantities $c_{1p_r}, c_{2p_r}, c_{3p_r}, c_{4p_r}, c_{5p_r}$ [44];

e. 1 - *the temperature effect*, developed in the form of radial displacement, is illustrated by the quantities $C^{\bullet}_{1T}, C^{\bullet}_{2T}$ [44, 55].

4. Stress states

Radial and annular stresses

Notations:

$(\sigma_1)_{jx}, (\sigma_2)_{jx}$ – radial and annular stresses for the cylindrical element $j=1,3$; $\lfloor(\sigma_1)_{1x}\rfloor_{p_1,\Delta T_1}, \lfloor(\sigma_2)_{1x}\rfloor_{p_1,\Delta T_1}$ – the radial and annular stresses developed by the pressure p_1 and the thermal gradient ΔT_1, specific to the cylindrical element 1; $(c_{i\sigma r})_{jx}$, $(c_{i\sigma i})_{jx}$ - influence factors for the radial and radial stresses developed in the cylindrical elements 1 and 3 ($j=1,3$); $\lfloor(\sigma_1)_{3x}\rfloor_{p_1,p_2,\Delta T_1}, \lfloor(\sigma_2)_{3x}\rfloor_{p_1,p_2,\Delta T_1}$ – the radial and annular stresses developed by the pressures p_1, p_2 and the thermal gradient ΔT_3, specific to the cylindrical element 3; M_{1x}, Q_{1x}, T_{1x} – the radial, unitary bending moment, the unitary shearing force and the unitary annular force, dependent on the current distance x_1, along the cylindrical element 1, under the action of the connection loads M_{01} and Q_{01} (fig. 2); M_{3x}, Q_{3x}, T_{3x} – the unitary radial bending moment, the unitary shear force and the unitary annular force, dependent on the current distance x_3, along the cylindrical element 3, under the action of the connection loads M_{02} and Q_{02} (fig. 2).

Note: After solving the equality (5), the signs of the connection loads are analyzed. If the sign is

negative, proceed to a new representation in figure 2, so that, further, it can be correctly established which are the mechanically most demanding surfaces. It is desirable that the maximum demands exist on the surfaces that do not come into direct contact with the working agents.
Next, we move on to the assessment of the *radial and annular stresses*, along the sections of the tube for the clean gas evacuation, for a flat state of static stress.

Action of external loads

The radial σ_1 and annular σ_2 stresses, constant along the length of cylindrical elements 1 and 3 (fig. 2), have the forms:

- *For the cylindrical element 1* (fig. 2):

$$\left[(\sigma_1)_{1x}\right]_{p_1,\Delta T_1} = \left[(\sigma_1)_{1x}\right]_{p_1} + \left[(\sigma_1)_{1x}\right]_{\Delta T_1} = p_1 \cdot R_{m1} / (2 \cdot \delta_1) + E_1 \cdot \alpha_1 \cdot \Delta T_1 ; \quad (30)_1$$

$$\left[(\sigma_2)_{1x}\right]_{p_1,\Delta T_1} = \left[(\sigma_2)_{1x}\right]_{p_1} + \left[(\sigma_2)_{1x}\right]_{\Delta T_1} = p_1 \cdot R_{m1} / \delta_1 + E_1 \cdot \alpha_1 \cdot \Delta T_1 ; \quad (30)_2$$

$$\left\lfloor (\sigma_2)_{1x} \right\rfloor_{p_1} = 2 \cdot \left\lfloor (\sigma_1)_{1x} \right\rfloor_{p_1} . \quad \left\lfloor (\sigma_1)_{1x} \right\rfloor_{\Delta T_1} = \left\lfloor (\sigma_2)_{1x} \right\rfloor_{\Delta T_1} = E_1 \cdot \alpha_1 \cdot \Delta T_1 . \quad (30)_3$$

- *For the cylindrical element 3* (fig. 2):

$$\left[(\sigma_1)_{3x}\right]_{p_1,p_2,\Delta T_1} = \left[(\sigma_1)_{3x}\right]_{p_1,p_2} + \left[(\sigma_1)_{3x}\right]_{\Delta T_3} = (p_1 - p_2) \cdot R_{m3} / (2 \cdot \delta_3) + E_3 \cdot \alpha_3 \cdot \Delta T_3 ; \quad (31)_1$$

$$\left[(\sigma_2)_{3x}\right]_{p_1,p_2,\Delta T_1} = \left[(\sigma_2)_{3x}\right]_{p_1,p_2} + \left[(\sigma_2)_{3x}\right]_{\Delta T_1} = (p_1 - p_2) \cdot R_{m3} / \delta_3 + E_3 \cdot \alpha_3 \cdot \Delta T_3 ; \quad (31)_2$$

$$\left\lfloor (\sigma_2)_{3x} \right\rfloor_{p_1,p_2} = 2 \cdot \left\lfloor (\sigma_1)_{3x} \right\rfloor_{p_1,p_2} ; \quad \left\lfloor (\sigma_1)_{3x} \right\rfloor_{\Delta T_1} = \left\lfloor (\sigma_2)_{3x} \right\rfloor_{\Delta T_1} = E_3 \cdot \alpha_3 \cdot \Delta T_3 . \quad (31)_3$$

Action of the connection loads

In this case, the variation of the connection loads, calculated in the separation planes of the constructive elements (cylindrical elements and flat plate), have the forms [4, 5]:

- ***For the cylindrical element 1*** (fig. 2):

$$M_{1x} = M_{01} \cdot (f_4)_{1x} - (1/k_1) \cdot Q_{01} \cdot (f_2)_{1x} ; \quad (32)_1$$

$$Q_{1x} = 2 \cdot k_1 \cdot M_{01} \cdot (f_2)_{1x} - Q_{01} \cdot (f_3)_{1x} ; \quad (32)_2$$

$$T_{1x} = 2 \cdot k_1 \cdot R_{m1} \cdot \left\lfloor k_1 \cdot M_{01} \cdot (f_3)_{1x} - Q_{01} \cdot (f_1)_{1x} \right\rfloor , \quad (32)_3$$

where:

$$(f_1)_{1x} = e^{-k_1 \cdot x_1} \cdot cos\,(k_1 \cdot x_1) ; \; (f_2)_{1x} = e^{-k_1 \cdot x_1} \cdot sin\,(k_1 \cdot x_1) ; \quad (32)_4$$

$$(f_3)_{1x} = e^{-k_1 \cdot x_1} \cdot \left[cos\,(k_1 \cdot x_1) - sin\,(k_1 \cdot x_1) \right] = (f_1)_{1x} - (f_2)_{1x} ; \quad (32)_5$$

$$(f_4)_{1x} = e^{-k_1 \cdot x_1} \cdot \left[cos\,(k_1 \cdot x_1) + sin\,(k_1 \cdot x_1) \right] = (f_1)_{1x} - (f_2)_{1x} . \quad (32)_6$$

For the cylindrical element 3 (fig. 2):

$$M_{3x} = M_{02} \cdot (f_1)_{3x} - (1/k_3) \cdot Q_{02} \cdot (f_2)_{3x}; \quad (33)_1$$

$$Q_{3x} = 2 \cdot k_3 \cdot M_{02} \cdot (f_2)_{3x} - Q_{02} \cdot (f_3)_{3x}; \quad (33)_2$$

$$T_{3x} = 2 \cdot k_3 \cdot R_{m3} \cdot \left[k_3 \cdot M_{02} \cdot (f_3)_{3x} - Q_{02} \cdot (f_1)_{3x} \right], \quad (33)_3$$

where:

$$(f_1)_{3x} = e^{-k_3 \cdot x_3} \cdot cos\,(k_3 \cdot x_3);\; (f_2)_{3x} = e^{-k_3 \cdot x_3} \cdot sin\,(k_3 \cdot x_3); \quad (33)_4$$

$$(f_3)_{3x} = e^{-k_3 \cdot x_3} \cdot \left[cos\,(k_3 \cdot x_3) - sin\,(k_3 \cdot x_3) \right] = (f_1)_{3x} - (f_2)_{3x}; \quad (33)_5$$

$$(f_4)_{3x} = e^{-k_3 \cdot x_3} \cdot \left[cos\,(k_3 \cdot x_3) + sin\,(k_3 \cdot x_3) \right] = (f_1)_{3x} + (f_2)_{3x}, \quad (33)_6$$

the current elevations x_1 and x_3 being measured along cylindrical elements 1 and 3, starting from the separation planes with plate 2 (fig. 2).

The expressions of the radial and annular stresses developed by the connection loads along the cylindrical elements have the following forms:

- ***For the cylindrical element 1*** (fig. 2):

$$\left\{ (\sigma_1)_{1x}; (\sigma_2)_{1x} \right\} = \left\{ \left[(\sigma_1)_{1x} \right]_{p_1, \Delta T_1} \cdot \left(c_{i\sigma r} \right)_{1x}; \; \left[(\sigma_2)_{1x} \right]_{p_1, \Delta T_1} \cdot \left(c_{i\sigma i} \right)_{1x} \right\}; \quad (34)_1$$

$$\left(c_{i\sigma r} \right)_{1x} = 1 + \left\{ \left(\pm 6 \cdot M_{1x} / \delta_1^2 \right) / \left[p_1 \cdot R_{m1} / (2 \cdot \delta_1) + E_1 \cdot \alpha_1 \cdot \Delta T_1 \right] \right\}; \quad (34)_2$$

$$\left(c_{i\sigma i} \right)_{1x} = 1 + \left\{ \left[\pm 6 \cdot \mu_1 \cdot M_{1x} / \delta_1^2 + T_{1x} / \delta_1 \right] / \left[p_1 \cdot R_{m1} / \delta_1 + E_1 \cdot \alpha_1 \cdot \Delta T_1 \right] \right\}. \quad (34)_3$$

- ***For the cylindrical element 3*** (fig. 2):

$$\left\{ (\sigma_1)_{3x}, (\sigma_2)_{3x} \right\} = \left\{ \left[(\sigma_1)_{3x} \right]_{p_1, p_2, \Delta T_3} \cdot \left(c_{i\sigma r} \right)_{3x}, \; \left[(\sigma_2)_{3x} \right]_{p_1, p_2, \Delta T_3} \cdot \left(c_{i\sigma i} \right)_{3x} \right\}; \quad (35)_1$$

$$\left(c_{i\sigma r} \right)_{3x} = 1 + \left\{ \left[\pm 6 \cdot M_{3x} / \delta_3^2 \right] / \left[(p_1 - p_2) \cdot R_{m3} / (2 \cdot \delta_3) + E_3 \cdot \alpha_3 \cdot \Delta T_3 \right] \right\}; \quad (35)_2$$

$$\left(c_{i\sigma i} \right)_{3x} = 1 + \left\{ \left[\pm 6 \cdot \mu_3 \cdot M_{3x} / \delta_3^2 + T_{3x} / \delta_3 \right] / \left[(p_1 - p_2) \cdot R_{m3} / \delta_3 + E_3 \cdot \alpha_3 \cdot \Delta T_3 \right] \right\}. \quad (35)_3$$

Note: The plus sign in equations $(33)_{2,3}$ and $(35)_{2,3}$ is taken into account for the inner surfaces of the cylindrical components $j = 1, 3$ (fig. 2), according to the scheme accepted for the study.

In the sense of the above, the variations of the functions M_{1x}, T_{1x}, respectively M_{3x}, T_{3x} must be analyzed. The sections where these sizes are maximum are positioned, reflecting the bending stress (M_{1x}, M_{3x}), respectively the tension/compression stress in the annular direction (T_{1x}, T_{3x}). The elevations are deduced (x_{1M} - for the radial, unitary moment M_{1x} and x_{1T} - for the unitary annular force T_{1x}); (x_{3M} - for the radial unit bending moment M_{3x} and x_{3T} - for the annular unit force T_{3x}):

$$\left\{ x_{1M},\ x_{1T} \right\} = \frac{1}{k_1} \cdot \left\{ arctg \left(\frac{Q_{01}}{Q_{01} - 2 \cdot k_1 \cdot M_{01}} \right) ; arctg \left(\frac{2 \cdot k_1 \cdot M_{01} - Q_{01}}{Q_{01}} \right) \right\}, \quad (36)_1$$

$$\left\{ x_{3M},\ x_{3T} \right\} = \frac{1}{k_3} \cdot \left\{ arctg \left(\frac{Q_{02}}{Q_{02} - 2 \cdot k_3 \cdot M_{02}} \right) ; arctg \left(\frac{2 \cdot k_3 \cdot M_{02} - Q_{02}}{Q_{02}} \right) \right\}. \quad (36)_2$$

Equivalent stresses

Notations

$\left\lfloor \left(\sigma_{ech} \right)_{1x} \right\rfloor_{p_1, \Delta T_1}$, $\left\lfloor \left(\sigma_{ech} \right)_{3x} \right\rfloor_{p_1, p_2, \Delta T_3}$ - equivalent stresses evaluated according to the pressures acting on the cylindrical elements 1 and 3 and the corresponding thermal gradients, as external loads with constant values; $\left\lfloor \left(\sigma_{ech} \right)_{1x} \right\rfloor_{p_1}$, $\left\lfloor \left(\sigma_{ech} \right)_{1x} \right\rfloor_{p_1, p_2}$ – equivalent stresses established based on the thermal effect of elements 1 and 3; $\left\lfloor \left(\sigma_{ech} \right)_{1x} \right\rfloor_{M_{1x}, T_{1x}}$, $\left\lfloor \left(\sigma_{ech} \right)_{1x} \right\rfloor_{M_{3x}, T_{3x}}$ - equivalent stresses evaluated in relation to the unit radial moments M_{1x} and M_{3x}, respectively the tensile/compressive unit forces T_{1x} and T_{3x}; $\left\{ \left(\sigma_{ech} \right)_{1x} \right\}_{max}$, $\left\{ \left(\sigma_{ech} \right)_{3x} \right\}_{max}$ - total equivalent stresses, calculated by summing the influences given by the external and connecting loads; σ_{1a}, σ_{3a} - the admissible resistance of the material of cylinder 1 or 3 ((fig. 2); , $\left(\sigma^{\bullet}_{ech} \right)_{1x}$, $\left(\sigma^{\bullet}_{ech} \right)_{3x}$ - equivalent stresses calculated with the influence of unit shearing forces Q_{1x} and Q_{3x}; $\left\lfloor \left(\sigma^{\bullet\bullet}_{ech} \right)_{1x} \right\rfloor_{max}$, $\left\lfloor \left(\sigma^{\bullet\bullet}_{ech} \right)_{3x} \right\rfloor_{max}$ - maximum equivalent stresses calculated with the influence of pressure, temperature, unit radial bending moment, of the bond shear forces and of the shear given by the connection unit shear forces (individual effects).

Equivalent stresses developed by external loads – constants

In the context of the assumption that the pressures and thermal gradients - external loads - are constant values along the cylindrical elements 1 and 3, the equivalent stresses, in this case, are not dependent on the elevation (the theory of the energy of shape variation is taken into account - (***Huber– Hencky – Mises*** variants) [54, 56]:

- ***For the cylindrical element 1*** (fig. 2):

$$\left[\left(\sigma_{ech} \right)_{1x} \right]_{p_1, \Delta T_1} = \sqrt{ \begin{array}{c} \left[\left(\sigma_1 \right)_{1x} \right]^2_{p_1, \Delta T_1} + \left[\left(\sigma_2 \right)_{1x} \right]^2_{p_1, \Delta T_1} - \\ - \left[\left(\sigma_1 \right)_{1x} \right]_{p_1, \Delta T_1} \cdot \left[\left(\sigma_2 \right)_{1x} \right]_{p_1, \Delta T_1} \end{array} } ; \quad (37)_1$$

$$\left[\left(\sigma_{ech} \right)_{1x} \right]_{p_1, \Delta T_1} = \sqrt{ \begin{array}{c} 3 \cdot \left[p_1 \cdot R_{m1} / \left(2 \cdot \delta_1 \right) \right]^2 + \\ + 3 \cdot \left[p_1 \cdot R_{m1} / \left(2 \cdot \delta_1 \right) \right] \cdot \left(E_1 \cdot \alpha_1 \cdot \Delta T_1 \right) + \left(E_1 \cdot \alpha_1 \cdot \Delta T_1 \right)^2 \end{array} }, \quad (37)_2$$

or, for individual effects:

$$\left\lfloor\left(\sigma_{ech}\right)_{1x}\right\rfloor_{p_1} = \sqrt{3}\cdot p_1\cdot R_{m1}/\left(2\cdot\delta_1\right);\ \left\lfloor\left(\sigma_{ech}\right)_{1x}\right\rfloor_{\Delta T_1} = E_1\cdot\alpha_1\cdot\Delta T_1\ . \qquad (37)_3$$

- ***For the cylindrical element 3*** (fig. 2):

$$\left[\left(\sigma_{ech}\right)_{3x}\right]_{p_1,p_2,\Delta T_3} = \sqrt{\begin{matrix}\left[\left(\sigma_1\right)_{3x}\right]^2_{p_1,p_2,\Delta T_3} + \left[\left(\sigma_2\right)_{3x}\right]^2_{p_1,p_2,\Delta T_3} - \\ -\left[\left(\sigma_1\right)_{3x}\right]_{p_1,p_2,\Delta T_3}\cdot\left[\left(\sigma_2\right)_{3x}\right]_{p_1,p_2,\Delta T_3}\end{matrix}}; \qquad (37)_4$$

$$\left[\left(\sigma_{ech}\right)_{3x}\right]_{p_1,p_2,\Delta T_3} = \sqrt{\begin{matrix}3\cdot\left[\left(p_1-p_2\right)\cdot R_{m3}/\left(2\cdot\delta_3\right)\right]^2 + \\ +3\cdot\left[\left(p_1-p_2\right)\cdot R_{m3}/\left(2\cdot\delta_3\right)\right]\cdot\left(E_3\cdot\alpha_3\cdot\Delta T_3\right)+\left(E_3\cdot\alpha_3\cdot\Delta T_3\right)^2\end{matrix}}\ , \qquad (37)_5$$

or, for individual effects:

$$\left\lfloor\left(\sigma_{ech}\right)_{3x}\right\rfloor_{p_1,p_2} = \sqrt{3}\cdot\left(p_1-p_2\right)\cdot R_{m3}/\left(2\cdot\delta_3\right);\left\lfloor\left(\sigma_{ech}\right)_{3x}\right\rfloor_{\Delta T_3} = E_3\cdot\alpha_3\cdot\Delta T_3\ . \qquad (37)_6$$

Equivalent stresses developed by the connection loads

In the present case, it is considered that the connection loads are dependent on the variable length along the considered cylindrical element.

The appropriate relationships are adopted:

- ***For the cylindrical element 1*** (fig. 2):

$$\left(\sigma_{1M}\right)_{1x} = 6\cdot M_{1x}/\delta_1^2;\ \left(\sigma_{2M}\right)_{1x} = \mu_1\cdot\left(\sigma_{1M}\right)_{1x};\left(\sigma_{1T}\right)_{1x} = 0;\left(\sigma_{2T}\right)_{1x} = T_{1x}/\delta_1; \qquad (38)$$

the equivalent stresses existing inside or outside cylinder 1 can be evaluated with relations of the form:

$$\left[\left(\sigma_{ech}\right)_{1x}\right]_{M_{1x},T_{1x}} = \sqrt{\left(\sigma_{1M}\right)^2_{1x} + \left[\left(\sigma_{2M}\right)_{1x}+\left(\sigma_{2T}\right)_{1x}\right]^2 - \left(\sigma_{1M}\right)_{1x}\cdot\left[\left(\sigma_{2M}\right)_{1x}+\left(\sigma_{2T}\right)_{1x}\right]}\ , \qquad (39)$$

respectively:

$$\left[\left(\sigma_{ech}\right)_{1x}\right]_{M_{1x},T_{1x}} = \sqrt{\left(1-\mu_1+\mu_1^2\right)\cdot\left(\sigma_{1M}\right)^2_{1x} + \left(2\cdot\mu_1-1\right)\cdot\left(\sigma_{1M}\right)_{1x}\cdot\left(\sigma_{2T}\right)_{1x}}\ . \qquad (40)$$

In the case of neglecting the effect of the unit stretch/compression force, the following is reached:

$$\left[\left(\sigma_{ech}\right)_{1x}\right]_{M_{1x}} = \left(\sigma_{1M}\right)^2_{1x}\cdot\sqrt{\left(1-\mu_1+\mu_1^2\right)};\ \left[\left(\sigma_{ech}\right)_{1x}\right]_{T_{1x}} = T_{1x}/\delta_1\ . \qquad (41)$$

- ***For the cylindrical element 3*** (fig. 2):

$$\left(\sigma_{1M}\right)_{3x} = 6\cdot M_{3x}/\delta_3^2;\ \left(\sigma_{2M}\right)_{3x} = \mu_3\cdot\left(\sigma_{1M}\right)_{3x};\left(\sigma_{1T}\right)_{3x} = 0;\left(\sigma_{2T}\right)_{3x} = T_{3x}/\delta_3; \qquad (42)$$

the existing equivalent stresses on the inside or outside of cylinder 1 can be evaluated with relations of the as:

$$\left[\left(\sigma_{ech}\right)_{3x}\right]_{M_{3x},T_{3x}}=\sqrt{\left(\sigma_{1M}\right)_{3x}^{2}+\left[\left(\sigma_{2M}\right)_{3x}+\left(\sigma_{2T}\right)_{3x}\right]^{2}-\left(\sigma_{1M}\right)_{3x}\cdot\left[\left(\sigma_{2M}\right)_{3x}+\left(\sigma_{2T}\right)_{3x}\right]}, \tag{43}$$

respectively:

$$\left[\left(\sigma_{ech}\right)_{3x}\right]_{M_{3x},T_{3x}}=\sqrt{\left(1-\mu_{3}+\mu_{3}^{2}\right)\cdot\left(\sigma_{1M}\right)_{3x}^{2}+\left(2\cdot\mu_{3}-1\right)\cdot\left(\sigma_{1M}\right)_{3x}\cdot\left(\sigma_{2T}\right)_{3x}}. \tag{44}$$

When neglecting the effect of the unit stretching/compression force T_{3x}, the equation is reached:

$$\left[\left(\sigma_{ech}\right)_{3x}\right]_{M_{3x}}=\left(\sigma_{1M}\right)_{3x}^{2}\cdot\sqrt{\left(1-\mu_{3}+\mu_{3}^{2}\right)};\qquad \left\lfloor\left(\sigma_{ech}\right)_{1x}\right\rfloor_{T_{3x}}=T_{3x}/\delta_{3}. \tag{45}$$

Note: The equivalent stresses developed by the connection loads must be calculated in the planes where they are extreme (expressions (4. 75) $_1$ and (4. 75) $_2$).

Equivalent stresses (with the effect of unit shear forces)

The shear stresses developed by the unit shear forces and unit radial bending moments, for cylindrical elements 1 and 3, can be evaluated with the relation:

$$\left\{\tau_{1x},\tau_{3x}\right\}=\left\{Q_{1x}/\delta_{1},\ Q_{3x}/\delta_{3}\right\}, \tag{46}$$

where Q_{1x} and Q_{3x} have the forms (32) $_2$, (33) $_2$.

When the shear effect is also taken into account, the expression of the equivalent stress changes according to the expression [56]:

$$\begin{Bmatrix}\left(\sigma_{ech}^{\bullet}\right)_{1x}\\ \left(\sigma_{ech}^{\bullet}\right)_{3x}\end{Bmatrix}=\begin{Bmatrix}\sqrt{\left(\sigma_{ech}\right)_{1x}^{2}+3\cdot\tau_{1x}^{2}}\\ \sqrt{\left(\sigma_{ech}\right)_{3x}^{2}+3\cdot\tau_{3x}^{2}}\end{Bmatrix}. \tag{47}$$

This time, the influence of the unitary shearing force Q_{1x}- relation (32) $_2$ – respectively Q_{3x} - equality (33) $_2$, in the possible assessment of the maximum values of the equivalent stresses, according to the expressions (38), also intervenes. The estimated sections along cylinders 1 and 3 (fig. 2) can be calculated using the expressions:

$$\begin{Bmatrix}x_{1Q}\\ x_{3Q}\end{Bmatrix}=\begin{Bmatrix}\left(1/k_{1}\right)\cdot arctg\left\lfloor\left(k_{1}\cdot M_{01}+Q_{01}\right)/\left(k_{1}\cdot M_{01}\right)\right\rfloor\\ \left(1/k_{3}\right)\cdot arctg\left[\left(k_{3}\cdot M_{02}+Q_{02}\right)/\left(k_{3}\cdot M_{02}\right)\right]\end{Bmatrix}. \tag{48}$$

Equalities can be used:

$$\left\{\left(\sigma_{ech}\right)_{1x}\right\}_{max}=\left[\left(\sigma_{ech}\right)_{1x}\right]_{p_{1},\Delta T_{1}}+\left[\left(\sigma_{ech}\right)_{1x}\right]_{M_{1x},T_{1x}}+\tau_{1x}, \tag{49}$$

for cylinder 1, respectively:

$$\left\{\left(\sigma_{ech}\right)_{3x}\right\}_{max}=\left[\left(\sigma_{ech}\right)_{3x}\right]_{p_{1},p_{2},\Delta T_{1}}+\left[\left(\sigma_{ech}\right)_{3x}\right]_{M_{3x},T_{3x}}+\tau_{3x}, \tag{50}$$

for cylinder 3.

The total equivalent stress can also be evaluated by means of partial equivalent stresses, of the pressure, thermal effect, unit radial bending moments, the unit stretch/compression forces, respectively the shear stresses, written in the following forms:

$$\left\lfloor \left(\ddot{\sigma}_{ech} \right)_{1x} \right\rfloor_{max} = c_p \cdot \left\lfloor \left(\sigma_{ech} \right)_{1x} \right\rfloor_{p_1} + c_{\Delta T} \cdot \left\lfloor \left(\sigma_{ech} \right)_{1x} \right\rfloor_{\Delta T_1} + + c_M \cdot \left[\left(\sigma_{ech} \right)_{1x} \right]_{M_{1x}} + c_T \cdot \left[\left(\sigma_{ech} \right)_{1x} \right]_{T_{1x}} + c_Q \cdot \sqrt{3} \cdot \tau_{1x} , \quad (51)$$

for cylinder 1, respectively:

$$\left\lfloor \left(\ddot{\sigma}_{ech} \right)_{3x} \right\rfloor_{max} = c_p \cdot \left\lfloor \left(\sigma_{ech} \right)_{3x} \right\rfloor_{p_1, p_2} + c_{\Delta T} \cdot \left\lfloor \left(\sigma_{ech} \right)_{1x} \right\rfloor_{\Delta T_3} + + c_M \cdot \left[\left(\sigma_{ech} \right)_{3x} \right]_{M_{3x}} + c_T \cdot \left[\left(\sigma_{ech} \right)_{3x} \right]_{T_{3x}} + c_Q \cdot \sqrt{3} \cdot \tau_{3x} , \quad (52)$$

for cylinder 3.

In the previous relationships $c_p , c_{\Delta T} , c_M , c_T , c_Q$, are selection factors for the effect of specified loads: pressure/pressures, thermal gradient, unit radial bending moment, unit annular tension/compression force, unit shear force. When the coefficients have values equal to unity, the load effect is present, while when the coefficients have zero values, it is removed.

Note: It is necessary to evaluate the maximum values of the equivalent stresses - the relations (49) and (50), respectively (51) and (52) - on the surfaces of the cylindrical elements 1 and 3, to be compared with the admissible resistance characteristic of the construction materials, under the operating conditions. Thus, $\left\{ \left(\sigma_{ech} \right)_{1x} \right\}_{max} \leq \sigma_{1a}$ or $\left\{ \left(\sigma_{ech} \right)_{3x} \right\}_{max} \leq \sigma_{3a}$.

5. Conclusions

In what precedes, the analysis of the stress states developed in the cylindrical sections of the cleaned gas exhaust tube is considered. The two sections can be made of different materials or of the same material, in which case the calculation relationships are adapted accordingly. Working hypotheses, specific to the considered case, are considered. The basic hypothesis, accepted in this case, is that the flat plate of the cyclone, to which the exhaust tube is fixed, is an extended construction (characteristic of supercyclones - large sizes), without mutually influencing the edges, both for deformations and for stresses.

An interesting mention is to introduce into the study the mechanical characteristics of the construction material at the time of the analysis, it being known that the respective values change during the use of the cyclone. Only in this way is a correct evaluation of the prescription of extending the service period of the mechanical structure, or not ($\sigma_{cd} = c_d \cdot \sigma_c$; σ_{cd} – yield limit of the tested material after the period of use; c_d - the degradation factor of the characteristics of the metallic material).

References

[1] Wang, Lingjuan. *Theoretical study of cyclone design*. PhD. Thesis, Texas A&M University, USA, 2004. https://core.ac.uk/download/pdf/147123938.pdf.

[2] Corleciuc (Mitucă), Melania, I. R. Iatan, I. Durbaca, and C. Ciocoiu. "General aspects regarding the movement of solid particles inside cyclones with tangential feeding, used for dedusting dry industrial gases (I)." / "Aspecte generale privind mişcarea particulelor solide în interiorul cicloanelor cu alimentare tangenţială, folosite pentru desprăfuirea gazelor industriale uscate (I)." *Sinteze de Mecanică Teoretică şi Aplicată* 14, no. 1 (2023): 45 – 54.

[3] Corleciuc (Mitucă), Melania, I. R. Iatan, I. Durbacă, and C. Gh. Ciocoiu. "General aspects regarding the movement of solid particles inside cyclones with tangential feeding, used for dedusting dry industrial gases (II)." / "Aspecte generale privind mişcarea particulelor solide în interiorul cicloanelor cu alimentare tangenţială, folosite pentru desprăfuirea gazelor industriale uscate (II)." *Sinteze de Mecanică Teoretică şi Aplicată* 14, no. 2 (2023): 119 - 130.

[4] Corleciuc (Mitucă), Melania, I. R. Iatan, I. Durbacă, Luminiţa Georgiana Enăchescu, Mădălina Anca Dumitrescu, and C. G. Ciocoiu. "Opinions regarding the assessment of presure drop in tangential feed cyclones for cleaning industrial dry gases." *Hidraulica Magazine*, no. 2 (June 2023): 15 – 24.
[5] Griffiths, W. D., and F. Boysan. "Computational fluid dynamics (CFD) and empirical modeling of the performance of a number of cyclone samplers." *Journal of Aerosol Science* 27, no. 2 (1996): 281–304.
[6] Bohnet, M., and Th. Lorenz. "Separation efficiency and pressure drop of cyclones at high temperatures." pp. 17 – 23. Clift, R., and K. P. J. Seville (Eds.). *Gas cleaning at high temperatures*. 1st edition. Springer-Science + Business Media, B. V., 1993.
[7] ***. *Separation equipments: General design considerations of cyclone separators, centrifuges, separation equipments*. National Programme Technology Enhanced Learning (NPTEL) – Chemical Engineering – Chemical Engineering Design II. Accessed January 16, 2024. https://nptel.ac.in/courses/103103027/pdf/mod5.pdf.
[8] Silva Lora, Electo. *Control of air pollution in the sugar industry* / *Controle da poluição do ar na indústria açucareira*. Federal School of Engineering of Itajubá / Escola Federal de Engenharia de Itajubá. Society of Sugar Technicians of Brazil / Sociedade dos Técnicos Açucareiros do Brasil – STAB, 2000.
[9] Gimbun, J., T.S.Y. Choong, A. Fakhru'L-Razi, and G. T. Chuah. "Prediction of the effect of dimension, particle density, temperature, and inlet velocity ob cyclone collection efficiency." *Jurnal Teknologi, Universiti Teknologi Malaysia* 40 (F) (June 2004): 37 – 50.
[10] Alămoreanu, Elena, Gh. Buzdugan, N. Iliescu, I. Mincă, and M. Sandu. *Mechanical Engineering Calculation Guide I Îndrumar de calcul în ingineria mecanică*. Bucharest, Technical Publishing House, 1996.
[11] Iatan, I. R. *Circular and ring-shaped plates, embossed and perforated* / *Plăci circulare şi inelare, gofrate şi perforate*. Bucharest, MatrixRom Publishing House, 2012.
[12] L'Hermite, R. *Resistance of materials (Theoretical and experimental)* / *Resistance des materiaux (Theorique et experimentale)*, vol. 1. Paris, Dunod Publishing House, 1954.
[13] Timoshenko, S. P., and S. Woinovsky – Krieger. *Theory of flat and curved plates* / *Teoria plăcilor plane şi curbe*. Bucharest, Technical Publishing House, 1968.
[14] Kantorovici, B. Z. *The basis for the development of chemical machines and devices* / *Osnovî rasceta himicskih maşin i apparatov*. Moscow, G.N.T.I.M.L., 1952.
[15] Kantorovici, B. Z. *Mechanical and chemical industries* / *Maşinî himiceskoi promâşlennosti*. Moscow, Maşghiz Publishing House, 1957, 1965.
[16] ***. *The Mechanical Engineer's Handbook* / *Manualul inginerului mecanic*. Bucharest, Technical Publishing House, 1973.
[17] Babiţkii, F. I., et al. *Calculation and design of equipment for oil refineries* / *Rascet i konstruirovanie apparaturî neftepereratâvaiuşcih zavodov*. Moscow, Nedra Publishing House, 1965.
[18] Baker, E. H., L. Kovalevsky, and F. L. Rish. *Structural analysis of shells*. New York, McGraw Hill Book Company, 1972.
[19] Buzdugan, Gh., A. Petre, A. Beleș, M. Blumenfeld, C. Mitescu, I. Constantinescu, V. Cosac, R. Voinea, and C. Voicu. *Collection of problems from the resistance of materials* / *Culegere de probleme din rezistenţa materialelor*. Bucharest, Didactic and Pedagogical Publishing House, 1978.
[20] Iatan, I. R., and Carmen T. Popa. *Thermo-mechanical stresses in smooth circular plates* / *Solicitări termo-mecanice în plăci circulare netede*. Bucharest, MatrixRom Publishing House, 2010.
[21] Buzdugan Gh. *Material Resistance* / *Rezistenţa materialelor*. Bucharest, Publishing House of the Romanian Academy, 1986.
[22] Jinescu, V. V. *Calculation and construction of chemical, petrochemical and refinery equipment* / *Calculul şi construcţia utilajului chimic, petrochimic şi de rafinării*, vol. 1. Bucharest, Didactic and Pedagogical Publishing House, 1983.
[23] Jinescu, V. V. *Technological equipment for process industries* / *Utilaj tehnologic pentru industrii de proces*, vol. 1. Bucharest, Publishing House, 1983.

Modeling and Simulating the Operation of the Pneumatic Cylinders

Prof. PhD Eng. **Anca BUCUREȘTEANU**[1,*]

[1] University POLITEHNICA of Bucharest

* ancabucuresteanu@gmail.com

Abstract: *This paper presents the simulation and mathematical models necessary for studying the behavior of the pneumatic cylinders in static and dynamic conditions. The mathematical models are simplified, accessible and adaptable to different applications; they can be used in the design phases of new pneumatic units in the industrial fields. The models for cylinders with or without braking at travel end are presented. Depending on each system, these models can be supplemented with models of equipment for regulation and distribution, in order to study the respective systems. The proposed models try to take into consideration the particularities of the pneumatic systems: compressible working environment, maximum working pressure limited to 10 bar at the most, specific damping effects, etc.*

Keywords: *Mathematical models, static and dynamic mode, pneumatic cylinders, simulation*

1. Introduction

Pneumatic cylinders are motors that transform the pneumatic energy, characterized by the pressure and flow received in a certain time, into mechanical energy provided in the form of a linear displacement of a force at the same time [1].
There is a large typology of pneumatic cylinders that are manufactured by specialized companies and are available for industrial applications in different fields: production equipment and machines (machine-tools, presses, injection machines), mobile equipment, light industry, robotics etc. [2, 3, 4, 5, 6]. Cylinders can operate in open or closed systems [1, 5].
These motors are powered by means of specific equipment [1, 2, 3] from a source defined, among other things, by a maximum working pressure, usually expressed in [bar], and a maximum flow rate expressed in [Nm^3/s]. Due to the compressibility of the air, the pressure and flow rate can change depending on load, the DN of the unit and the length of the pipes. The characteristics of the equipment influence each other.
In these conditions, a series of approximations and linearizations of the proposed mathematical models are needed to easily create applicable models. Moreover, the operation of each pneumatic cylinder is also influenced by a series of constructive parameters: the type of the seals used, the friction coefficients of the live elements compared to the fixed ones, the existence of accessories such as the locking and/or braking systems on one or both ends of the cylinder stroke, the operating method, the length of strokes etc. For these reasons, the author tries to include also these types of parameters in the mathematical models.

2. Simplified Mathematical Model of the Pressure Source

The maximum working pressure p_{Max}, the maximum velocity v_{Max} allowed by the cylinder and the active surface S_1 of the piston (the surface on which the pressure actuates) are considered to be given values. The second surface will be denoted by S_2 and is the one that removes the existing air left after the previous actuation.
When the maximum pressure is reached, the cylinder is blocked because of a resistive force higher than the one that can be overcome or because the cylinder reached the end of the stroke. In these cases, the flow provided by the source becomes null.
Regarding the proposed model, it is assumed that at the supply moment there is no air in the piston chamber, nor in the piston supply pipes, because the air had been evacuated during the previous actuation. It is also considered that this total volume will be filled at the initial p_0 atmospheric pressure, after which the piston stroke can be achieved, depending on the load.
Under these conditions, the flow rate supplied as a function of pressure will be:

$$Q_{(p)} = \begin{cases} Q_M; p \le p_0 \\ Q_M \frac{p_M - p}{p_M - p_0} \; ; p_0 < p \le p_{Max} \\ 0; p > p_{Max} \end{cases} \tag{1}$$

$$Q_M = S_1 v_{Max} \tag{2}$$

As it is shown in Figure 1 also, the mathematical model above is characterized by the linearization of the dependence between flow and pressure.

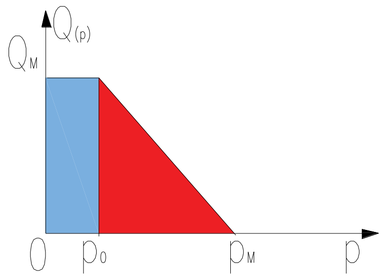

Fig. 1. Characteristic of the pressure – flow source

The pressure source will ensure a flow rate in the range [0, Q_M] at an instantaneous pressure that will not exceed the p_M value.

3. Simplified Mathematical Model of the Pneumatic Cylinder

Let consider the cylinder in Figure 2.

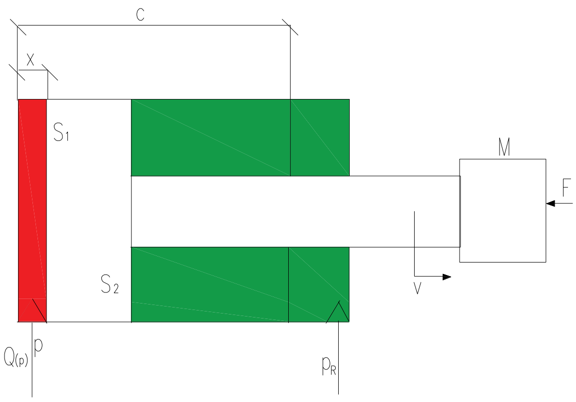

Fig. 2. Pneumatic cylinder to be actuated

The piston of the cylinder goes on stroke c against the resistive force F, moving the mass M. The instantaneous velocity is v and appears as a function of the pressure of the source p, which actuates on the surface S_1 of the piston and of the return pressure p_R that actuates on the surface S_2. The instantaneous position of the piston is given by the size x.
If the flow rate $Q_{(p)}$ and the force F are considered as inlet quantities, the following mathematical model can be taken into consideration:

$$M\frac{d^2x}{dt^2} + b\frac{dx}{dy} + F_F + F = pS_1 - p_R S_2 \tag{3}$$

$$Q_{(p)} = Q_1 + Q_2 + Q_3 \tag{4}$$

In the relations above it was also denoted: t - time, b - linearized damping coefficient, F_F – friction force in the mobile seals, Q_1 – useful flow rate, which entails the movement of the piston, Q_2 – flow rate lost through the mobile seals of the piston, Q_3 - flow rate lost due to the air compressibility.
The useful flow rate Q_1 will be:

$$Q_1 = S_1 \frac{dx}{dt} \tag{5}$$

The lost flow, if any, can be considered as:

$$Q_2 = ap \tag{6}$$

The coefficient a is the one that ensures the proportionality between the lost flow rate and the instantaneous pressure.
The flow rate Q_3, the one lost due to the compressibility of the air, can be expressed considering that the transformations undergone by the air in the cylinder body are of isothermal or adiabatic type.
In the case of the isothermal transformation (for longer durations, of the order of minutes), it is considered:

$$pV = ct \tag{7}$$

In this relation, V is the instantaneous volume in the active chamber of the cylinder.
By deriving the relation above as a function of time, it shall be obtained:

$$Q_3 = \frac{dV}{dt} = \frac{V}{p}\frac{dp}{dt} \sim \frac{V_{Med}}{p_{Med}}\frac{dp}{dt} \tag{8}$$

In this latest relation, there were denoted also: V_{Med} – the average volume of air, which can be considered as $cS_1/2$ and p_{Med} – the average pressure during operation equal to $p_M/2$.
In the case of the adiabatic transformation (for shorter durations, of the order of a few seconds) it will be considered:

$$pV^{\gamma} = ct. \tag{9}$$

After derivation, the following expression will be obtained for the flow rate:

$$Q_3 = \frac{dV}{dt} = \frac{V}{p\gamma}\frac{dp}{dt} \sim \frac{V_{Med}}{\gamma p_{Med}}\frac{dp}{dt} \tag{10}$$

Besides the sizes already defined, in the relation above there is also γ – the adiabatic coefficient considered to be γ = 1.4.
The linearized damping coefficient b in the relation (3) is more difficult to determine, as it depends on several constructive factors, out of which some are specific to the assembly in question. Thus, the longer the return pipes and the more numerous the local resistances, the higher the value.
If there is no backpressure on the return and the length of the hose is negligible, it will be considered $p_R = p_0$.
The mathematical model above applies to the cylinders that do not have braking at the end of the stroke. If the braking is available, the return pressure p_R will be defined as follows:

$$p_R = \begin{cases} p_{R1}; & x \le c - c_F \\ p_{R2} = p_{R1} + \Delta p; & c - c_F < x \le c \end{cases} \tag{11}$$

In the relation above, it was also denoted: p_{R1} – back pressure before braking, p_{R2} - back pressure during braking, Δp – pressure drop due to braking (assumed to be constant), c_F – stroke made under braking.

4. Simulation of the Pneumatic Cylinder Operation in Dynamic Mode

Based on the presented mathematical models, simulations were carried out for different variants, by means of Matlab - Simulink programs packages [7].
The behavior of a pneumatic cylinder with the following characteristics was studied: D – piston diameter 40 mm, d – rod diameter d = 20 mm, total stroke c = 1000 mm, braking stroke c_F = 10% c, maximum imposed velocity v_{Max} = 0.5 m/s. The reduced mass that can be moved is M = 50 Kg and the resistive force is F = 600 N.
The friction forces were neglected and the damping coefficient was considered to be b = 100 N/m/s, including the damping provided by the return devices and pipes.
The pneumatic source can operate at the maximum pressure p_{Max} = 6 bar.
For the first simulation, it was considered that the supply pressure is of step - type and the compressibility of the air in the start-up phase was not taken into account.
In this case, the characteristic shown in Figure 3 was obtained for the stroke velocity.

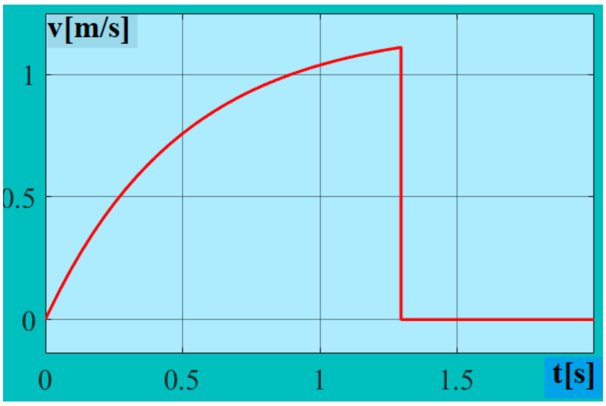

Fig. 3. Characteristic of the velocity for supply with constant pressure (step)

It can be noticed that the velocity increases even above the imposed value, and the stroke is completed in approximately 1.3 seconds as in Figure 4.

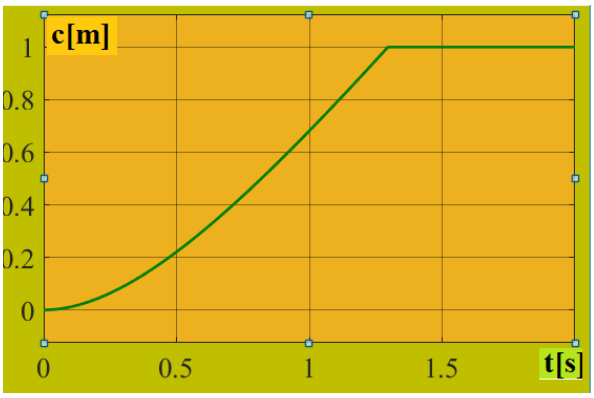

Fig. 4. Characteristic of the travel for supply with constant pressure (step)

This characteristic shows, as the previous one, that the lack of braking at the end of the stroke leads to the sudden stop of the cylinder.
Next, it was considered that the supply is made with the pressure-dependent flow rate, according to the relations (1) and (2) and the characteristic in Figure 1. In this case, the velocity v has the characteristic shown in Figure 5.
The maximum velocity in this case is below 0.2 m/s, therefore below the allowed maximum. The time necessary for the entire stroke is approximately 14 s.

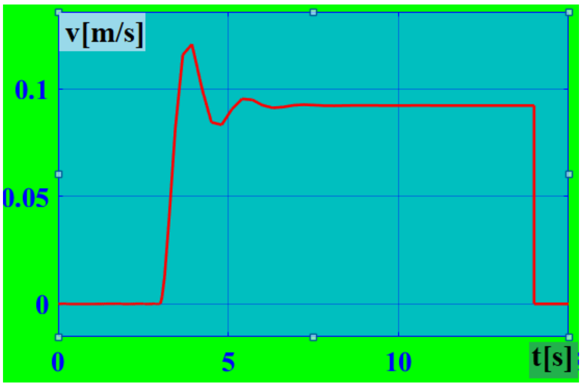

Fig. 5. Characteristic of the velocity for supply with the flow rate Q(p), a function of pressure

As it can be seen from the stroke characteristic presented in Figure 6, the absence of braking at the end of the stroke entails the sudden stop.

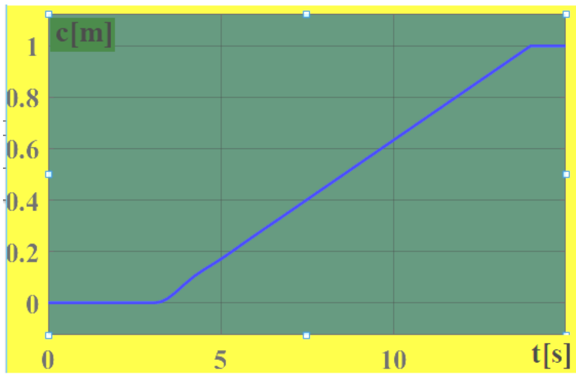

Fig. 6. Characteristic of the stroke for supply with the flow rate Q(p), a function of pressure

At the moment of making the stroke c, the stop is sudden and the pressure p will reach the maximum value p_{Max} and the supplied flow will become zero. The evolution of the pressure over the entire stroke is shown in Figure 7.

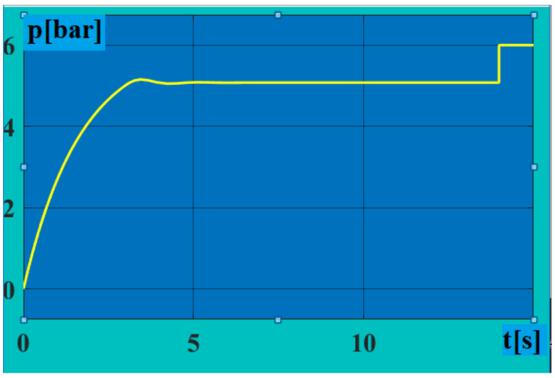

Fig. 7. Characteristic of pressure for supply with the flow rate Q(p)

The characteristic of the source and the dependence of the flow rate on the pressure lead to the increase of the time necessary for completing the stroke.
The lack of braking at the end of the stroke can entail the destruction of the unit because of the sudden stops over time.
Then it was considered that the source is of the type above (Q(p)) and the braking is performed during the last part of the stroke, on the length c_F, [1]. The diagram in Figure 8 was used for the simulation.

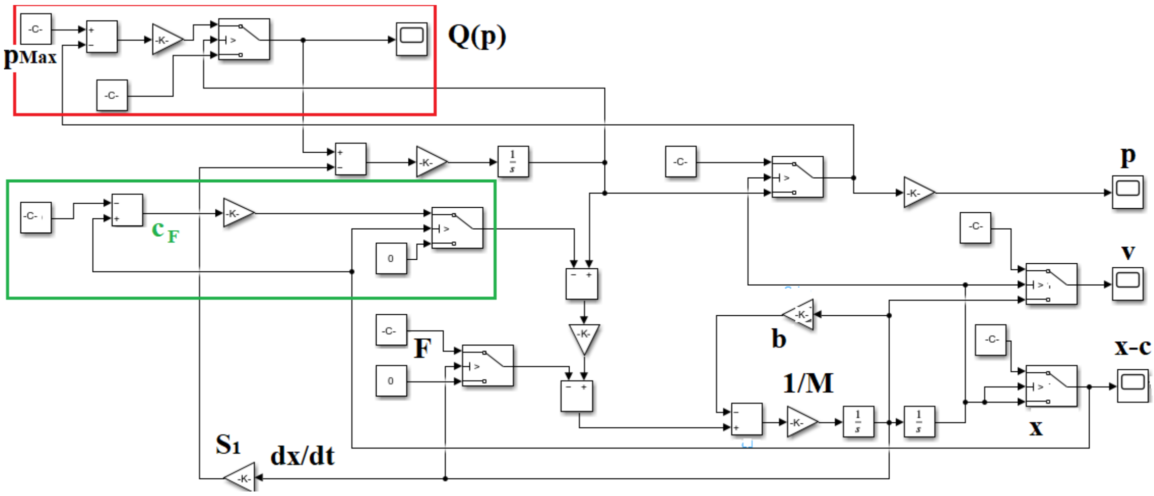

Fig. 8. Simulation diagram for the model with variable pressure and braking at the end of the stroke

The flow rate generation module as a function of the pressure Q(p) can be seen in the upper part of the diagram and immediately below is presented the module that simulates the braking on the segment of stroke c_F.
The characteristic of the flow rate Q(p) on the entire stroke is presented in Figure 9.

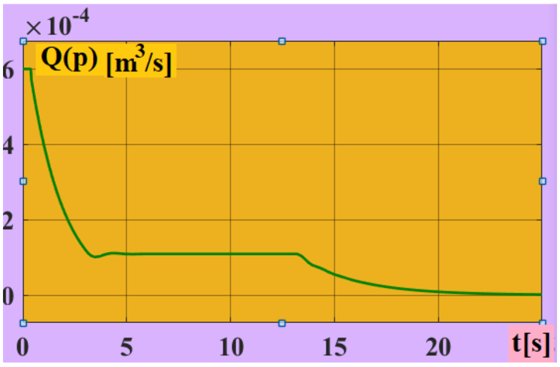

Fig. 9. Characteristic of the source

Initially, the maximum flow is the one programmed for the maximum allowed velocity, after which, increasing the pressure, the flow decreases along the stroke without braking. At the start of the braking, the pressure increases even more, which leads to the decrease of the flow that becomes zero at the end of the stroke.
The evolution of the pressure p is shown in Figure 10.

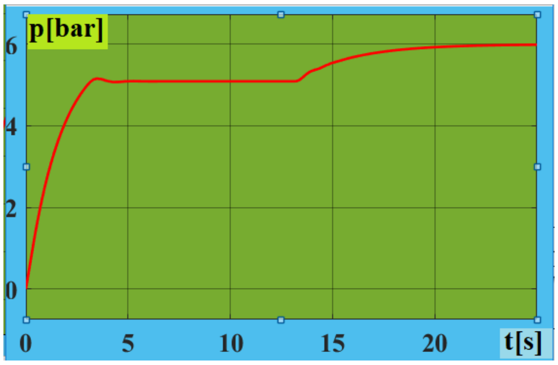

Fig. 10. Evolution of the pressure from the active chamber of surface S_1

The pressure increases until the stroke starts, then – at the beginning of the braking (approximately after 14 s) – the pressure increases until the end of the stroke when it will reach the value p_{Max} = 6 bar.
The pressure must overcome the resistive force; afterwards, the stroke starts with the velocity v, according to the characteristic in Figure 11.

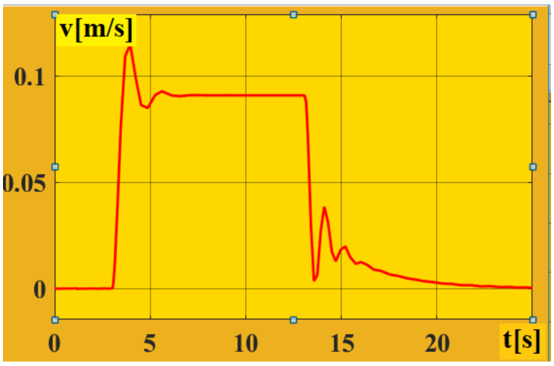

Fig. 11. Characteristic of velocity

The maximum velocity is approximately 0.13 m/s, lower than the maximum allowed. The movement is made with constant velocity up to second 14, after which the braking intervenes and the velocity decreases; the stopping is performed after 20 s from the moment of the supply.
The moment of stopping and the development of the stroke over time is viewed in the form of the instantaneous displacement x and/or of the stroke c as shown in Figure 12.

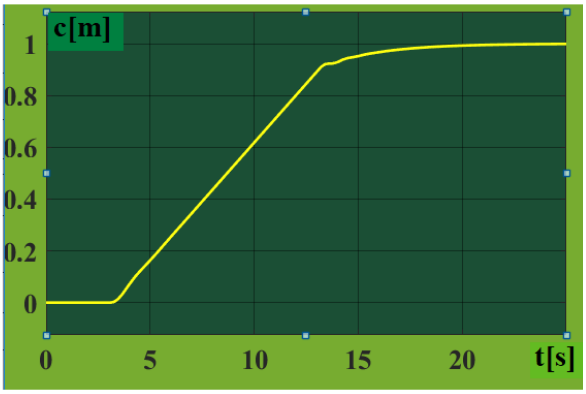

Fig. 12. Characteristic of displacement

From the moment when the braking at the end of the stroke becomes active, the velocity decreases and the effect of damping at the end of the stroke is reduced. In the case of the cylinders with braking at the end of the stroke, the damping (coefficient b) too is improved.

5. Conclusions

Due to the operation with a very compressible environment, the modeling and simulation of the pneumatic cylinders raises much more problems than in the case of the hydraulic cylinders.
The development of models which allow the determination of theoretical characteristics similar to the real ones requires the acceptance of some approximations and linearization.
As for the hydraulic drives, due to the high modulus of elasticity of the oil (about 1.5x10^4 daN/cm^2), the flow is slightly influenced by the pressure. In the case of the pneumatic cylinders, it can be considered that the pressure and the flow rate influence each other isothermally or adiabatically.
The damping coefficient b is variable, depending on the cylinder, but also on the elements of the pneumatic diagram, on the length and DN of the pipes, much more in the case of the pneumatic drive than in the case of the hydraulic drive.

Due to the high velocities developed by the pneumatic cylinders, if big strokes and high masses are involved, the braking at the end of the stroke becomes mandatory.
In order to create correct models, experimental determinations and measurements are necessary for each individual case.
The Matlab - Simulink program package ensures the possibility of creating useful models.

References

[1] Bucuresteanu, Anca, and Daniela Isar. *Pneumatic Elements and Systems. Industrial Applications/Elemente si sisteme pneumatice. Aplicatii industriale.* Bucharest, Certex Publishing House, 2007.
[2] ***. Catalogues and leaflets AIRON, FESTO, PARKER, BOSCH REXROTH.
[3] Moreno, S., and E. Peulot. *Pneumatics in Automation Production Systems/La pneumatique dans les systèmes automatisés de production*. Paris, Éditions Casteilla, 2001.
[4] Johnson, James L. *Introduction to Fluid Power*. U.S.A., Publisher: Delmar Cengage Learning, 2001.
[5] Ali, H.I., S.M. Noor, S.M. Bashi, and M.H. Marhaban. "A review of pneumatic actuators (modeling and control)." *Australian Journal of Basic and Applied Sciences* 3, no. 2 (2009): 440-454.
[6] Rahmat, M.F., N.H. Sunar, S.S. Salim, M.Z. Abidin, A.M. Fauzi, and Z.H. Ismail. "Review on modeling and controller design in pneumatic actuator control system." *International Journal on Smart Sensing and Intelligent Systems* 4, no. 4 (December 2011): 630-661.
[7] ***. MATLAB - SIMULINK Software package.

ISSN 1453 – 7303 **“HIDRAULICA” (No. 1/2024)**
Magazine *of Hydraulics, Pneumatics, Tribology, Ecology, Sensorics, Mechatronics*

Considerations regarding the Recovery and Utilization of Residual Heat from Data Centers

Assoc. Prof. PhD. Eng. **Adriana TOKAR**[1,*], Univ.Asst. PhD. student Eng. **Daniel MUNTEAN**[1], Univ.Asst. PhD. student Eng. **Dănuț TOKAR**[1], Lecturer PhD. Eng. **Daniel BISORCA**[1], Assoc. Prof. PhD. Eng. **Mihai CINCA**[1]

[1] University Politehnica Timișoara

* adriana.tokar@upt.ro

Abstract: *In the context of the acceleration of the need to store and process data and digital telecommunications, which leads to an increase in global electricity consumption and greenhouse gas emissions, the need for research to find reliable, efficient, and cost-effective solutions to reduce energy consumption and the recovery of the residual heat produced by the data centres is an increasingly urgent one. The article presents aspects that refer to the recovery of residual energy from data centres and its use for the preparation of domestic hot water, but also for the preparation of the thermal agent necessary for heating installations in buildings and respectively modern heating systems, with the mention that the latter work at a low temperature regime.*

Keywords: *Waste heat recovery, data centres, heating systems, district heating, domestic hot water*

1. Introduction

The rapid increase in the need for data storage and processing and digital telecommunications have recently generated a massive development of the data center (DC) industry. Although the digitization of various fields of human activity brings major benefits to the quality of his life, the secondary effects that appear because of this trend must also be assumed and solutions found to reduce the negative effects. Considering the exponential increase in human dependence on IT devices and services, an increase in energy consumption for manufacturing and powering these devices is also generated [1].

Taking into account the fact that DC operation is continuous, 24/24 h, 365 days per year, and it assumes as operating characteristics high requirements for safety in operation, high heat flow density, high energy consumption and carbon emissions, it is essential to make energy consumption more efficient and to recover residual heat and reuse it, a fact that leads both to the reduction of energy consumption and to the reduction of the carbon footprint [2,3].

Another problem that needs to be addressed concerns the applications in which the potential of recovered thermal energy can be used so that the technical solutions are as reliable, efficient and profitable as possible.

2. General characteristics of DC and the prediction of their development in the future

DC are spaces with a special destination within a building where IT systems and associated components are located that together carry out data processing, storage and distribution operations, they may include: server complex, data storage systems, storage systems backup, network infrastructure, electricity supply, fire alarm systems, security system and systems for maintaining the indoor climate at the parameters corresponding to the DC class.

According to the ASHRAE thermal guides for data center operating, DCs are classified according to the climatic parameters that must be maintained in the respective space in order to maintain high reliability and energy-efficient operation. The classes in which DCs falls are shown in Fig.1 [4].

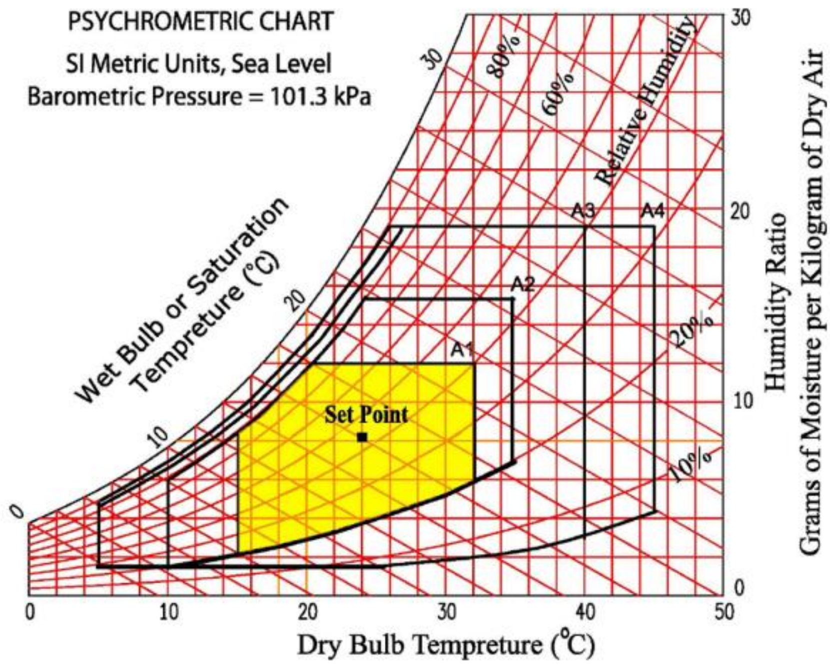

Fig. 1. ASHRAE thermal guides for data center operating [4]

A rapid increase in the needs for data processing, data storage and digital telecommunications is expected, which will normally lead to an increase in energy consumption in this sector and also in greenhouse gas emissions. Currently, DCs energy consumption is estimated at 3% of global electricity consumption and greenhouse gas emissions at 4% [5]. Recent reports predict an increase in DC of 12–14% over the next two to five years, thus resulting in an increase in consumption of up to 1/5 of global electricity consumption by 2025 [5,6].
Considering these expectations, the energy efficiency of the DCs has recently become the main concern of operators, ahead of availability and security aspects. Even when running in idle mode, the servers consume a significant amount of electricity, so other measures must be considered, such as shutting them down for the idle period or consolidating the workload. Of course, these measures to reduce energy consumption will lead to a reduction in system performance, so a balance must be found in the process of determining suitable technical solutions [7].

3. Applications for the use of energy recovered from DC

Considering that the potential of recoverable energy from DC residual heat varies depending on their size, the characteristics of the equipment used and the classification class of the DC, the applications for its subsequent use will be of two types, namely: local use, by integrating the energy under the form of hot water in the own heating installation and hot water supply for consumption and centralized use by providing thermal energy, as a prosumer, to the city's district heating system.

3.1 Local use of recovered energy

The local use of recovered energy is chosen as a technical solution for situations where the amount of thermal energy recovered is less than or equal to the total thermal energy required to cover the needs of the buildings in which the DC is located, for space heating in the winter and the production of domestic hot water in the summer.
For the recovery of residual heat from DC, an air-water heat exchanger connected to the primary circuit of a water-water heat pump can be used, which will raise the temperature of the heating agent so that it can still be used as needed in the thermal heating installation or for the production and accumulation in a hot water tank (HWT) of domestic hot water. The functional scheme of the

waste heat recovery installation and the production of thermal energy in the form of hot water is presented in Fig. 2.

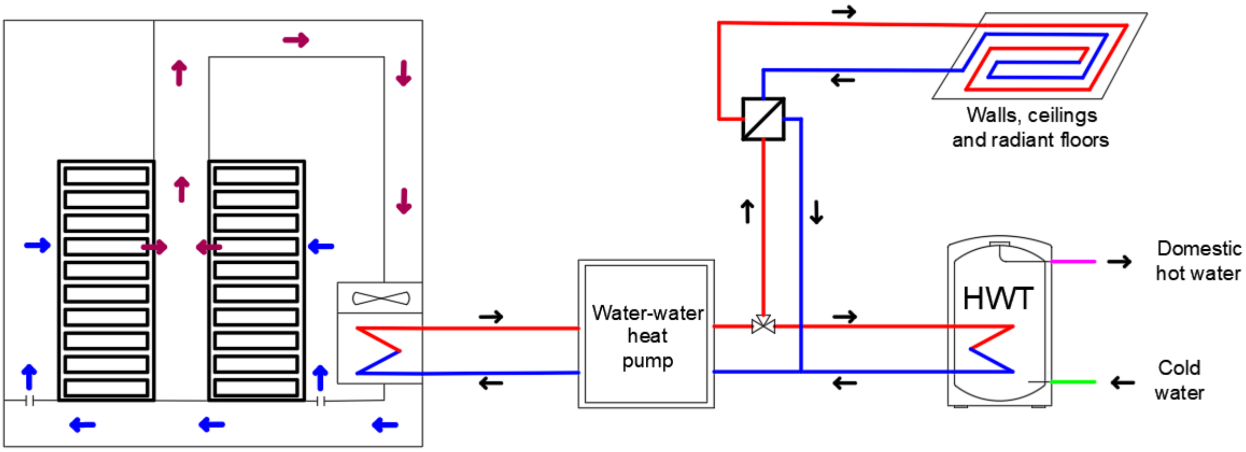

Fig. 2. Functional scheme of the recovery and local use installation

3.2 Introducing the recovered energy into the heating system

Traditional district heating systems are composed of thermal plants that produce and pump hot water or steam through pipes to provide heat to metropolitan areas. A heating system incorporates a heat generating unit, a transmission and distribution network, substations and heat consumers.
Most district heating systems use various energy sources, including coal or natural gas and waste incineration, or incorporate renewable energy sources (RES), such as geothermal, solar, or energy recovered from waste heat produced from various sources such as wastewater, industrial surplus energy or residual heat from DCs.
Today, district heating systems enable the long-distance distribution of thermal energy and the use of an increasing percentage of renewable energy, thus increasing the fight against global warming and the energy crisis. For this reason, sustainable heating systems will have to ensure planning structures, low costs linked to efficient operation and strategic investments, an aspect illustrated in Fig. 3 [8].

Fig. 3. The concept of 4th Generation District Heating [9]

The heating systems are also classified mainly according to the source of energy used, the temperature regime of the thermal agent and the efficiency of the equipment used in the process of production and distribution of the thermal energy supplied to the final consumers.

We thus identify a transition of heating systems starting with the first generation characterized by a high temperature regime of the thermal agent up to 200ºC towards the following generations which are characterized by a decrease in the temperature of the supplied thermal agent and the use of a wider range of energy sources among where RES are also found (Fig.4).

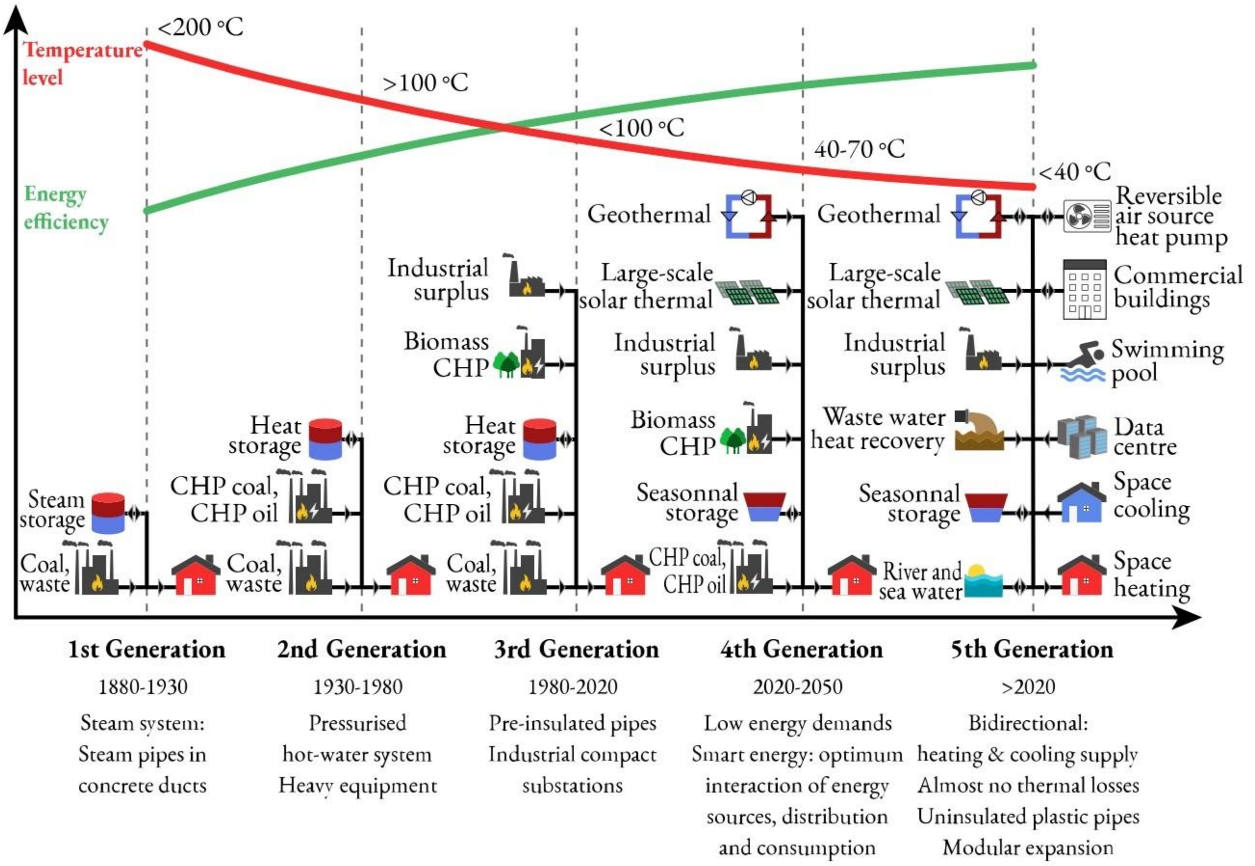

Fig. 4. The evolution of the district heating systems generations [10]

An important aspect that must be taken into account when we talk about RES integration is the fact that the temperature of the thermal agent produced by these sources is lower than in the case of the classic ones, so that the use of additional equipment is required to raise the temperature of the agent to the necessary value to it could finally be used by the consumers of the heating system, in most cases using water-to-water heat pumps (Fig. 5).

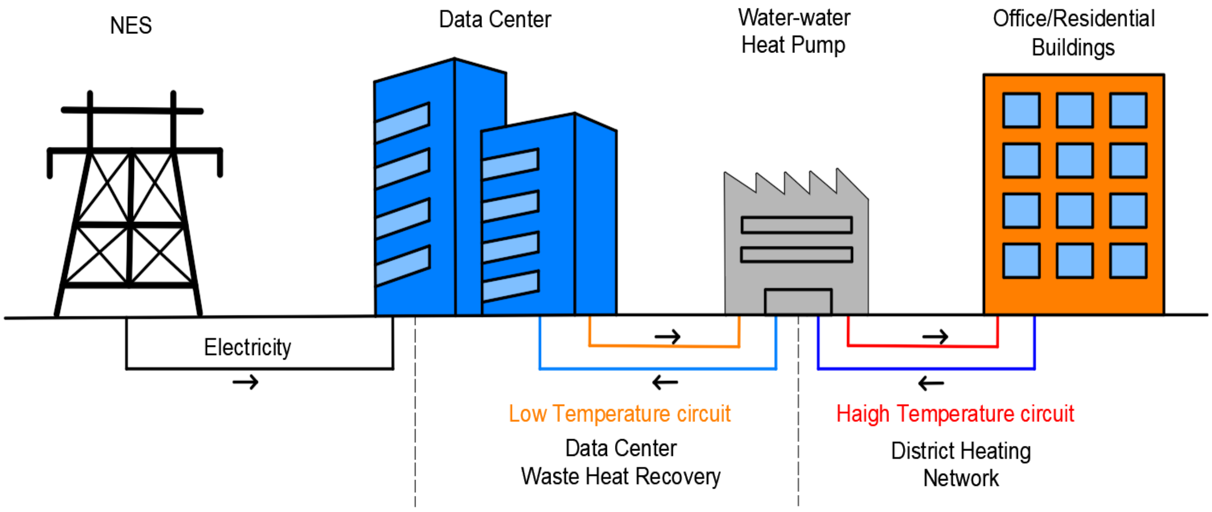

Fig. 5. Integration of thermal energy recovered from data centers in the district heating systems

4. Conclusions and future directions

The residual energy potential in the EU presented in specialized literature is estimated to be approximately 2860TWh/year [11] of which approximately 56TWh/year comes from the DC sector [12]. So, the residual energy potential recoverable from DC is a source for the preparation of hot water in various applications: domestic hot water, thermal agent for heating installations with walls, ceilings and/or radiant floors and thermal agent for heating systems ready for transition from in the 4th to 5th generation. Thus, the residual energy recovery systems and the applications for which the recovered energy is used, can be based on a temperature between 35ºC and 70ºC [13].

As future directions, we propose the realization of a pilot installation in a server room for the purpose of evaluating the residual energy potential that can be used and identifying the optimal solutions for applicability.

References

[1] Belkhir, Lotfi, and Ahmed Elmeligi. "Assessing ICT global emissions footprint: Trends to 2040 & recommendations." *Journal of Cleaner Production* 177 (2018): 448-463.

[2] Yuan, Xiaolei, Yumin Liang, Xinyi Hu, Yizhe Xu, Yongbao Chen, and Risto Kosonen. "Waste heat recoveries in data centers: A review." *Renewable and Sustainable Energy Reviews* 188 (December 2023): 113777.

[3] Yuan, Xiaolei Damon, Xuetao Zhou, Jinxiang Liu, Yu Wang, Risto Kosonen, and Xinjie Xu. "Experimental and numerical investigation of an airflow management system in data center with lower-side terminal baffles for servers." *Building and Environment* 155 (May 2019): 308-319.

[4] ASHRAE. *Thermal Guidelines for Data Processing Environments – Expanded Data Center Classes and Usage Guidance*. Whitepaper prepared by ASHRAE Technical Committee (TC) 9.9, 2011.

[5] Huang, Pei, Benedetta Copertaro, Xingxing Zhang, Jingchun Shen, Isabelle Löfgren, Mats Rönnelid, Jan Fahlen, Dan Andersson, and Mikael Svanfeldt. "A review of data centers as prosumers in district energy systems: Renewable energy integration and waste heat reuse for district heating." *Applied Energy* 258 (January 2020): 114109.

[6] Andrae, Anders. "Total consumer power consumption forecast." Paper presented at the Nordic Digital Business Summit, Helsinki, Finland, October 5, 2017.

[7] Dayarathna, Miyuru, Yonggang Wen, and Rui Fan. "Data Center Energy Consumption Modeling: A Survey." *IEEE Communications Surveys & Tutorials* 18, no. 1 (2016): 732-794.

[8] Lund, Henrik, Sven Werner, Robin Wiltshire, Svend Svendsen, Jan Eric Thorsen, Frede Hvelplund, and Brian Vad Mathiesen. "4th Generation District Heating (4GDH) Integrating smart thermal grids into future sustainable energy systems." *Energy* 68 (April 2014): 1-11.

[9] Muntean, Daniel, Matei Mîrza, Adriana Tokar, and Dănuț Tokar. "Simulations regarding the Modernization of the District Heating System in Timisoara by Controlling the Supply and Regulating the Temperature of the Heating Agent." *Hidraulica Magazine*, no. 1 (March 2022): 76-84.

[10] Muntean, Daniel, Matei Mirza, Adriana Tokar, and Danut Tokar. "Modernization of the Heat Supply System of the University of Agricultural Sciences and Veterinary Medicine of Banat, from Timisoara." Paper presented at World Multidisciplinary Civil Engineering-Architecture-Urban Planning Symposium WMCAUS 2022, Prague, Czech Republic, September 5–9, 2022.

[11] Charlotte, Elton. "Europe could be powered by recycled heat from data centres and fridges, report reveals." *Euronews.green*, February 27, 2023. Accessed February 13, 2024. https://www.euronews.com/green/2023/02/27/europe-could-be-powered-by-recycled-heat-from-data-centres-and-fridges-report-reveals.

[12] Oró, Eduard, Paolo Taddeo, and Jaume Salom. "Waste heat recovery from urban air cooled data centres to increase energy efficiency of district heating networks." *Sustainable Cities and Society* 45, (February 2019): 522-542.

[13] Montagud-Montalva, Carla, Emilio Navarro-Peris, Tomas Gomez-Navarro, Ximo Masip-Sanchis, and Carlos Prades-Gil. "Recovery of waste heat from data centres for decarbonisation of university campuses in a Mediterranean climate." *Energy Conversion and Management* 290 (August 2023): 117212.

Density and Viscosity Effects of Hydraulic System Working Fluid

Associate Professor PhD Eng. **Fănel ȘCHEAUA**[1,*]

[1] "Dunărea de Jos" University of Galati, MECMET Research Center

* fanel.scheaua@ugal.ro

Abstract: *Fluid actuation systems have proven their efficiency over time to ensure the solution of the most difficult tasks in most industries. Today we are witnessing the implementation of these systems on most of the machines and equipment that make up the stationary and mobile industry. This development is highlighted by the well-designed construction of the components, which have been modernized over time, thus enabling actuation solutions for the most divers working bodies. The working principles of fluidic drives are presented, which are based on the circulation of the working fluid that constitutes the support of this drive, the types of fluids as well as the effects related to the density and viscosity of these fluids for the operation of the hydraulic system.*

Keywords: *Hydraulic actuation, fluid density, viscosity, bulk modulus*

1. Introduction

Fluidic systems (figure 1) have been used by human communities since the beginning of their existence by using the force of water flow, or the movement of atmospheric masses represented by winds to solve certain domestic tasks related to water supply, irrigating land surfaces that they were used for growing plants, or grinding grains. Such evidence is present everywhere in the world where there have been important civilizations of mankind.

Actuations began to be used to solve other tasks with reference to various actions after the theoretical bases related to Blaise Pascal's principle were established in the 17th and 18th centuries according to which pressure is transmitted identically in all fluid directions, and later in the 18th century when Daniel Bernoulli established the energy conservation law, the kinetic-molecular theory of gases, as well as the law of fluids displacement in a fluid current tube in his published work entitled HYDRODYNAMICA (1738).

The century of sustained development of hydraulic systems was the 20th century in which water distribution systems in large cities were designed with forced actuation based on the force of steam, and later also actuation systems with high pressure values were implemented.

Regarding the fluids used to achieve the actuation, water was used in the force actions, being a liquid that has abundance and a low cost price, but it came with disadvantages related to reduced lubrication and the accentuated tendency of corrosion on the component elements of the systems with which it came in contact.

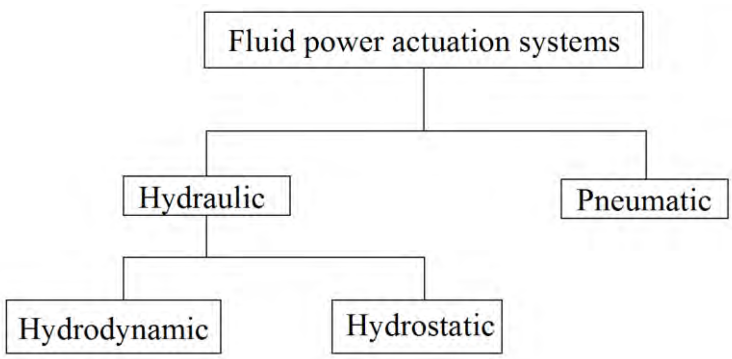

Fig. 1. Fluidic actuation classification

2. Main principles of fluidic systems

The possibility of energy transmission and conversion between different sources and receivers is highlighted, which can be achieved through the fluidic link that highlights the working fluid within a type of system. The energy source that can provide mechanical energy to a fluidic system can be of the electrical or thermal type, the energy is impregnated into the working fluid to then be used to drive a motor that can be rotary or linear.
The hydraulic system (figure 2) presupposes the existence of a hydraulic generator represented by a pump-type volume unit that has the ability to take a fluid on the suction area and send it to the network through the discharge connection. The hydraulic energy thus obtained from the continuous operation of the pump is in the form of fluid flow and pressure capable of acting directly on the moving parts of a motor that can be rotary or linear causing its rotor to come into action. The connection between the pump and the motor is ensured by the presence of circuit pipes and connecting elements of specific construction.
The advantages of using this type of system are represented by the reduced dimensions of the components that can provide high value powers, multiple possibilities of layout and assembly of the constituent elements of the circuit, as well as high efficiency values in operation.

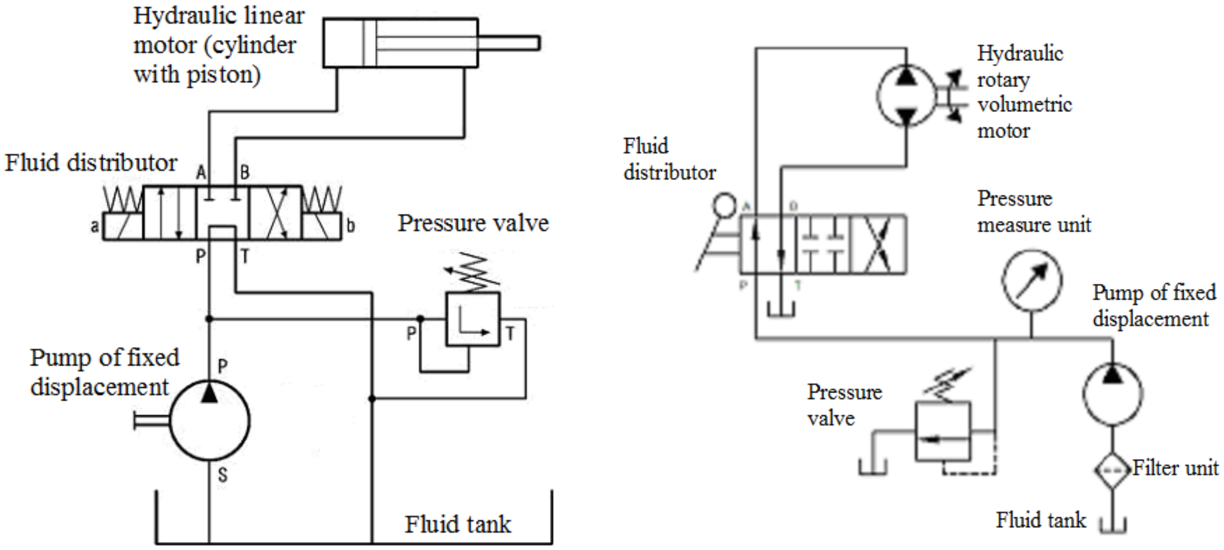

a) linear motor hydraulic actuation b) rotary motor hydraulic actuation

Fig. 2. Principle of hydraulic actuation in open circuit

All power hydraulics applications are carried out by means of the working fluid which constitutes the support of energy transmission and conversion.

3. Hydraulic fluids

The working fluids used in industrial hydraulics for multiple drives are represented by mineral oils that are circulated through complex working circuits inside various components such as pumps, motors or various other devices that are intended for the distribution of the volume of circulated fluid, or the adjustments of the values of pressure or flow required during the operation of the plant to carry out various work tasks.
In particular, there are hydraulic drives for the equipment and machines used in construction, agriculture, but also for the car, shipbuilding, mining, or aviation industries, so it can be said that we have a clear coverage with drives hydraulics of industrial branches.
In order for the work process to take place in optimal conditions, the working fluid must have a good behaviour in terms of energy transfer, but at the same time have lubricating, cooling, or insulating qualities so as to avoid leakage to outside.

There is a classification of working areas for industrial hydraulics, and this can be done by classes for stationary hydraulics, mobile hydraulics and hydraulics used in the aeronautical industry.
For each individual class, a fluid class is adopted to suit the work and environmental requirements.
It must be said that a fluid used for marine applications must be designed in such a way as to have absorption properties (biodegradable) so that in case of contact with water it does not affect the marine environment.
Hydraulic fluids are mineral and synthetic. Fluids of mineral origin are obtained from petroleum, and synthetic fluids are obtained by sintering.
Mineral oils are enriched with additives aimed at obtaining certain properties for the resulting mixture, which relate to ensuring anti-wear properties, rust and oxidation inhibition properties, viscosity index improvement properties and others.
Table 1 shows the typologies of additive hydraulic fluids that are usually marked with the indicator H for hydraulic oil and A for additive, (acc. STAS 9691-94) together with their own characteristics.

Table 1: Hydraulic fluid with proper values

Characteristics	H18A	H32A	H46A	H60A
Density (at 25 $^{\circ}$C) (g/cm^3)	0.900	0.900	0.905	0.905
Kinematic Viscosity (at 40 $^{\circ}$C) (cSt)	21.2	33.4	49.0	63.7
Conventional Viscosity ($^{\circ}$E)	3.0	4.5	6.5	8.4
Flammability point ($^{\circ}$C)	150	175	180	190
Temperature range for use ($^{\circ}$C)	-30 +85	-30 +85	-25 +85	-20 +85

Depending on the stress range of working fluids in hydrostatic actuation systems, fluids intended for light stress (used in circuits with pressure up to 15 MPa) are presented, being represented by mineral oils marked with H (H32-H100), fluids used in medium pressure circuits (up to 30 MPa) being considered medium stresses applied to the working fluid where additive fluids are used, and for the higher pressure group pressure fluids (45 MPa) are used which are additive.
The density of hydraulic fluid can vary depending on temperature, pressure, and the specific composition of the fluid.
Due to operation conditions the temperature of the hydraulic fluid increases, while the density value decreases. This is because as temperature rises, the molecules within the fluid gain kinetic energy and move further apart, resulting in decreased density.
Hydraulic fluids are typically designed to operate within certain temperature ranges to maintain their desired viscosity and performance characteristics.
Changes in pressure can also affect the density of hydraulic fluid.
Contaminants such as air bubbles, water, or foreign particles can affect the density of hydraulic fluid. If air is present in the fluid, it can decrease the overall density. Similarly, water contamination can alter the density and also affect the fluid's performance and lubricating properties.
In industrial applications, it's crucial to monitor and control the factors that can influence hydraulic fluid density to ensure optimal performance and efficiency of hydraulic systems. This often involves maintaining proper temperature, pressure, and fluid cleanliness within specified limits.
In order to calculate the fluid density at a given pressure, the fluid compressibility is considered. The hydraulic fluids density can be affected by pressure due to compression effects.
One commonly used equation to estimate the fluid density under pressure values is the Bulk Modulus equation:

$$\frac{dV}{V} = -\frac{dp}{K} \Rightarrow K = -V\frac{dp}{dV} = \rho\frac{dp}{d\rho} \quad (1)$$

Where:

dp – pressure change;
ρ - fluid density;
K - fluid bulk modulus.

The bulk modulus (K) represents the fluid resistance to compression; it's a material experimentally determined property and can be found in material data sheets.
Given the fluid density at atmospheric pressure (ρ0) and its bulk modulus (K), we can estimate the density (ρ) at a different pressure (p) using the equation:

$$\rho = \rho_0 \cdot e^{\left(\frac{p_0 - p}{K}\right)} \quad (2)$$

Three pressure ranges are considered for analysis and a common fluid density specific value for hydraulic oil, as presented in table 2.

Table 2: Initial values for fluid density and pressure

Item no.	Pressure values *(MPa)*	Initial fluid density *(kg/m3)*
1.	15	900
2.	30	
3.	45	

The calculated fluid density values applying the working pressure amounts considering the specific adiabatic bulk modulus values for hydraulic fluid at 40°C are presented in table 3.

Table 3: The calculated values for fluid density function of bulk modulus and pressure

Item no.	Pressure values *(MPa)*	Bulk modulus *(K) (MPa)*	Fluid density *(kg/m3)*
1.	15	1780	907.59
2.	30	1935	914.07
3.	45	2125	919.11

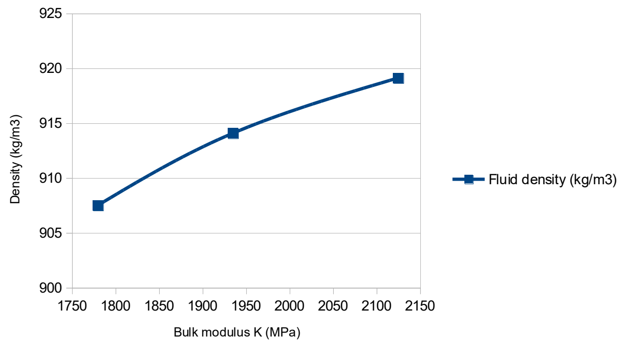

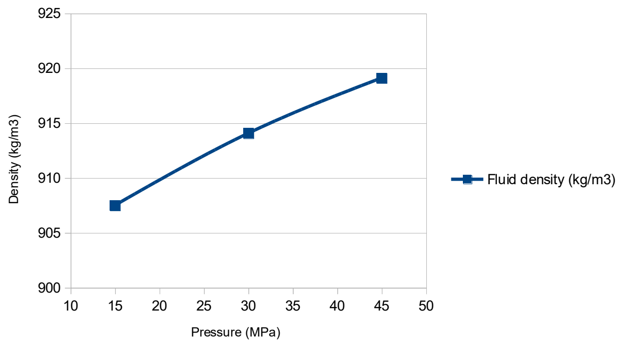

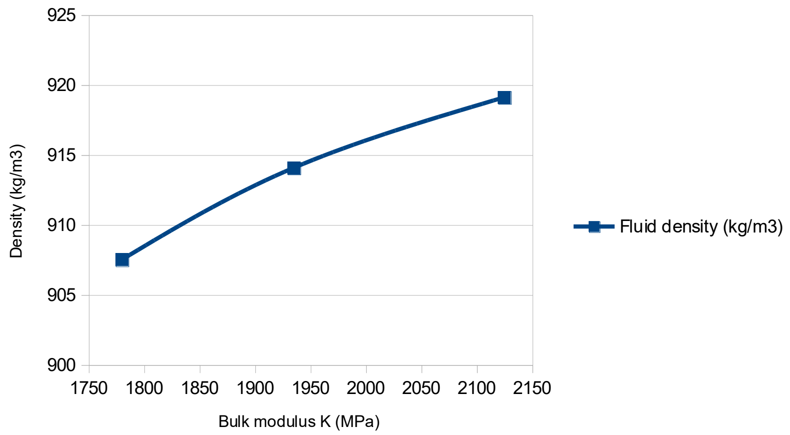

Fig. 3. The diagrams for density obtained values

The viscosity of hydraulic fluid can vary due to several factors, and understanding these variations is crucial for maintaining the efficiency and functionality of hydraulic systems.

$$\tau = \mu \frac{du}{dt} \quad (3)$$

Temperature has a significant impact on the viscosity of hydraulic fluid. As temperature increases, the viscosity typically decreases, making the fluid less resistant to flow.
As temperature decreases, viscosity tends to increase, making the fluid more resistant to flow. This viscosity-temperature relationship is essential for ensuring proper lubrication and efficient operation of hydraulic components over a range of operating temperatures.
Extreme pressure conditions, such as those encountered in high-pressure hydraulic systems or under certain operating conditions, can cause changes in viscosity due to changes in fluid density and molecular arrangement. These effects are usually accounted for in the design and selection of hydraulic fluids.
The viscosity of hydraulic fluid can also vary with shear rate, which is the rate at which adjacent fluid layers move relative to each other. Within hydraulic systems, fluid undergoes shear as it flows through narrow channels, valves, and other circuit components.
Under high shear rates, hydraulic fluids may exhibit shear thinning behavior, where viscosity decreases with increasing shear rate. This property is desirable as it helps maintain consistent fluid flow and minimizes energy losses within the system.
Different types of hydraulic fluids, such as mineral oil-based, synthetic, or water-based fluids, have distinct viscosity profiles based on the types and proportions of additives, base oils, and other components.
Manufacturers formulate hydraulic fluids to meet specific performance requirements, including viscosity at various temperatures and operating conditions.
Contaminants such as water, air, particulate matter, or degradation byproducts can affect the viscosity of hydraulic fluid. Water contamination can cause emulsification and changes in viscosity, leading to reduced lubricating properties and potential damage to system components.
Proper fluid maintenance and filtration are essential for minimizing the impact of contaminants on fluid viscosity.
When there is a need to adopt a certain hydraulic fluid for an application viscosity is an important parameter.
During operation of the hydraulic circuit higher values of viscosity ensure a reduction in operating temperatures. This is because a low viscosity hydraulic fluid will reduce the volumetric efficiency of pumps and cause fluid overheating.
Also the low viscosity hydraulic fluids lead to increased friction and circuit components wear, while some fluids with high viscosity values will cause poor mechanical efficiency, operating with a tendency to wear over time.

The best solution for hydraulic fluid adoption involves best oil viscosity in terms of volumetric and mechanical pump efficiency and in order to realize the respective project, must be considered the main requirements for the circuit main components, at specific temperature values range.

4. Conclusions

The density and viscosity of hydraulic fluid play crucial roles in the operation and efficiency of hydraulic circuits of the technological equipment.
The density of hydraulic fluid affects its ability to transmit pressure efficiently within the system.
Fluids with higher density can transmit pressure more effectively, leading to improved system response and performance.
Regarding the system dynamics a higher fluid density can result in increased inertia and damping effects within the system, affecting its dynamic response. This can impact factors such as system oscillations, response time, and stability.
Hydraulic pumps must overcome the pressure created by the fluid stream. Higher fluid density means higher pressure, which can increase the load on the pump and affect its efficiency.
The hydraulic fluid viscosity determines the resistance of the fluid to be circulated within the hydraulic circuit. Higher viscosity fluids experience greater internal friction, leading to energy losses and reduced efficiency within the system.
Viscosity influences the thickness of the lubricating film between moving parts. Optimal viscosity ensures adequate lubrication to minimize wear and prevent metal-to-metal contact.
Viscosity affects the efficiency and performance of hydraulic pumps. Higher viscosity fluids require more energy to pump, potentially reducing overall system efficiency.
Selecting hydraulic fluids with appropriate density and viscosity for the specific application is crucial. The fluid should provide adequate pressure transmission while minimizing energy losses due to viscosity.
Both density and viscosity properties of the hydraulic fluid are temperature-dependent.
Monitoring and controlling fluid temperature within recommended limits are essential to maintain optimal fluid properties and system performance.
Regular fluid analysis and maintenance practices, such as filtration and contamination control, help preserve fluid properties and ensure consistent circuit performance over time.
Hydraulic circuit design should consider the fluid properties to minimize pressure drops, optimize component sizing, and enhance overall system efficiency.
In summary, the density and viscosity of hydraulic fluid significantly impact system performance, efficiency, and component longevity.
Proper selection, maintenance, and system design considerations are essential for achieving optimum circuit operation.

References

[1] Axinti, G., and A.S. Axinti. *Hydraulic and pneumatic drives – Components and systems, Functions and features/Acţionări hidraulice şi pneumatice – Componente și sisteme, Funcții și caracteristici*. Vol. 1. Chişinău, Tehnica-Info Publishing House, 2008.
[2] Axinti, S., and F.D. Șcheaua. *Introduction to industrial hydraulics/Introducere în hidraulica industrială*. Galati, Galati University Press, 2015.
[3] Axinti, G., and A.S. Axinti. *Hydraulic and pneumatic drives – Bases of Calculation, Design, Operation, Reliability and Drive Diagrams/Acţionări hidraulice şi pneumatice – Baze de Calcul, Proiectare, Exploatare, Fiabilitate și Scheme de Acționare*. Vol. 3. Chişinău, Tehnica-Info Publishing House, 2009.
[4] Wu, J. B., and L. Li. "Pipeline pressure loss in deep-sea hydraulic systems considering pressure-dependent viscosity change of hydraulic oil." *Journal of Marine Science and Engineering* 9, no. 10 (2021): 1142.
[5] Deuster, S., and K. Schmitz. "Bio-based hydraulic fluids and the influence of hydraulic oil viscosity on the efficiency of mobile machinery." *Sustainability* 13, no. 14 (2021): 7570.
[6] Bair, S., and P. Michael. "Modelling the pressure and temperature dependence of viscosity and volume for hydraulic fluids." *International Journal of Fluid Power* 11, no. 2 (2010): 37-42.
[7] Knežević, D., S. Laloš, M. Jocanović, and V. Karanović. "Effect of bulk modulus of fluid on the dynamic behavior of the hydraulic system." *ANNALS of Faculty Engineering Hunedoara – International Journal of Engineering* 14, no. 1 (2016): 243-246.

New Drought Index Implementation at Station 15130, Valle de Bravo, Mexico

Dr. **Maritza ARGANIS**[1,*], M.Eng. **Margarita PRECIADO**[2,*], Dr. **Faustino DE LUNA**[1,*]

[1] Nacional Autonomous University of Mexico, Institute of Engineering, Av. Universidad 3000. Ciudad Universitaria, Coyoacán, CDMX, C.P. 0451 (Arial, 10pt, Regular)

[2] Mexican Institute of Water Technology IMTA, Paseo Cuauhnáhuac 8232 Progreso, Morelos, C.P. 62550 (Arial, 10pt, Regular)

* MArganisJ@iingen.unam.mx; preciado@tlaloc.imta.mx; FLunaC@iingen.unam.mx

Abstract: *This research focused on meteorological drought problem a phenomenon that has affected several countries and has had significant impacts on various water uses, including human, agricultural, and industrial consumption. To address this problem, the NDI index was applied, which uses precipitation and mean air temperature data, and the RASP method to the annual data of the Presa Valle de Bravo weather station, in Edomex., Mexico. This analysis allowed the identification of two periods of severe drought: one of approximately 8 years and another that began in 2019 and seems to continue. In addition, a decreasing trend was detected in the daily runoff volumes to the Presa Valle de Bravo from 1994 to early 2024. These results are indicative of the need to conduct regional studies to confirm the duration of droughts and to implement resource management policies that allow for anticipation and water shortage prevention contingencies due to meteorological droughts.*

Keywords: *Valle de Bravo Reservoir, Precipitation, Droughts, Daily inflow volumes, Trend*

1. Introduction

Droughts are prolonged scarce precipitation climatic events that can have significant effects on water availability. In various parts of the world, an increase in the frequency and intensity of droughts has been observed, affecting water security and sectors such as agriculture, livestock, and the supply of water for human consumption. In this research, an analysis was carried out with annual data of annual precipitation and mean air temperature from the Presa Valle de Bravo station15130, Edomex., Mexico, using the new drought index NDI (New Drought Index in English) described in the methodology of Bonacci et al., 2023 [1].

2. Methodology

In simple terms, a drought is defined as the decrease or absence of rainfall relative to the annual index and, contrary to what is assumed, it is a normal and recurring event that occurs cyclically in all climatic zones of the world, although with greater intensity and recurrence in arid and semi-arid zones. In Mexico, these phenomena occur cyclically and when they occur, they cause a water imbalance in the water cycle, as the availability of the resource is insufficient to meet the needs of living beings. A drought can last on average from one to three years, and it ends when the rains return and the normal precipitation index is recovered and the functioning of the water bodies is restored.
Drought is mainly classified into three types: meteorological, agricultural, and hydrological. These different typologies of drought "identify the beginning, the end, and the degree of severity of the same". All types of drought originate from the same cause: the lack of rain, therefore, when "only rain is taken into account", we are talking about meteorological drought. It is this type of drought that is attributed to the beginning of the hydrological imbalance, as it is when an interruption in the weather is perceived for one or more seasons; this type of drought is difficult to specify, since its effects or incidence are different depending on the place where it occurs; for example, in Bali, meteorological drought is defined as "the period with absence of rain in six days", while in Spain it is considered as meteorological drought a period that can reach up to two consecutive years without precipitation [2] (Esparza M, 2014). Drought, when combined with scarcity, often generates

a social catastrophe, as the situation of scarcity worsens. Although drought is a less spectacular phenomenon, its impact is silent and progressive. Often, it is not easily perceived until its attack is already underway. The lack of rain and the decrease in water resources can have devastating consequences on the availability of food, the health of the population, and the local economy. Awareness and proper management of drought are fundamental to mitigate its effects and prevent social crises.

2.1 New drought index (NDI)

The drought indices traditionally used consider the main variable to be precipitation and/or evapotranspiration of the analyzed site [3-6], Bonacci et al.,2023 [1] proposed to include in the analysis of droughts and in a standardized form both total precipitation and mean air temperature, taking into account that this variable is commonly reported at weather stations and that evapotranspiration depends on it, which is more difficult to estimate. The new drought index (NDI) is calculated with equation (1)

$$NDI_i = \left(\frac{\mathrm{P}_i - \mathrm{P}_m}{S_p}\right) - \left(\frac{\mathrm{T}_i - \mathrm{T}_m}{S_T}\right) \tag{1}$$

where NDI_i is the new drought index in year *i* or month *i*, P_i is the total precipitation in year *i*, P_m is the mean precipitation of the entire recording period, S_p is the standard deviation of the precipitation of the entire recording period; T_i is the mean temperature in year *i*, T_m is the average temperature of the entire recording period and S_T is the standard deviation of the mean temperature over the entire recording period.

2.2 RAPS Method

The Rescaled Adjusted Partial Sums (RAPS) method aids in defining statistically significant time periods in which changes in average values occur throughout a time series [7]. This method estimates the series of partial sums with equation 2.

$$RAPS_i = \sum_{i=1}^{k} \frac{(y_i - y_m)}{S_y} \tag{2}$$

where y_i, represents la analized variable in a given time interval, *i*, y_m, the average value of the entire analysis series, S_y, the standard deviation, *n*, the number of data in a series, *k ∈(1, 2…, n)*, the counter of sums for the *k* analyzed time unit in a series of the total, *n*.
In t case of applying this method directly to the NDI_i, the ΣNDi sums were calculated as it is a standardised variable.

2.3 Identification of potential drought periods and their severity

Trend, homogeneity, and independence tests were applied to the annual precipitation and temperature series (Escalante and Reyes, 2002) [8]. Additionally, with the RAPS and the NDi sums, time periods are identified in which increasing and decreasing behaviors are observed in the series, upward and downward trends; and to these time periods, statistical tests are applied, for example, the Student's t-test to accept or reject a null hypothesis; in this analysis, the null hypothesis for the sums of the temperature series, precipitation, and NDI was that there is a significant change it means the analyzed period compared to complete original series mean, a significance level of 0.05 was considered. Additionally, linear regressions were performed whose lines slopes help to classify droughts and in this way their severity is investigated.

2.4 Study site

Climatological Station 15130 Valle de Bravo is located at municipality of Valle de Bravo, state of Mexico. It is situated at an altitude of 1,840 meters above sea level and has a temperate sub-humid climate with summer rains. This station was founded in 1948 and is operated by the National Meteorological Service (SMN) of Mexico. It measures a variety of meteorological parameters, including temperature, humidity, precipitation, wind speed, and wind direction [9]. The meteorological station 15130 Presa Valle de Bravo was selected, located near the dam of the same name, which is part of the main dams of the Cutzamala System that supply water to the State of Mexico and Mexico City.

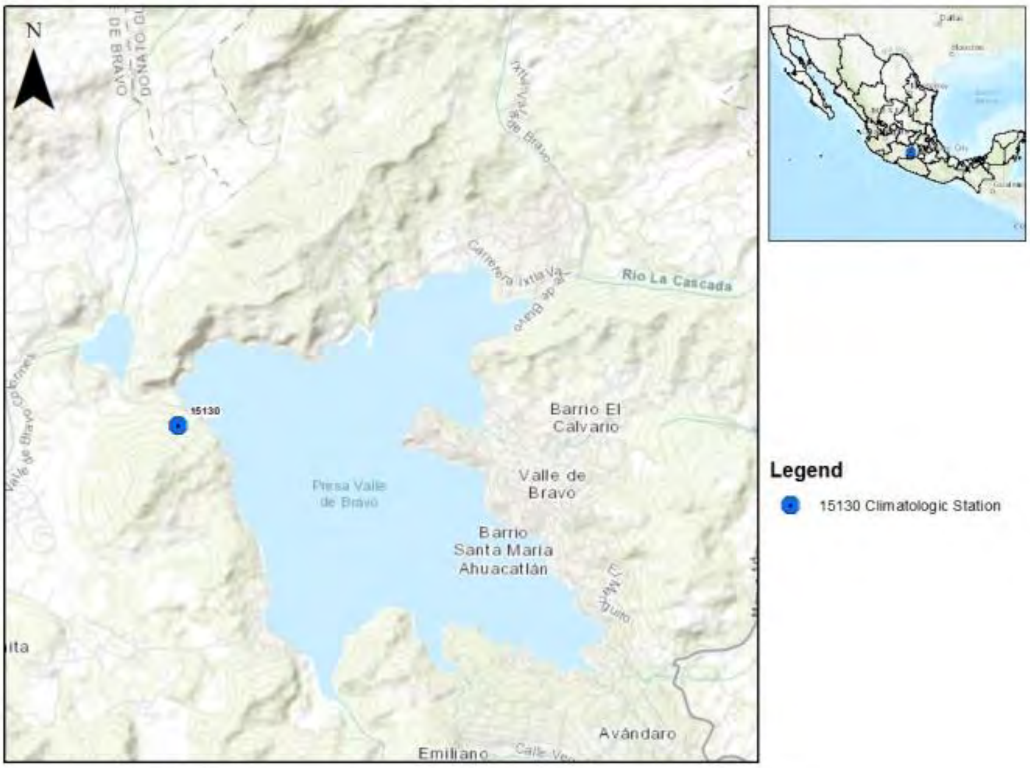

Fig. 1. Climatological station 15130 location Presa Valle de Bravo, Valle de Bravo, Edomex, Mexico. Source: Own design

Monthly average Records air precipitation and temperature were almost complete for period from 1969 to 1989 and from 2009 to 2020. From these data, annual series, maximum values, minimums, and their statistical mean and standard deviation were estimated. (Table 1).

Table 1: Minimum values, maximums, mean, and standard deviation of the total annual precipitation and the average annual temperature. Station 15130 Valle de Bravo, Mex.

Value	Precipitation, mm	Temperature, °C
Min	685.8	18.16
Max	1116.4	20.21
Mean	896.27	19.01
Standard Deviation	112.25	0.56

3. Application and results

3.1 Precipitation Data Series

In Figure 2, Data from annual precipitation series and the observed trend lines in two identified groups are observed. The series turned out to be independent, homogeneous, and without a trend.

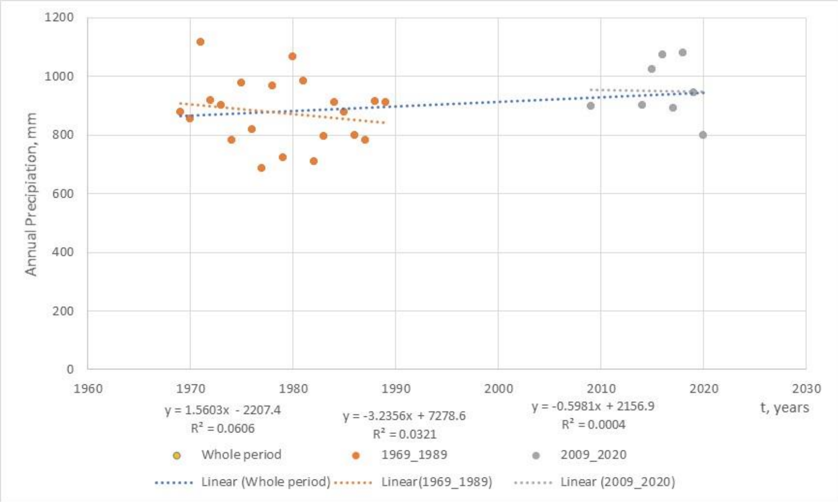

Fig. 2. Total annual precipitation series, Station 15130 Valle de Bravo, Edomex., Mexico

3.2 Average Air Temperature Data Series

In Figure 3, data from the annual precipitation series and the observed trend lines in two identified groups are observed. Series turned out to be dependent, non-homogeneous, and with a trend.

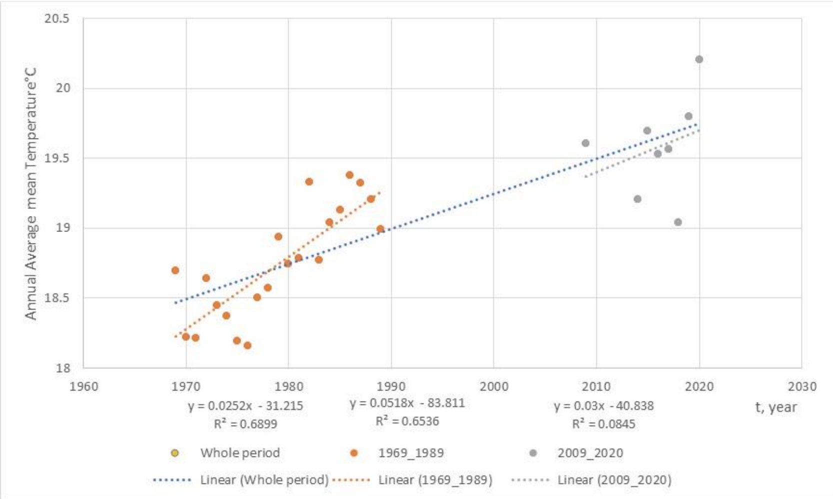

Fig. 3. Annual average temperature series, Station 15130 Valle de Bravo, Edomex., Mexico

3.3 NDIi

Annual drought indices are observed in Figure 4.

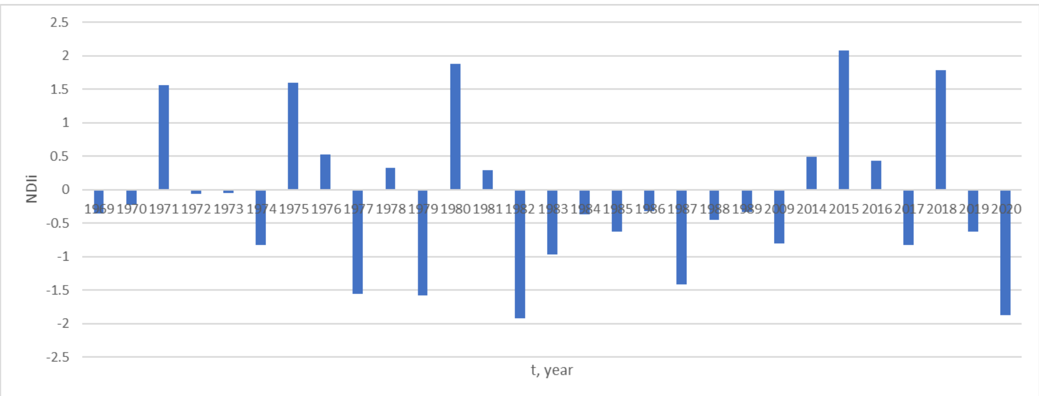

Fig. 4. Annual NDIi, Station 15130 Valle de Bravo, Edomex., Mexico

3.4 RAPSi and ΣNDIi

RAPSi of precipitation and average annual temperature as well as SNDIi appear in Figures 5 to 7 and in Tables 2 to 4 the identified periods of variation of the RAPSI and of the SNDi sums are indicated with their statistics and probability value student's t-test p.

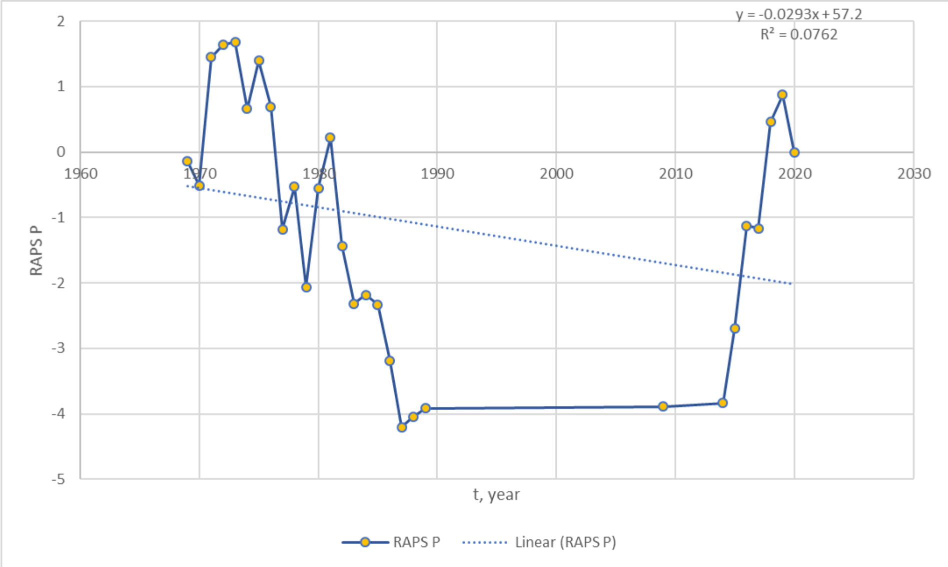

Fig. 5. RAPs of annual precipitation

Table 2: Periods identified with changes in the RAPSi, statistics and result from Student's t-test p. Annual precipitations

Periods	Mean	Standard deviation	p $_{t\text{-test}}$	Result
1969-1981	898.176923	126.661913	0.94	Mean are not different
1982-1987	813.5	72.053841	0.12	Mean are not different
1988-1989	912.6	2.54558441	0.87	Mean are not different
2009-2020	951.16125	98.9425115	0.22	Mean are not different

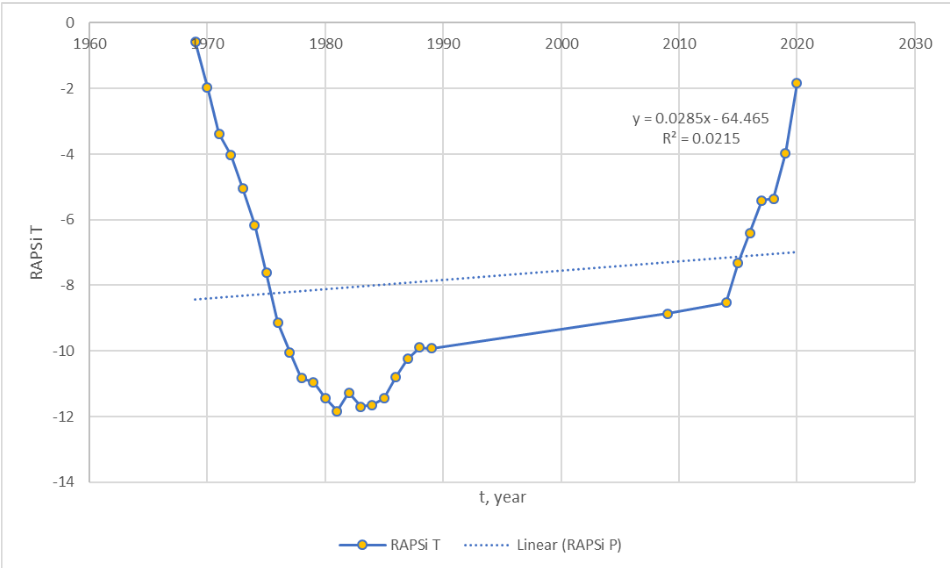

Fig. 6. RAPs of Average annual temperature

Table 3: Periods identified with changes in the RAPSi, statistics and result from Student's t-test p. Average annual temperature

Periods	Mean	Standard deviation	p t-test	Result
1969-1981	18.50	0.25495214	0	Means are different
1982-1989	19.15	0.21	0.56	Means are not different
2009-2020	19.25	0.36	0.07	Means are not different

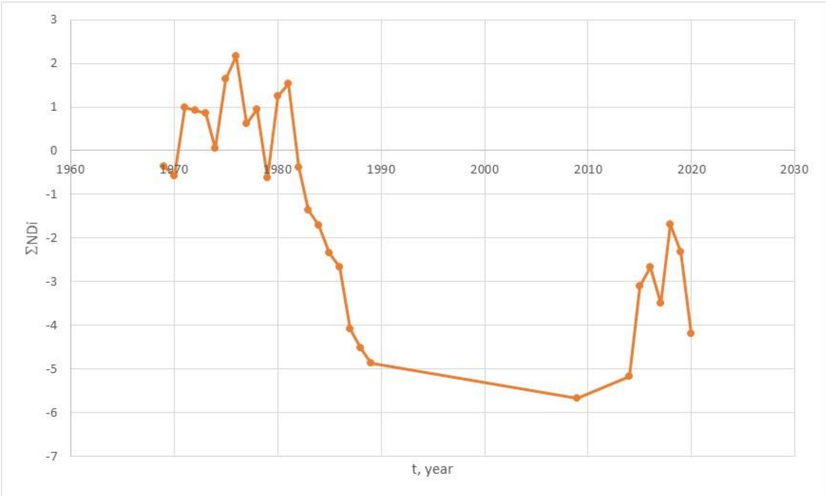

Fig. 7. Annual ΣNDIi annuals

Table 4: Periods identified with changes in the RAPSi, statistics and result from Student's t-test p. Average annual temperature

Periods	Mean	Standard deviation	p t-test	Result
1969-1981	0.73	0.88	0	Mean is different
1982-1989	-2.74	1.61	0.54	Mean is not different
2009-2018	-3.63	1.52	0.1	Mean is not different
2019-2020	-3.26	1.33	0.31	Mean is not different

Finally, linear trend lines were obtained for each identified period of the SNDIi to establish the severity of the drought at the site of the climatological station Presa Valle de Bravo with the help of their slopes. In Figure 8, generated by Python, these results are observed.

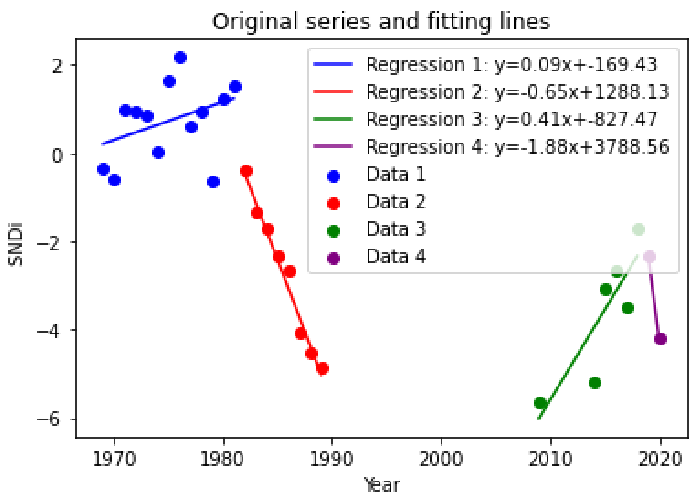

Fig. 8. SNDi Regressions at periods for droughts severity identification on analyzed site

From Figure 8 and taking into account strongly negative slope, it is observed that in the period from 1982 to 1989 a severe drought episode occurred, but a severe drought is notable in the period from 2019 to 2020, in which the slope in absolute terms is almost three times steeper.

3.5 Inflow volume Behavior into Presa Valle de Bravo

Daily volumes series of inflow to the Presa Valle de Bravo is observed in Figure 9, which illustrates the variation over time of the main dams that feed the Cutzamala system in Mexico.

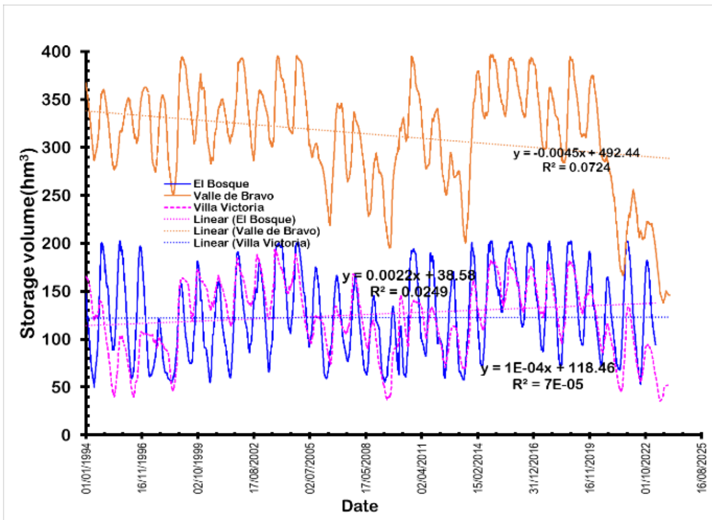

Fig. 9. Behavior of inflow volumes to the main dams of the Cutzamala System, Mexico

From Figure 9, a downward trend line is observed from daily runoff volume into the Presa Valle de Bravo, observing a descent that is becoming increasingly pronounced from 2019 and until the beginning of 2024.

4. Conclusions

A newly proposed drought index application for climatological station situated in an area prone to severe droughts yielded promising results. This index, which integrates both precipitation and temperature data, effectively addresses the challenge of evapotranspiration estimation uncertainty encountered in other methods.
By subjecting precipitation and temperature data to independent reviews, including tests for independence, homogeneity, and trends, along with employing the RAPSi method, no statistically significant changes in the mean of precipitation data during the analyzed periods were detected. However, notable deviations from randomness, non-homogeneity, and a discernible trend were observed in the temperature data. Notably, changes in the mean temperature were noted between 1969 and 1981, but such changes were not evident thereafter.
The analysis conducted for New Drought Index (SNDi) sums revealed statistically significant mean differences compared to the total series from period spanning 1969 to 1981. However, no differences were observed in subsequent periods. Linear regressions facilitated the identification of two significant drought periods: one lasting 8 years and another potentially initiating in 2019 and extending into 2020, with indications of persistence fueled by recent local precipitation scarcity reports contributing to the dam near to study site. Concurrently, daily runoff volumes to the Valle de Bravo dam exhibited a declining trend, notably from 2019 onwards.
The aforementioned research on precipitation and temperature patterns also has significant implications for addressing anthropogenic actions affecting water usage. A comprehensive analysis of stations at nearby reservoirs is essential to understand how human activities are impacting water availability and distribution in the region. This, in turn, can provide critical insights to develop water management policies and practices that mitigate negative human activities impacts and promote sustainable use of this vital resource.

Acknowledgments

We appreciate the official data sources available for free use on the internet.

References

[1] Bonacci, Ognjen, Duje Bonacci, Tanja Roje-Bonacci, and Adrijana Vrsalović. "Proposal of a new method for drought analysis." *Journal of Hydrology and Hydromechanics* 71 (2023): 1-11. https://doi.org/10.2478/johh-2022-0030.

[2] Esparza, Miguel. "Drought and water scarcity in Mexico: Current situation and future perspectives." / "La sequía y la escasez de agua en México: Situación actual y perspectivas futuras." *Secuencia*, no. 89 (2014): 193-219. Accessed January 24, 2024. http://www.scielo.org.mx/scielo.php?script=sci_arttext&pid=S0186-03482014000200008&lng=es&tlng=es.

[3] Scordo, Facundo, Maria Cintia Piccolo, and Gerardo Miguel E. Perillo. "Application of the Standardized Precipitation Evapotranspiration Index (SPEI) to determine extreme climatic events in the Andean and Extra Andean Patagonia Argentina." / "Aplicación del índice estandarizado de precipitación y evapotranspiración (SPEI) para determinar eventos climáticos extremos en la Patagonia Andina y Extra Andina Argentina." *Geociencias* 37, no. 2 (2018): 423-436.

[4] Ortiz-Gómez, Ruperto, Julio C. Cardona-Díaz, Fidel A. Ortiz-Robles, and Pedro Alvarado-Medellin. "Characterization of droughts by comparing three multi-scale indices in Zacatecas, Mexico." / "Caracterización de las sequías mediante la comparación de tres índices multiescalares en Zacatecas, México." *Tecnología y Ciencias del Agua* 9, no. 3 (2018): 47-91.

[5] Campos-Aranda, Daniel Francisco. "Evolution of common indices for detection and monitoring of meteorological droughts." / "Evolución de los índices comunes de detección y seguimiento de sequías meteorológicas." *Tecnología y Ciencias del Agua* 11, no. 1 (2020): 375-409.

[6] Villazón Gómez, Juan Alejandro, Pavel Noris Noris, and Roberto Alejandro García Reyes. "Use of the standardized precipitation index for the evaluation of drought intensity in the province of Holguín." / "Uso del índice de precipitación estandarizado para la evaluación de la intensidad de la sequía en la provincia de Holguín." *Idesia (Arica)* 39, no. 4 (2021): 103-109.

[7] Garbrecht, J., and G.P. Fernandez. "Visualization of trends and fluctuations in climatic records." *Water Resources Bulletin* 30, no. 2 (1994): 297–306.

[8] Escalante-Sandoval, C., and L. Reyes-Chávez. *Statistical techniques in hydrology* / *Técnicas estadísticas en hidrología*. Mexico City: Faculty of Engineering, National Autonomous University of Mexico, 2002.

[9] National Metereological Service / Servicio Meteorológico Nacional (SMN). "Climate normals by state." / "Normales climatológicas por estado." 2023. Accessed January 15, 2024. https://smn.conagua.gob.mx/es/climatologia/informacion-climatologica/normales-climatologicas-por-estado.

High-Performance Techniques and Technologies for Monitoring and Controlling Environmental Factors

PhD student Eng. **Marius-Valentin DUMITRESCU[1],** Senior Lecturer Dr. Eng. **Ionuț VOICU[2],** PhD student Eng. **Aurelia-Florentina VASILICA[1],** Dr. Eng. **Mariana PANAITESCU[2,*],** Dr. Eng. **Fănel-Viorel PANAITESCU[2]**

[1] Doctoral School of Energy Engineering, National University of Science and Technology POLITEHNICA, Bucharest, Romania

[2] Constanta Maritime University, Faculty of Naval Electro-Mechanics, Romania

* panaitescumariana1@gmail.com

Abstract: *The impact of air quality inside residential buildings and constructions on the health of residents and workers has been studied very little in recent years. In the school environment, students are constantly exposed to mixtures of airborne substances from a wide variety of sources both in classrooms and in the school environment. Exposure to such factors of students influences, in the long term, physiological development, dynamics, quality of life, life expectancy, without being aware of the dangers in the air and being able to make decisions on reducing exposure to the risk factor. In the short term, poor air quality in classrooms leads to a decrease in attention and concentration, both for the student and the teaching staff. The research is motivated by the following: a) The lack of data and studies carried out in Romania, and their relationship with the change in student behavior during the school program; b) Laboratories and practice workshops in high schools are totally different from classrooms from the point of view of air quality and internal factors that contribute to pollution due to the equipment and specific, different activities carried out in these spaces. The novelty of this study is brought by the fact that, at the same time as the monitoring and data acquisition of air quality (inside and outside), there will be a monitoring and data acquisition of real-time biometric measurements of the subjects directly exposed to this environment, via a bracelet attached to the subject's arm. This bracelet is designed to perform biometric measurements without disturbing the subjects in the activities in which they are involved. These measurements are made with 9 different sensors for: pulse, blood oxygen (SPO_2), air flow (respiration), body temperature, electrocardiogram (ECG), galvanic skin response (GSR - sweat), blood pressure (sphygmomanometer), patient position/movement, and muscle sensor/electromyography (EMG). The data thus obtained will be centralized on a PC and analyzed later. At the end, an ecological equipment capable of ensuring the ventilation of the space and a constant air quality, by monitoring the values of the compounds in the air, will be created experimentally.*

Keywords: *Monitoring, air, quality, data, biometric, measurement, sensor, health, worker*

1. Introduction

The impact of air quality inside residential buildings and constructions on the health of residents and workers has been studied very little in recent years. In the school environment, students are constantly exposed to mixtures of airborne substances from a wide variety of sources both in classrooms and in the school environment. Exposure to such factors of students influences, in the long term, physiological development, dynamics, quality of life, life expectancy, without being aware of the dangers in the air and being able to make decisions on reducing exposure to the risk factor. In the short term, poor air quality in classrooms leads to a decrease in attention and concentration, both for the student and the teaching staff. Students and teachers often complain, after several hours of study, of dizziness and headaches, without specifying a specific cause, even if the window of the study room has been open for a long time. In certain situations, the 10-minute breaks are not enough to recover the student and ventilate the classroom, especially since the quality of the external air is not always accurately known. Temperature, humidity, CO_2 level, oxygen level, etc. are not being monitored, and in certain situations due to the location of the school, these values can be a negative factor for air quality. The same thing happens in some improperly ventilated workplaces.

The reason for this study appeared after a simple experiment carried out in the premises of a school, namely: in the mechatronics laboratories, a small electronic device was made that measured the concentration of oxygen in the air. At the beginning of the class, the device indicated values of 20% oxygen in the air, with the passage of time this value continuously decreased until it reached the value of 18% oxygen in the air. Initially, a malfunction of the equipment was suspected, but the next day it also indicated 20% oxygen in the air initially, gradually decreasing to 17-18% oxygen in the air during the day. If the percentage of oxygen varies so much over the course of a day, what are the values of the other elements in the air, dust, temperature, humidity, carbon dioxide, etc., and what are the influences on the student's behavior and performance? [1], [2]

The mixed monitoring device has 2 components in its structure: one fixed and one mobile. The fixed one continuously monitors the air parameters in the work areas on board the ship, and the mobile one is mounted on the worker's hand to monitor his/her 8 biometric values during the work schedule. Thus, we can have a better view of the working conditions on board the ship and a real-time monitoring of the health (and stress) of the workers on the ship.

The data thus collected can be corroborated for the realization of safety strategies and the creation of low-risk working conditions. Two identical sets were built and fitted into one ship (along with a wide range of sophisticated monitoring and calibration instruments.) The instruments were exposed to common indoor pollution sources in a semi-controlled experiment and during normal ship operation. The results indicate that none of the sensors requires individual calibration. The readings taken by them are within the margins of error specified by the manufacturer.

Thus, the sensor responses were very consistent and correlated with much more expensive instruments. The combination of data provided by the sensors is still being analyzed. Classic air quality monitoring technology has reached its technological and cost limits.

As spatial monitoring improves, pollution sources, dispersion patterns and health effects can be better addressed while reducing reliance on predictive models; hence, the need to supplement conventional air quality monitoring networks with alternative, punctual, local approaches capable of capturing fine changes in these levels of variability and in environmental microsystems. Passive sampling ensembles, mobile monitoring, and emerging sensor technologies are all approaches that have been used to address spatial coverage.

The sensor market has boomed in recent years, resulting in economical, low-power, miniature, self-contained (and usually easy-to-internet) air quality monitoring units. Although these units were less accurate when first marketed, subsequent generations demonstrate improved reliability and accuracy. Equipment made with these tools includes real-time, location-specific data collection. The results can be used as an educational tool, promoting air quality awareness, while contributing to changing time activity patterns to reduce harmful exposure to air pollutants. This revolution in sensors and related applications can provide sustainable solutions for applications in monitoring, education, community monitoring, supplementing ambient air monitoring networks or even compliance assessment.

Equipment made with these tools, attached to human subjects, allows the acquisition of data and the creation of a new picture of the compliance of working conditions and the anticipation of undesirable events. It is only a matter of time before shipping vessels have integrated systems to monitor air quality metrics as well as personnel biometrics.

2. Material and methods

In this work we propose to present 3 case studies:

1) monitoring and acquisition of air quality data with the help of a biometric bracelet (one fixed, the other mobile) [3, 4];
2) universal device for monitoring electromagnetic radiation [5];
3) universal indoor air quality monitoring device [6, 7].

All 3 case studies target common aspects of operational performance for the set of tools used:

- low unit cost
- small form factor
- increased reliability
- use of new generations of sensors
- compatibility with the power and communication systems of the study locations

• compatibility with study site monitoring programs
• issuing alarms
• minimal electrical interference with existing systems
• low energy consumption
• operation period without intervention for 5 years
• ability to easily switch to the new generation of sensors (still under development).

2.1 Case study 1: Biometric bracelet for measuring

The equipment is designed for the monitoring and acquisition of real-time air quality data (indoor and outdoor) [3]. Real-time biometric measurements of subjects directly exposed to the air in the study location will be carried out by means of a bracelet attached to the arm of the subject, without creating discomfort to the analyzed subjects involved in current activities. For the measurements, 9 different sensors are used that give information about: pulse, blood oxygen, air flow (respiration), body temperature, electrocardiogram, galvanic skin response, blood pressure, patient position / movement and muscle condition (electromyography sensor). Later this obtained data will be stored on a hard disk and analyzed. The information obtained from the analyzed subjects is applicable and useful in many fields of activity (on ships, especially in the engine compartment, where the air undergoes alterations of the quality parameters). Deterioration of air quality can lead to stagnation of the subjects' activity as a result of the deterioration of the state of health.
The biometric bracelet can be used in two versions: one fixed, the other mobile.
In the fixed version, the sensors used for data transmission are (Figure 1) [4]:
• Optical dust sensor: GP2Y1010AU0F Sharp
• Sensor for NO_3, CO, NH_3: MiCS-6814 SGX Sensortech
• Temperature and humidity pressure sensor: BME 680 BOSCH.

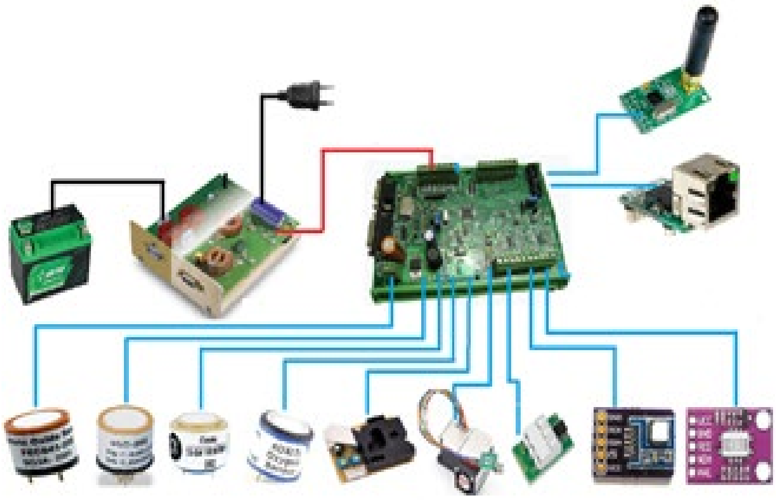

Fig. 1. Fixed unit - Block diagram

In the second version, the sensors used for data transmission are (Figure 2) [4]:
• MAX30100 Maxim Integrated pulse oximeter and integrated heart rate sensor
• Sensor for NO_3, CO, NH_3: MiCS-6814 SGX Sensortech
• Temperature and humidity pressure sensor: BME 680 BOSCH
• Motion sensor (accelerometer): MPU-6000 InvenSense
• Body temperature sensor
• Sweat sensor.

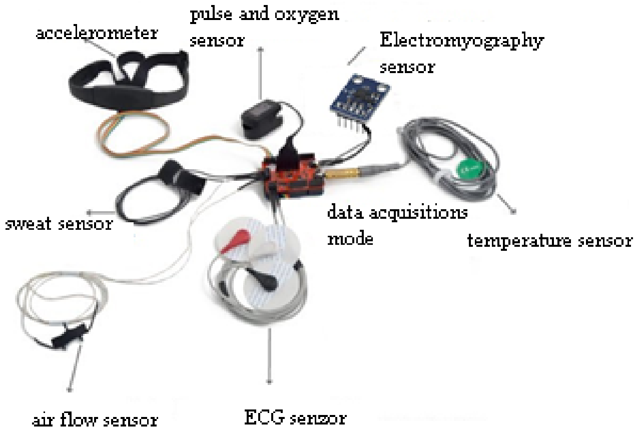

Fig. 2. Mobile unit scheme

Techniques used:

- The Autodesk EAGLE program was used for the electronic design.
- Software development Prototyping ARDUINO I.D.E.
- For creating Office diagrams.
- For PLX-DAQ data acquisition via RS232 converted to USB.

3 tests were performed:

- Test 1, a short series of controlled tests aimed at testing equipment performance;
- Test 2, different variable quantities of the monitored elements were placed in the work area in turn and data was collected from the two equipment pieces;
- Test 3, the equipment was exposed to a series of common sources of internal emissions, specific to the work area.

The results and their graphic interpretation are presented in Table 1, respectively Figure 3, for 1000 values for the NO_2 sensor, the CO sensor and the NH_3 sensor.

Table 1: Results for air quality

Current time	Sensor Values NO_2	Sensor Values CO NH_3	Sensor Values NH_3
16:30:40	0.00	2.00	1.00
16:30:54	12.00	79.00	0.00
17.56.32	15.00	1.00	3.00
17.56.43	8.00	1.00	10.00
17.56.44	0.00	0.00	1.00
17.56.46	0.00	4.00	1.00

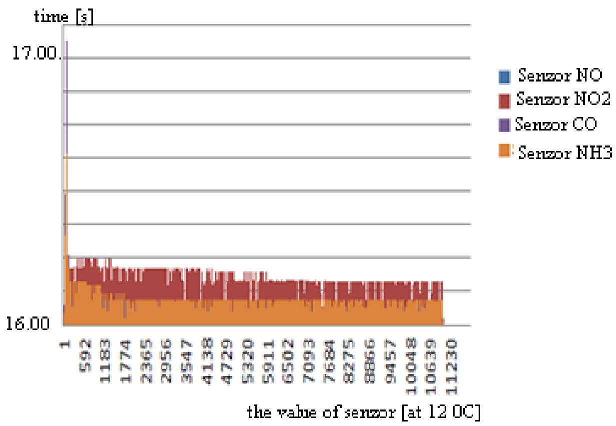

Fig. 3. The values of sensors in current time

Reference values for air quality indicators (according to OG no. 582/2002) measured in air for 1 hour, alert threshold measured for 3 consecutive hours:

- SO_2-350 pg / m^3; Alert threshold-500 µg / m^3
- NO2-200 µg / m^3 NO_2; Alert threshold-400 µg / m^3
- Particulate matter (PM10) - value at 24 h-50 µg / m^3 PM10; Maximum evaluation threshold - at 24 hours - 60% of the daily limit value (30 µg / m^3)
- CO-Maximum average daily value of 8 hours-10 µg / m^3
- Ozone - the maximum daily value of the averages for 8 hours-120 µg / m^3; Alert threshold at 1 hour-240 µg / m^3.

The measured data were compared with the values indicated by the standard certified equipment (gas analyzer) [8, 9].

The experiments showed that the choice of sensors with **I2c** communication was a good, viable, feasible choice. Sensor readings are within prescribed tolerances. No sensor calibration is required. The constructive dimensions of the bracelet were not very small when first realized, but they can be considerably reduced in the case of industrial manufacturing.

2.2 Case study 2: Universal Device for Monitoring Electromagnetic Radiation

It complements the family of universal devices for monitoring Indoor Air Quality Universal Device [7] and Outdoor Air Quality Monitoring Universal Device [10]. "Composed of the basic unit with the role of interpretation, storage, display, online retransmission of information, received from one or more sensory modules, with a narrow spectrum, specialized for the area of interest to be monitored, these sensor modules are connected to the base unit via the I2C communication line via the quick jacks, which allow them to be changed in a few seconds. Thus, one or more sensors can be attached depending on the area or areas to be monitored, thus achieving an exact identification of the area and the source generating electromagnetic radiation" [10]. The design of the electronic scheme of the equipment prototype was developed with EAGLE software. The prototype wiring was made in our own laboratory, following the final, perfected version, to be made in a factory specialized in wiring (Figure 4) [10].

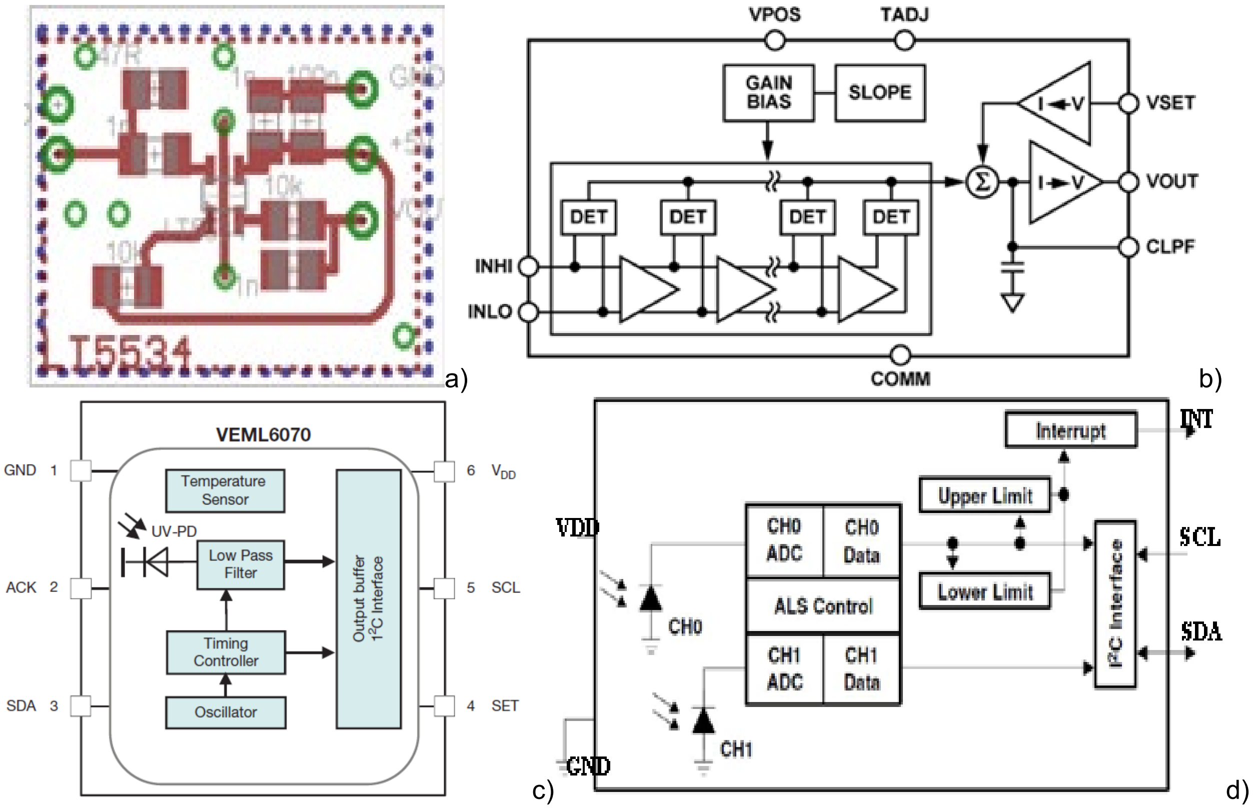

Fig. 4. The block diagram of device

Where:
a) the electrical equipment; b) communication equipment; c) UV radiation sensor; d) converter light intensity into a digital signal output.
The data obtained can be synchronized with local time (LT) or with Coordinated Universal Time (UTC) and can be imported into table programs for further analysis. The data acquisition was made through the "Tera Term" program, which offers the possibility of accessing data both on a serial local communication and accessing the data over the Internet. The following were monitored in the four study locations: the variation of the daily average of electric field strength during a week, daily average of density of power for electromagnetic radiation during a week (Table 2) [10]. The obtained values were compared with the values imposed by the legislative restrictions (Table 3) [10].

Table 2: Results for monitoring electromagnetic radiations

Current time	Frequency Domain			
	Zone 1 ***100 kHz - 7 GHz*** ***S (W/m²)***	***Zone 2*** ***925 MHz – 960 MHz*** ***S (W/m²)m)***	***Zone 3*** ***1805 MHz – 1880 MHz*** ***S (W/m²)***	***Zone 4*** ***2110 MHz – 2170 MHz*** ***S (W/m²)***
Day 1	0.0539	0.0495	0.0010	0.0095
Day 2	0.0495	0.0584	0.0013	0.0099
Day 3	0.0398	0.0500	0.0012	0.0082
Day 4	0.0384	0.0512	0.0013	0.0072
Day 5	0.0046	0.0489	0.0010	0.0070
Day 6	0.0024	0.0006	0.0003	0.0001
Day 7	0.0023	0.0005	0.0003	0.0001

where S (W/m^2) is the power density for electromagnetic radiation during a week.

Table 3: Results for monitoring power density for electromagnetic radiation - Comparative analysis

Frequency Domain	S (W/m^2)	
	Restrictions on exposure to time	***Measured average weekly value***
Zone 1 100 kHz-7 GHz	-	0.0282
Zone 2 925 MHz - 960 MHz	-	0.02612
Zone 3 1805 MHz - 1880 MHz	-	0.00131
Zone 4 2110 MHz - 2170 MHz	-	0.006

As it results from the comparative analysis in the areas where the measurements were performed, the persons are not exposed to the danger of electromagnetic irradiation, the registered values being below the standard values recommended by the European legislation. "*The need to monitor electromagnetic emissions on areas of interest has led to the design and implementation of this versatile, adaptable, easy-to-use and maintenance equipment that can be used in different environments to be monitored*" [10].

2.3 Case study 3: Universal indoor air quality monitoring device

The design and manufacture of this device aims to create a versatile, adaptable, easy-to-use and maintain equipment in different environmental area.
This device works with a wide variety of sensors: gas sensor (volatile organic compounds, carbon dioxide), digital gas sensor for air quality breakout (Total Volatile Organic Compounds, CO2, metal

oxide), sensor which operates over a wide supply range, combined temperature and barometric pressure sensor, a 3-sensor device suitable for gas leak detection air quality monitoring (for unhealthful gases like Carbon monoxide, Nitrogen dioxide, Ethanol, Hydrogen, Ammonia, Methane, Propane, Iso-butane).
The data are acquired using the TeraTerm program and stored in **xls**. format [11]. After this, they can be numerically or graphically visualized (Figure 5).

1	DATA	TEMP	HUM	PRES	ALT	CO2	Tvoc	NH3	CO	NO2
2	[2020-01-3	26.22	32.63	724.95	396.52	400	0	0.68	4.39	0.14
3	[2020-01-3	26.23	32.63	724.95	396.52	400	0	0.68	4.39	0.14
4	[2020-01-3	26.3	32.53	724.95	396.52	400	0	0.68	4.39	0.14
5	[2020-01-3	26.24	32.53	724.95	396.52	400	0	0.68	4.39	0.14
6	[2020-01-3	26.29	32.43	724.93	396.74	400	0	0.68	4.39	0.14
7	[2020-01-3	26.33	32.43	724.93	396.74	400	0	0.68	4.39	0.14
8	[2020-01-3	26.3	32.33	724.95	396.52	400	0	0.68	4.39	0.14
9	[2020-01-3	26.33	32.33	724.95	396.52	400	0	0.68	4.39	0.14
10	[2020-01-3	26.33	32.23	724.96	396.29	401	0	0.68	4.39	0.14
11	[2020-01-3	26.39	32.21	724.96	396.29	401	0	0.68	4.39	0.14
12	[2020-01-3	26.46	32.12	724.96	396.29	401	0	0.68	4.39	0.14

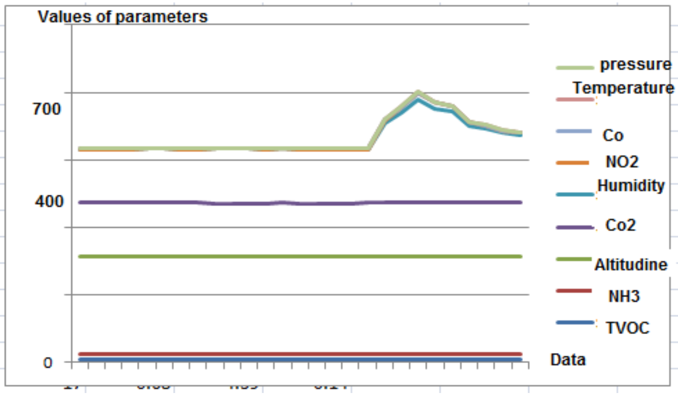

Fig. 5. The values of parameters in current time

The average values of the monitored parameters are calculated and taken into consideration, and these values are centralized. Finally, the values obtained with calibrated devices are checked. Choosing such a device is advantageous because: sensors can be chosen from the profile industry depending on the lowest price and the most reliable design, data can be accessed locally or online, as many sensors as possible can be mounted on the base plate depending on the number of parameters desired to be monitored, various databases can be created for different air quality parameters.

3. Conclusions

Atmospheric emissions, with potential impact on natural ecosystems and a human well-being, may result in potential impact at local and regional levels, in a cross-border context and on a global scale.
Due to the dispersive nature of the offshore environment and the lack of receptors in the vicinity of the offshore infrastructure, locally high concentrations of emissions will last a short time and are unlikely to be detectable, except in the immediate vicinity of activities. The concern regarding atmospheric emissions, implicitly air quality in the offshore area, has increasingly focused on global warming and climate changes that can modify the average values of air quality parameters. An increase in CO_2 in global gas concentrations greenhouse can increase temperatures at the soil surface. An increase in methane will involve global climate changes and contribute to air quality deterioration at a regional level, through the production of ozone at a reduced level, which can be to the detriment of health and may have an impact on vegetation, crops and ecosystems. CO can have direct effects on human health (asphyxiation), and may indirectly contribute to climate change. NOx emissions generate photochemical pollution in the presence of solar radiation. The reduced level of ozone is the main chemical pollutant formed, with by-products including nitric and sulfuric acid and settleable dusts of nitrates.

These devices are useful in the land and offshore area to assess the volume of gases emitted by each source of pollution in the atmosphere. They allow the estimation of the worst case of emissions to be put in the context of the inventories of national and international emissions and to evaluate the global contribution of these gases, because the potential impacts from atmospheric emissions are globally cumulative.

Acknowledgments

Authors gratefully acknowledge to this material support path received under Project BLOW 2023-2028- Black Sea FLoating Offshore Wind, Grant Agreement Nº: 101084323.

References

[1] World Health Organization (WHO). "The World Health Report 2008 - Primary Health Care: Now More Than Ever." *ReliefWeb*, October 1, 2008. Accessed February 12, 2024. https://reliefweb.int/report/world/world-health-report-2008-primary-health-care-now-more-ever.
[2] UNICEF, UN Children's Fund. "Clear the air for children: The impact of air pollution on children." *ReliefWeb*, March 22, 2017. Accessed February 12, 2024. https://reliefweb.int/report/world/clear-air-children-impact-air-pollution-children.
[3] Panaitescu, Mariana, Fanel-Viorel Panaitescu, Marius-Valentin Dumitrescu, and Valeriu-Nicolae Panaitescu. "The Impact of Quality Air in The Engine Room on the Crew." *TransNav - The International Journal on Marine Navigation and Safety of Sea Transportation.*13, no. 2 (June 2019): 409-414.
[4] Dumitrescu. Marius-Valentin. *Studies on techniques and technologies for monitoring and control of environmental factors*. Doctorate Report. Politehnica University of Bucharest, Romania, 2018.
[5] Panaitescu, Mariana, Fanel-Viorel Panaitescu, and Marius-Valentin Dumitrescu. "Electromagnetic radiation monitoring universal device." Paper presented at the Conference "Advanced Topics in Optoelectronics, Microelectronics and Nanotechnologies X", Constanta, Romania, August 20-23, 2020.
[6] Dumitrescu, Marius-Valentin. *Studies on techniques and technologies for monitoring and control of environmental factors*, 2-86. Bucharest, Politehnica Press, 2018.
[7] Panaitescu, Mariana, Marius Valentin Dumitrescu, and Fanel-Viorel Panaitescu. "Indoor air quality monitoring universal device." Paper presented at the 8th ModTech International Conference on Modern Technologies in Industrial Engineering, Iasi, Romania, June 23-27, 2020.
[8] Dumitrescu, M.V., F.V. Panaitescu, M. Panaitescu, and V.N. Panaitescu. "A prediction model for monitoring indoor air quality." Paper presented at the 10th ModTech International Conference on Modern Technologies in Industrial Engineering, Mamaia, Romania, June 22-25, 2022.
[9] Afriso S.R.L. Accessed June 2, 2023. http://www.afriso.ro.
[10] Viegi, G., M. Simoni, A. Scognamiglio, S. Baldacci, F. Pistelli, L. Carrozzi, and I. Annesi-Maesano. "Indoor air pollution and airway disease." *International Journal of Tuberculosis and Lung Disease* 8, no. 12 (December 2004): 1401.
[11] Slim, Xavier. "Free lightweight server manager." *Softonic*. Accessed August 23, 2023. https://tera-term.en.softonic.com/.

Insights on Hydroponic Systems: Understanding Consumer Attitudes in the Cultivation of Hydroponically Grown Fruits and Vegetables

Assoc. Prof. Ph.D. Eng. **Ștefan ŢĂLU**[1,*]

[1] Technical University of Cluj-Napoca, The Directorate of Research, Development and Innovation Management (DMCDI), Constantin Daicoviciu Street, no. 15, Cluj-Napoca, 400020, Cluj county, Romania

[*] stefan_ta@yahoo.com or stefan.talu@auto.utcluj.ro

Abstract: *This study examines consumer attitudes toward fruits and vegetable cultivation in hydroponic systems, shedding light on how consumers perceive and interact with this innovative agricultural approach. Socio-demographic factors, such as gender, age, and education level, emerged as significant influencers on the frequency of consuming fruits and vegetables grown hydroponically. The frequency of consuming hydroponically grown fruits and vegetables is notably shaped by consumers' knowledge regarding the quality and safety of produce from this farming method. Furthermore, this analysis reveals consumer preferences, concerns, and motivations, providing valuable insights for stakeholders in the hydroponic industry to improve consumer satisfaction and promote the adoption of hydroponic fruits and vegetable cultivation practices. This study offers practical implications to assist farmers and food retailers in navigating the hydroponic fruits and vegetable market effectively.*

Keywords: *Hydroponic systems, fruits and vegetable cultivation, consumer attitudes, perceptions, preferences, agricultural innovation*

1. Introduction

As climate change advances, biodiversity diminishes, and the world population expands, there is an increasing urgency to transition away from conventional agricultural practices and adopt innovative, technology-driven methods for food production.
"Geoponics" refers to the science or practice of agriculture, specifically focusing on soil cultivation and management. It encompasses various techniques and methods related to soil preparation, fertilization, irrigation, and crop cultivation. The term "geoponics" is derived from Greek, where "geo" means "earth" and "ponos" means "work" or "labor," emphasizing the labor-intensive nature of agricultural practices involving soil.
Hydroponics originates from the Greek words "hydro," which translates to water, and "ponos," meaning labor. Essentially, hydroponics refers to an innovative agricultural method, that entails the cultivation of plants without traditional soil mediums. Instead, it relies on water, nutrient solutions, and oxygen to nourish and sustain plant growth, presenting a soilless gardening approach that revolutionizes conventional farming practices [1, 2]. Plants can be grown in a variety of media such as sand, gravel, rock wool, coconut fiber, and sponge cubes. The choice of substrate encompasses considerations such as porosity, capillarity, oxygenation, chemical inertness, and biological inertness. The ability of a medium to retain moisture depends on factors such as particle size, shape, and porosity. Every medium presents its own set of advantages and drawbacks, with the selection process influenced by factors like accessibility, expense, quality, and the specific hydroponic system employed. In hydroponics, potential savings of 70% to 90% are expected, depending on the type of crop and the hydroponic system. While the basic principles of hydroponics are not novel and have been employed in traditional commercial greenhouses for the past four decades, the technology underlying hydroponics has evolved considerably since then [2].
Hydroponic systems are categorized into water-culture or medium-culture systems. In water-culture systems, plants are either suspended directly in the nutrient solution - as in NFT (Nutrient Film Technique) or raft systems - or their roots are misted with the solution (as in aeroponics) [3]. These systems can be open, where the solution flows past the roots without recycling, or closed, where surplus solution is recovered and reused. In contrast, medium-culture systems utilize a solid substrate, such as sand, to support plant roots. Examples include ebb-and-flow systems, where the nutrient solution floods the grow bed before draining back to a reservoir, and drip systems,

where the solution is delivered to plants via drip irrigation. Sub-irrigation systems, on the other hand, rely on capillary action to transport the nutrient solution to plant roots. Plants obtain nutrients by dissolving fertilizer salts in water. There are two options for acquiring nutrient solutions: buying a ready-made commercial solution or preparing a custom stock solution. The optimal formulation depends on variables such as plant species, growth stage, harvestable plant part, season, and outdoor environmental conditions.

Hydroponic agriculture primarily relies on highly soluble inorganic salts as fertilizers to create nutrient solutions, although certain inorganic acids are also utilized. Extensive research has been conducted on plant nutrition within hydroponic systems, categorizing the essential nutrients into three main groups: primary, secondary, and trace or micro-nutrients. These nutrient solutions are carefully balanced to provide plants with optimal nutrition for growth and development. Primary nutrients such as nitrogen, phosphorus, and potassium are crucial for basic metabolic functions and structural integrity. Secondary nutrients, including calcium, magnesium, and sulfur, play essential roles in enzyme activation and overall plant health. Additionally, trace or micro-nutrients like iron, zinc, and copper are required in smaller quantities but are equally vital for various physiological processes, such as photosynthesis and hormone regulation. The precise control over nutrient composition and availability in hydroponic systems ensures that plants receive all necessary elements for robust growth and high-quality yield, making it an efficient and effective method of cultivation with potential applications in diverse agricultural contexts [1-5].

Medium-culture hydroponic systems are prone to the accumulation of pathogenic microorganisms with each successive crop. For optimal results, sterilization of the system between each crop is recommended. Steam sterilization is generally effective, while chemical sterilization is employed when steam sterilization is not feasible. Crops grown using this method include microgreens, greens, tomatoes, peppers, strawberries, herbs, and medicinal cannabis. No definitive conclusions have been reached regarding the nutritional superiority of hydroponically cultivated produce compared to soil-grown counterparts [2].

Hydroponics capitalizes on its unique ability to optimize spatial resources. Unlike traditional methods that primarily rely on horizontal cultivation, hydroponics efficiently harnesses both the horizontal and vertical surface area. This innovative approach not only increases the overall yield per unit area but also resonates with the evolving trend toward vertical farming. Also, the benefits of hydroponics include the elimination of the need for weeding, the elimination of the necessity for crop rotation, and the reusability of materials, contributing to sustainability.

The nutrient management advantages of hydroponic systems contribute to higher yields, healthier plants, and more efficient resource utilization, making them an attractive option for modern agriculture in urban or densely populated areas with limited space availability. Hydroponics allows for continuous crop harvesting throughout the year, mitigating the environmental risks associated with pesticide or fertilizer runoff commonly observed in open-field agriculture.

In hydroponic systems, elevated humidity can foster the presence of various pests like midges or earthworms, posing a threat to crop health. However, hydroponic vegetable cultivation mitigates these risks through vigilant monitoring, ensuring plant well-being while eradicating weeds and preventing the spread of diseases and pests from prior crops. This approach eliminates the necessity for pesticides, promoting environmental protection. Even in cases where pesticides are employed in hydroponics, their containment prevents their entry into the natural ecosystem, unlike traditional agricultural practices. Furthermore, hydroponic systems promote the conservation of land and water resources, offering a more sustainable alternative to traditional farming methods. Hydroponics enables the efficient utilization of key resources like water, energy, space, capital, and labor, and entails lower financial investment than traditional farming, as it eliminates the need to purchase extensive farmland or costly machinery. Additionally, the advanced automation and environmental control features inherent to hydroponic setups reduce the reliance on human labor, thereby potentially lowering operational costs and enhancing work efficiency. Ultimately, hydroponics presents a sustainable and effective approach to plant cultivation, facilitating resource conservation and bolstering agricultural productivity [1-4]. Smart greenhouse (Fig. 1) technology takes these advantages to the next level by fine-tuning essential parameters crucial for the health and development of plants, thereby maximizing their growth potential. In terms of transportation, hydroponic farms can be established in urban areas or near consumption centers, minimizing the need for long-distance transportation, and thus reducing carbon emissions associated with food miles. In hydroponic cultivation, productivity increases by 30% due to the higher plant density on a smaller surface area and the fact that plant roots, having access to all the necessary water and nutrients, will no longer focus on procurement but on the growth of the aboveground parts and fruiting [2]. Compared to traditional agriculture, vertical farming technologies face economic challenges regarding energy consumption. Hydroponic crops require large amounts of energy due to the use of supplemental lighting, such as LED lights. Additionally, if non-renewable energy is used to meet these energy requirements, vertical farms could potentially pollute more than traditional farms or greenhouses. However, these issues can be easily addressed by looking at innovations in the field. Transitioning to renewable energy sources, alongside redesigning and optimizing lighting systems, could reduce the carbon footprint generated by this type of agricultural production in the future [1, 2].

Fig. 1. Examples of growing vegetables in productive commercial greenhouses (hydroponics)

Ongoing research is exploring the viability of cultivating additional vegetable varieties hydroponically for longer space missions to sustain astronauts' nutritional needs. On the other hand, hydroponics has certain limitations: a) Initial investment costs for hydroponic infrastructure, including lighting, pumps, and nutrient delivery systems, may be higher compared to traditional soil-based farming; b) Disease management can be challenging in hydroponic systems, as pathogens can spread rapidly through the circulating nutrient solution or between plants nearby, and c) Maintaining optimal nutrient balance and environmental conditions requires a certain level of expertise and ongoing monitoring, necessitating continuous education and training for successful operation.

In hydroponic farming, there are no weeds, diseases, or pests from previous crops due to the controlled environment. With plants grown in nutrient-rich water solutions instead of soil, there's no medium for weed growth, and controlled conditions minimize disease and pest risks, ensuring a cleaner and more efficient growing process. While hydroponics offers numerous benefits for modern agriculture, it's essential to weigh these advantages against the associated challenges and consider them in the context of specific farming goals and constraints. However, vertical farming will not replace traditional agricultural production; instead, it could serve as a complementary option, greatly needed in addressing agricultural challenges.

The worldwide hydroponics system market, in terms of revenue, was valued at approximately $12.1 billion in 2022, with expectations to surge to $25.1 billion by 2027. This growth trajectory signifies a remarkable compound annual growth rate (CAGR) of 15.6% from 2022 to 2027. Concurrently, the global hydroponics crop market, estimated at USD 37.7 billion in 2022, is forecasted to escalate to USD 53.4 billion by 2027, reflecting a steady CAGR of 7.2%. These

projections underscore the burgeoning significance and potential of hydroponics as a sustainable and efficient method of crop cultivation on a global scale [6].
Establishing a hydroponic farm necessitates a substantial initial investment, as the required equipment is both extensive and often pricey to procure and maintain. Various components such as HVAC systems, ventilation, irrigation systems, control systems, rails, and lighting represent the primary cost factors in a hydroponic operation. For instance, a 500-square-foot hydroponic farm may require up to $110,000 for a basic system that lacks full automation. Larger and more automated farms can incur costs ranging from $500,000 to $800,000 per 1,000 square feet, contingent upon the level of autonomous functionality desired. It's important to note that these expenses pertain solely to the setup of the farm; however, ongoing costs are also a consideration, as equipment upgrades are necessary every 3 to 4 years to enhance farm yield and productivity. This underscores the financial commitment required to establish and maintain a thriving hydroponic operation [6].
Globally, the hydroponics sector boasts over 700 active companies. Among them, approximately 300 startups have entered the market, each bringing innovative approaches to hydroponic farming.
Within the hydroponics market, key players such as Scotts Miracle-Gro from the US and Triton Foodworks Pvt. Ltd from India offers specialized products and expertise tailored to regional needs. Companies like Green Sense Farms and Gotham Greens in the US are known for their innovative indoor farming techniques, while Emirates Hydroponic Farm in the UAE demonstrates the potential for hydroponics in arid climates. Hydrodynamics International, American Hydroponics, and Advanced Nutrients provide essential equipment and nutrient solutions for hydroponic growers globally, ensuring optimal plant health and growth. Freight Farms and AeroFarms lead the way in containerized and vertical farming solutions, revolutionizing urban agriculture practices. Other notable players such as Vita Link in the UK, Nature's Miracle in India, and Bright Farms in the US focus on sustainable farming practices and localized production. Companies like Infarm in Germany and Badia Farms in the UAE explore modular and desert farming approaches, respectively, pushing the boundaries of hydroponic agriculture. Automation and control solutions are offered by companies like Argus Control Systems in Canada, while Logiqs BV in the Netherlands provides advanced conveyor systems for hydroponic greenhouse operations. Lighting solutions from LumiGrow, Inc. in the US and Signify Holding in the Netherlands optimize plant growth, while Hydroponic Systems International in Spain and Heliospectra AB in Sweden specialize in cutting-edge hydroponic technology development [6].
In Romania, many companies offer consultancy services in the field and design and produce hydroponic systems tailored to the surface area and conditions of each farmer. A diverse array of hydroponic systems is currently available, varying in cost, design, and method of manufacture [7-11]. These systems are developed utilizing a variety of software tools, each customized to cater to distinct requirements and preferences, particularly within the realm of hydraulic theory [12-15]. Each system, considering applications of modern dynamic systems theory [16, 17] and environmental informatics [18-21], offers its unique benefits, helping farmers to evaluate their options. Factors such as available space, budget constraints, and the farmer's level of expertise play a major role in choosing the most suitable hydroponic system [6].
At this moment in the world, there are millions of hectares of hydroponic crops found in supermarkets originating from hydroponic cultivation systems. However, in countries such as Japan, USA, Australia, Israel, Denmark, the Netherlands, Belgium, France, Germany, Iran, Italy, Russia Federation, and the United Kingdom, hydroponics represents a widespread modern agricultural technology applied extensively across various types of plants: vegetables, fruits, fodder, medicinal plants, flowers, and so forth [6]. In Romania, hydroponic cultures cultivated and developed within hydroponic greenhouses are still relatively uncommon.
There are numerous studies in this field focusing on consumer awareness regarding hydroponic cultivation systems [22-26]. However, there is a lack of information regarding how knowledge influences the frequency of consumption of foods produced through new farming techniques like hydroponic systems. Consumer attitude plays a significant role in this regard, as a positive attitude towards a food product can lead to increased consumption. Attitude, defined as one's thoughts or feelings about something, is often shaped by personal experiences with different aspects of the food, leading to preferences or aversions. When consumers lack prior experience with foods

produced using new farming techniques, their attitude is often formed by comparing them to foods produced through conventional methods. Additionally, consumer practices in food handling are crucial, with some consumers prioritizing the preservation of food quality and safety. This prioritization influences their choice to consume foods that are properly handled. Poor food handling practices can deter some consumers from consuming foods prepared both within and outside the household. This study aims to assess the understanding of Romanian consumer attitudes in vegetable cultivation of hydroponically grown fruits and vegetables, and how these factors influence the frequency of consumption of hydroponically produced foods.

2. Research method

To examine the factors influencing consumer preferences for hydroponically cultivated products, an exploratory marketing research initiative through a pilot survey was undertaken.
Table 1 presents the demographic characteristics of the Romanian participants, providing insights into the composition of the sample population. Firstly, in terms of gender distribution, the table indicates that out of the total 96 participants, 42 (43.75%) were men, while 54 (56.25%) were women. This balanced representation allows for a comprehensive examination of consumer preferences across gender lines. Secondly, the age distribution of the participants is delineated into five distinct groups. The largest proportion of participants falls within the age bracket of 41-56 years, with 33 individuals, representing 34.375% of the total sample. This is followed closely by the 57-65 years age group, comprising 30 individuals (31.25%). The age groups of 26-40 years and 18-25 years each account for 18.75% and 9.375% of the sample, respectively. Notably, the smallest proportion of participants falls within the age range of 66-82 years, constituting 6.25% of the total sample. The age of participants varied between 18 and 82 years, with an average of 50.57 years and a standard deviation of 16.83. This diverse age distribution enables a comprehensive analysis of consumer preferences across different life stages. Lastly, the majority of participants, 57 (59.375%), reported having completed a university education, while 39 (40.625%) indicated having completed high school. This distribution reflects a well-educated sample population, which may have implications for their purchasing behavior and preferences.
The research was carried out from January 10, 2024, to February 29, 2024. Additionally, gathering information about societal perspectives, beliefs, thoughts, and behaviors involves statistical measurement and recognition, rendering it a form of measurement. Furthermore, as it investigates and analyzes the relationships between independent and dependent variables, it can be classified as correlational. All statistical analyses were conducted using SPSS Software version 22.

Table 1: The demographic details of participants (n = 96)

Participants		Number [-]	Percent [%]
Gender	Men	42	43.75
	Women	54	56.25
Age group	18 - 25 years	9	9.375
	26 – 40 years	18	18.75
	41 – 56 years	33	34.375
	57 – 65 years	30	31.25
	66 - 82 years	6	6.25
Education	High school	39	40.625
	University	57	59.375

This involved conducting a pilot survey comprising 8 questions. The following questions were addressed to the participants:
Q1) How often do you consume organic fruits and vegetables in your diet?
Q2) Are you familiar with hydroponic systems for fruit and vegetable cultivation?
Q3) Have you ever purchased fruits and vegetables grown using hydroponic systems?

Q4) What factors influence your decision to purchase hydroponically cultivated fruits and vegetables?
Q5) Do you believe hydroponically grown fruits and vegetables have a longer shelf life compared to conventionally grown ones?
Q6) What sources do you rely on to gather information about hydroponic systems and their products?
Q7) How likely are you to recommend hydroponically grown fruits and vegetables to others?
Q8) Are you willing to pay a premium for hydroponically grown fruits and vegetables?

3. Results

Response options for Q1 were given in Table 2, with options: a) Several times a day, b) Once a day, c) and Several times a week.

Table 2: The answers of participants to Q1

Participants		No. [-]	Several times a day	Once a day	Several times a week
Gender	Men	42	1	7	34
	Women	54	1	9	44
Age group [years]	18 - 25	9	1	2	6
	26 – 40	18	3	5	10
	41 – 56	33	3	10	20
	57 – 65	30	1	8	21
	66 - 82	6	0	2	4
Education	High school	39	5	5	29
	University	57	3	14	40

Gender-wise, both men and women exhibit varied frequencies about organic fruit and vegetable consumption. Women tend to consume organic fruits and vegetables several times a day slightly more frequently than men, suggesting potential cultural or societal influences on dietary habits. Regarding age groups, there are notable differences in organic fruit and vegetable consumption patterns. Younger individuals (18-25 years) report lower frequencies of organic fruit and vegetable consumption, with a significant proportion indicating infrequent or negligible intake. Older age groups, particularly those aged 41-56 years and 57-65 years, report more frequent organic fruit and vegetable consumption, indicating potentially evolving dietary preferences with age. In terms of education level, participants with a university education show a higher frequency of organic fruit and vegetable consumption compared to those with a high school education. This observation hints at a possible association between higher education levels and healthier dietary habits, possibly due to increased access to nutritional information and resources among individuals with advanced education.

Response options for Q2 were given in Table 3, with options: a) Yes, b) Somewhat, or c) No.

Table 3: The answers of participants to Q2

Participants		Number [-]	Yes	Somewhat	No
Gender	Men	42	6	27	9
	Women	54	7	36	11
Age group [years]	18 - 25	9	3	4	2
	26 – 40	18	7	8	3
	41 – 56	33	8	20	5
	57 – 65	30	6	21	3

Participants		Number [-]	Yes	Somewhat	No
	66 - 82	6	1	4	1
Education	High school	39	5	26	8
	University	57	8	42	7

Both men and women exhibited varying levels of familiarity. The majority of participants from both genders responded affirmatively ("Yes"), with women slightly outnumbering men in this regard. Additionally, a notable portion of both genders indicated "Somewhat," suggesting some awareness but limited knowledge. Across different age groups, participants demonstrated diverse levels of familiarity. Younger individuals (18-25 years) tended to respond with "Somewhat" or "No," indicating lower familiarity compared to older age groups. Conversely, older participants, particularly those aged 41-56 years and 57-65 years, displayed a higher proportion of affirmative responses. Regarding education, participants with a university education showed a higher level of familiarity with hydroponic systems compared to those with a high school education. A greater proportion of university-educated participants responded affirmatively, highlighting a positive correlation between higher education levels and knowledge about hydroponic cultivation methods.

Response options for Q3 were given in Table 4, with options: a) Yes, b) I am not sure or c) No.

Table 4: The answers of participants to Q3

Participants		Number [-]	Yes	I am not sure	No
Gender	Men	42	5	29	8
	Women	54	8	39	7
Age group [years]	18 - 25	9	2	6	1
	26 – 40	18	3	13	2
	41 – 56	33	4	23	6
	57 – 65	30	2	26	2
	66 - 82	6	1	3	2
Education	High school	39	8	29	2
	University	57	10	44	3

Both men and women responded positively ("Yes") to having purchased fruits and vegetables grown using hydroponic systems. However, women show a slightly higher proportion of affirmative responses compared to men. Across age groups, there is a consistent trend of affirmative responses outweighing uncertainty or negative responses. Younger individuals (18-25 years) and those with a high school education exhibit a higher proportion of uncertainty ("I am not sure") regarding their purchases, indicating a possible lack of familiarity or understanding of hydroponic fruits and vegetables among these demographics. In contrast, older age groups, particularly those aged 41-56 years and 57-65 years, demonstrate higher levels of certainty ("Yes") regarding their purchases. Participants with a university education display a higher proportion of affirmative responses compared to those with a high school education, indicating potentially greater preference for hydroponic fruits and vegetables among individuals with higher educational attainment.

Response options for Q4 were given in Table 5, with options: a) Freshness and quality; b) Environmental sustainability; c) Health benefits; d) Price; e) Taste; f) Aesthetic appeal; g) Seasonality; h) Food education; i) Brand reputation; j) Certifications; k) Availability, and l) Gardening space limitations.

Table 5: The answers of participants to Q4

Participants		No. [-]	Fresh. and quality	Environ. Sustain.	Health benefits	Price	Taste	Aesthetic appeal
Gender	Men	42	2	3	8	6	4	3
	Women	54	3	6	10	9	3	3
Age group [years]	18 - 25	9	1	1	1	1	1	1
	26 – 40	18	2	1	2	3	2	1
	41 – 56	33	4	2	5	5	3	2
	57 – 65	30	3	3	5	5	2	1
	66 - 82	6	1	1	1	1	1	0
Education	High school	39	3	3	7	7	4	2
	University	57	6	4	11	8	4	3

Table 5: The answers of participants to Q4 (continued)

Participants		Season-ality	Food education	Brand reputation	Certifica-cations	Availa-bility	Gardening space limitations
Gender	Men	3	2	3	3	2	3
	Women	4	3	3	3	3	4
Age group [years]	18 - 25	1	0	1	0	0	1
	26 – 40	2	1	1	1	1	1
	41 – 56	2	2	2	2	2	2
	57 – 65	2	2	3	1	2	1
	66 - 82	0	0	0	0	1	0
Education	High school	3	1	2	3	2	2
	University	4	2	6	3	3	3

Men and women provided varying responses, with women slightly outnumbering men in participation. Both genders prioritized freshness and quality, health benefits, and price as key factors. Participants across different age groups and education levels showed similar trends in their responses. The 41-56 age group and university-educated participants had the highest participation rates. Freshness and quality were consistently cited as important factors by both genders and across age groups and education levels. Environmental sustainability, health benefits, and price were also significant considerations. Taste, aesthetic appeal, and availability were mentioned to a lesser extent but still contributed to participants' decision-making.

Response options for Q5 were given in Table 6, with options: a) Yes, b) I am not sure or c) No.

Table 6: The answers of participants to Q5

Participants		Number [-]	Yes	I am not sure	No
Gender	Men	42	4	35	3
	Women	54	5	39	10
Age group [years]	18 - 25	9	4	4	1
	26 – 40	18	5	11	2
	41 – 56	33	6	23	4
	57 – 65	30	4	24	2
	66 - 82	6	2	2	2

Participants		Number [-]	Yes	I am not sure	No
Education	High school	39	5	25	9
	University	57	6	44	7

Across various demographics, the majority of respondents expressed confidence in the extended shelf life of hydroponically grown fruits and vegetables. Specifically, 57% of men and 59% of women held this belief. In terms of age groups, 55% of participants aged 41-56 and 53% aged 57-65 believed in the superior shelf life of hydroponically cultivated fruits and vegetables, with slightly lower percentages among younger age groups. Regarding education level, 61% of university-educated individuals expressed confidence in the extended shelf life of hydroponically grown fruits and vegetables, compared to 51% of high school graduates.

Response options for Q6 were given in Table 7, with options: a) Internet research; b) Social media platforms; c) Journals; d) TV; e) Workshops; f) Hydroponic retailers or suppliers.

Table 7: The answers of participants to Q6

Participants		No. [-]	Internet research	Social media platforms	Journals	TV	Work-shops	Hydroponic retailers or suppliers
Gender	Men	42	21	12	2	3	2	2
	Women	54	27	15	1	3	2	6
Age group [years]	18 - 25	9	4	2	1	1	0	1
	26 – 40	18	6	3	1	2	2	4
	41 – 56	33	13	10	1	3	1	5
	57 – 65	30	11	8	1	1	1	8
	66 - 82	6	1	0	0	2	0	3
Education	High school	39	16	14	1	5	1	2
	University	57	23	17	1	6	1	9

Internet research emerged as the most common source across all categories, with a considerable portion of both men and women, spanning various age groups and education levels, relying on it. Social media platforms were also a popular choice, particularly among younger individuals aged 18-40 years and those with higher education levels. Journals were cited as a source by a notable percentage of participants, indicating an interest in more scholarly or in-depth information. TV and workshops were less frequently mentioned, suggesting that traditional media and face-to-face events play a smaller role in acquiring knowledge about hydroponic systems. Interestingly, hydroponic retailers or suppliers were selected by a significant proportion of respondents across all categories, underscoring the importance of direct engagement with industry professionals and suppliers in acquiring relevant information in this domain.

Response options for Q7 were given in Table 8, with options: a) Very likely; b) Likely; c) Neutral; d) Unlikely; e) Very unlikely.

Table 8: The answers of participants to Q7

Participants		No. [-]	Very likely	Likely	Neutral	Unlikely	Very unlikely
Gender	Men	42	4	6	25	4	3
	Women	54	7	7	36	3	1
Age group	18 - 25	9	1	1	4	2	1
	26 – 40	18	3	2	10	3	0

Participants		No. [-]	Very likely	Likely	Neutral	Unlikely	Very unlikely
[years]	41 – 56	33	4	3	22	3	1
	57 – 65	30	5	4	17	3	1
	66 - 82	6	1	1	2	1	1
Education	High school	39	4	4	25	5	1
	University	57	5	19	25	7	1

Both men and women provided responses across the spectrum, ranging from "Very likely" to "Very unlikely." However, men tended to have a slightly higher proportion of responses in the "Neutral" and "Unlikely" categories compared to women. Among different age groups, variations were observed. Younger individuals (18-25 years) were more inclined to select "Neutral" or "Unlikely" compared to older age groups. In contrast, those aged 41-56 years had a higher proportion of responses in the "Very likely" and "Likely" categories, indicating a stronger inclination towards recommending hydroponically grown fruits and vegetables. University-educated participants were more likely to recommend hydroponically grown fruits and vegetables, with a higher proportion selecting "Very likely" and "Likely" compared to those with a high school education.

Response options for Q8 were given in Table 9, with options: a) Strongly agree; b) Agree; c) Neutral; d) Disagree; e) Strongly disagree, or f) Unsure.

Table 9: The answers of participants to Q8

Participants		No. [-]	Strongly agree	Agree	Neutral	Disagree	Strongly disagree	Unsure
Gender	Men	42	2	2	12	20	3	3
	Women	54	2	2	14	32	2	2
Age group [years]	18 - 25	9	2	1	2	2	1	1
	26 – 40	18	1	1	3	11	1	1
	41 – 56	33	2	3	5	21	1	1
	57 – 65	30	1	2	5	20	1	1
	66 - 82	6	0	0	2	2	1	1
Education	High school	39	2	2	6	24	4	1
	University	57	2	3	10	36	5	1

Women generally displayed a higher proportion of agreement compared to men, suggesting potentially greater interest or perceived value in hydroponically grown fruits and vegetables among female participants. Across different age groups, opinions varied. Younger individuals (18-25 years) tended to express more uncertainty, possibly due to a lack of familiarity with the benefits associated with hydroponic fruits and vegetables. Conversely, older age groups, particularly those aged 41-56 years, were more likely to agree or strongly agree, indicating a greater appreciation for the environmental benefits of hydroponically grown produce with increasing age and experience. University-educated participants showed higher agreement levels compared to those with a high school education, who exhibited more varied responses.

4. Discussion

Various factors shape consumers' dietary preferences in a region, with both positive and negative influences. Age group segmentation is crucial in our interconnected society, where internet access facilitates diverse food experiences. Younger individuals often prefer processed foods, while older ones prioritize health-conscious choices. This contrast in food preferences likely arises from the increased incidence of age-related health conditions among older demographics. Extensive research highlights the connection between aging and the onset or worsening of conditions such as obesity, diabetes, cardiovascular diseases, osteoporosis, iron deficiency anemia, cancer, liver diseases, stroke, inflammatory bowel diseases, real diseases, arthritis, Alzheimer's disease, and other cognitive disorders. Older consumers adopt healthier eating habits as a means to prolong their longevity and mitigate healthcare expenses. Additionally, higher education levels empower individuals to make informed dietary decisions, leveraging the knowledge gained through academic pursuits. Educated consumers carefully consider the pros and cons of different food options, which highlights the importance of community-centered nutrition education programs tailored to individuals with lower educational attainment.

5. Conclusions

The pilot survey on Romanian consumer preferences for hydroponically grown products yielded valuable insights. Freshness and quality were key factors driving purchasing decisions across demographics, followed by considerations like environmental sustainability, health benefits, and price. Most participants trusted the extended shelf life of hydroponically grown produce and relied on internet research for information. These findings stress the importance of prioritizing product quality and sustainability in marketing efforts. Future research could focus on specific consumer segments for deeper insights and conduct longitudinal studies to track evolving preferences and assess marketing interventions' effectiveness in promoting hydroponic products.

Conflicts of Interest: The author declares no conflict of interest.
ORCID: Ştefan Ţălu, https://orcid.org/0000-0003-1311-7657.

References

[1] Velazquez-Gonzalez, Roberto S., Adrian L. Garcia-Garcia, Elsa Ventura-Zapata, Jose Dolores Oscar Barceinas-Sanchez, and Julio C. Sosa-Savedra. "A review on hydroponics and the technologies associated for medium- and small-scale operations." *Agriculture* 12, no. 5 (2022): 646.
[2] Kannan, M., G. Elavarasan, A. Balamurugan, B. Dhanusiya, and D. Freedon. "Hydroponic farming – A state of art for the future agriculture." *Materials Today: Proceedings* 68, no. 6 (2022): 2163-2166.
[3] Rozilan, M.R., A.S. Mohd Rodzi, A. Faiz Zubair, A.R. Hemdi, R. Deraman, N.D. Md. Sin. "Design and Fabrication of Nutrient Film Technique (NFT) Hydroponic System". In: Hassan, M.H.A., Zohari, M.H., Kadirgama, K., Mohamed, N.A.N., Aziz, A. (eds.) *Technological Advancement in Instrumentation & Human Engineering*. *ICMER 2021*. *Lecture Notes in Electrical Engineering*, vol. 882 (2023). Springer, Singapore. https://doi.org/10.1007/978-981-19-1577-2_11.
[4] Sambo, P., C. Nicoletto, A. Giro, Y. Pii, F. Valentinuzzi, T. Mimmo, P. Lugli, G. Orzes, F. Mazzetto, S. Astolfi, R. Terzano, and S. Cesco. "Hydroponic solutions for soilless production systems: issues and opportunities in a smart agriculture perspective." *Frontiers in Plant Science* 10 (July 2019): 923.
[5] Sales, Helder B.E., Adriano De S. Carolino, Ronald Z. De A. Nunes, Célio M. A. Macalia, Camila M. Ruzo, Camila Da C. Pinto, Jaqueline De A. Bezerra, Pedro H. Campelo, Ștefan Țălu, Luiz K. C. De Souza, and Edgar A. Sanches. "Advances in agricultural technology: a review of slow-release nanofertilizers and innovative carriers." *Communications in Soil Science and Plant Analysis* (March 2024).
[6] Marketsandmarkets Research Private Ltd. "Hydroponics market by type (aggregate systems and liquid systems), equipment, input (nutrients and grow media), crop type (vegetables, fruits, flowers), farming method (indoor and outdoor), crop area, and region - global forecast to 2027". *MarketsandMarkets*. Accessed March 10, 2024. https://www.marketsandmarkets.com/Market-Reports/hydroponic-market-94055021.html?gad_source=1&gclid=EAIaIQobChMIqu-2w7CBhQMVd5KDBx3JQgxCEAAYAiAAEgLq7fD_BwE.
[7] Paturu, P., and S. Varadarajan. "Design of Smart Hydroponics Product Service Systems - A Qualitative System Dynamics Perspective". In: Chakrabarti, A., Singh, V. (eds.) *Design in the Era of Industry 4.0*, vol. 2. *ICORD 2023*. *Smart Innovation, Systems and Technologies*, vol 342 (2023). Springer, Singapore. https://doi.org/10.1007/978-981-99-0264-4_37.
[8] Evelyn, G.L., J.E. Montiel, C.A. Chadwick, and F.R. Menchaca García. "Architecture proposal for low-cost hydroponic IoT based systems". In: Mata-Rivera, M., Zagal-Flores, R., Barría-Huidobro, C. (eds.) *Telematics and Computing*. *WITCOM 2019*. *Communications in Computer and Information Science*, vol 1053 (2019). Springer, Cham. https://doi.org/10.1007/978-3-030-33229-7_26.

[9] Mujtahidin, Muhammad Hanafi, Ahmad Feirdaous Mohd Shah, Ahmadul Sayyidi Amin Jais, Khalil Azha Mohd Annuar, and Mohd Razali Mohamad Sapiee, "Design and development of control and monitoring hydroponic system." *International Journal of Reconfigurable and Embedded Systems (IJRES)* 13, no. 1 (March 2024): 41-51.
[10] Niţulescu, Theodor, and Ştefan Ţălu. *Applications of descriptive geometry and computer aided design in engineering graphics / Aplicaţii ale geometriei descriptive şi graficii asistate de calculator în desenul industrial.* Cluj-Napoca, Risoprint Publishing House, 2001.
[11] Ţălu, Ştefan. *Micro and nanoscale characterization of three dimensional surfaces. Basics and applications*. Cluj-Napoca, Napoca Star Publishing House, 2015.
[12] Darshan, Katgeri, and Basavaraj Hubballi. "A review & progress on digital hydraulic pumps and valves." *Magazine of Hydraulics, Pneumatics, Tribology, Ecology, Sensorics, Mechatronics (HIDRAULICA)*, no. 1 (March 2019): 116-123.
[13] Marinescu, Alexandru-Daniel, Teodor Costinel Popescu, Alina-Iolanda Popescu, and Carmen-Anca Safta. "Approaches of the best maintenance strategies applied to hydraulic drive systems." *Magazine of Hydraulics, Pneumatics, Tribology, Ecology, Sensorics, Mechatronics (HIDRAULICA)*, no. 4 (December 2016): 63-68.
[14] Cristescu, Corneliu, Catalin Dumitrescu, Genoveva Vrânceanu, and Liliana Dumitrescu. "Considerations on energy losses in hydraulic drive systems." *Magazine of Hydraulics, Pneumatics, Tribology, Ecology, Sensorics, Mechatronics (HIDRAULICA)*, no. 1 (March 2016): 36-46.
[15] Țălu, Mihai, and Ştefan Țălu, *The calculation of pressure declines in hydraulic pipes. Stabilized and unstabilized regimes of flow. Theory, applications and computational programmes*. Craiova, Universitaria Publishing House, 2006.
[16] Cioruța, Bogdan, and Coman Mirela. "From classical systems thinking to modern dynamic systems theory: beyond the definitions and conceptual delimitations." *Magazine of Hydraulics, Pneumatics, Tribology, Ecology, Sensorics, Mechatronics (HIDRAULICA)*, no. 3 (September 2019): 76-85.
[17] Cioruța Bogdan. "From classical systems thinking to modern dynamic systems theory: beyond the system structure and properties." *Magazine of Hydraulics, Pneumatics, Tribology, Ecology, Sensorics, Mechatronics (HIDRAULICA)*, no. 1 (March 2020): 114-121.
[18] Cioruța, Bogdan, and Mirela Coman. "From human-environment interaction to environmental informatics (iv): filling the environmental science gaps with big open-access data." *Magazine of Hydraulics, Pneumatics, Tribology, Ecology, Sensorics, Mechatronics (HIDRAULICA)*, no. 2 (June 2019): 52-61.
[19] Coman, Mirela, and Bogdan Cioruța. "From human-environment interaction to environmental informatics (iii): the social-ecological systems dynamics in knowledge-based society." *Magazine of Hydraulics, Pneumatics, Tribology, Ecology, Sensorics, Mechatronics (HIDRAULICA)*, no. 1 (March 2019): 124-134.
[20] Cioruța, Bogdan, Mirela Coman, and Alexandru Lauran. "From human-environment interaction to environmental informatics (ii): the sustainability evolution as requirement of knowledge-based society." *Magazine of Hydraulics, Pneumatics, Tribology, Ecology, Sensorics, Mechatronics (HIDRAULICA)*, no. 2 (June 2018): 33-42.
[21] Cioruța, Bogdan, Mirela Coman, Alin-Andrei Cioruța and Alexandru Lauran. "From human-environment interaction to environmental informatics (i): theoretical and practical implications of knowledge-based computing." *Magazine of Hydraulics, Pneumatics, Tribology, Ecology, Sensorics, Mechatronics (HIDRAULICA)*, no. 1 (March 2018): 71-82.
[22] Spendrup, Sara, Karl-Johan Bergstrand, Rebecca Thörning, and Malin Hultberg. "Consumer attitudes towards hydroponic cultivation of vegetables – Specifically exploring the impact of the fertilisation strategy (using mineral origin or food waste as fertilisers)." *Food Quality and Preference* 113 (2024): 105085
[23] Balqiah, Tengku Ezni, Andreas Pardyanto, Rifelly Dewi Astuti, and Syahrial Mukhtar. "Understanding how to increase hydroponic attractiveness: economic and ecological benefit." *E3S Web of Conferences* 211 (2020): 01015. Paper presented at The 1st JESSD Symposium: International Symposium of Earth, Energy, Environmental Science and Sustainable Development 2020, Jakarta, Indonesia September 28-30, 2020.
[24] Nekesa, R., L. Njue, and G. Abong. "Influence of knowledge, attitude and practices of consumers on the consumption of hydroponically grown fruits and vegetables in Kiambu County, Kenya." *East African Journal of Science, Technology and Innovation* 4 (August 2023): 1-19.
[25] Yano, Yuki, Tetsuya Nakamura, Satoshi Ishitsuka, and Atsushi Maruyama. "Consumer attitudes toward vertically farmed produce in Russia: A study using ordered logit and co-occurrence network analysis." *Foods* 10, no. 3 (2021): 638.
[26] Gao, J., Abdullah Al Mamun, Qing Yang, Muhammad Khalilur Rahman, and Muhammad Mehedi Masud. "Environmental and health values, beliefs, norms and compatibility on intention to adopt hydroponic farming among unemployed youth." *Scientific Reports* 14 (2024) 1592.

Hydraulic Power Generation Unit Powered by Photovoltaic Energy

PhD. Eng. **Radu RĂDOI**[1,*], PhD. stud. Eng. **Bogdan TUDOR**[1], PhD. stud. Eng. **Ștefan ȘEFU**[1], PhD. stud. Eng. **Robert BLEJAN**[1]

[1] National Institute of Research & Development for Optoelectronics/INOE 2000, Subsidiary Hydraulics and Pneumatics Research Institute/IHP / Romania

* radoi.ihp@fluidas.ro

Abstract: *The conversion of solar energy into electricity can provide a solution to the following problems: access to electricity for users or applications in areas without access to the electricity grid and hybrid system operation of some equipment in order to reduce pollution due to conventional energy sources (internal combustion engines, mainly). In both cases, if hydraulic power is required at the end user (irrigation systems, waste compaction, lifting installations, various drive systems), this is obtained with the help of an electro-hydraulic pumping unit, powered by a battery, charged with the help of a group of PV panels.*

Keywords: *Photovoltaic supply, hydraulic power unit, hydraulic drive system*

1. Introduction

A specially designed photovoltaic system can be used to provide a hydraulic power unit in hard-to-reach areas without an electrical network. It can be built in the form of a unit that can be deployed quickly in the field alongside a group of photovoltaic panels. An actuation system using a solar-powered pumping group is suitable, for intermittent use day or night that operates on the basis of the energy provided by a photovoltaic system in combination with the energy stored in an accumulator. Thus, it is not necessary to dimension the photovoltaic system to support all the power required by the hydraulic pumping group. The system described in this article can greatly facilitate the implementation of a remotely controlled actuation system for actuating a valve, some mechanism, irrigation canal gate, etc. [1,2,3]. For applications in hard conditions, which require relatively high forces (torques), a hydraulic actuation can be used, and the system can also be equipped with an automation system and remote control via GSM or LoRa modem [4]. PrimeHyd company has developed a remote control system that provides wireless data transmission in real time and allows the operation of a valve from a distance of hundreds of km for customers in the mining field all over the world [5]. Another system is a solar-powered Hydraulic Power Unit (HPU) from Shafer Valve, an Emerson Company that provides hydraulic energy for valve automation in distant regions or places lacking reliable energy sources. Solar modules are tailored to meet the required watt-hour capacity, factoring in the peak sunlight hours at the specific location. Additionally, the solar modules can be installed remotely to accommodate hazardous area applications [6].

2. The photovoltaic system

The photovoltaic system for powering the compact hydraulic power unit is made as an off-grid system, totally independent of an electricity network. The system stores electricity in a battery, the stored energy can be used at night or in combination with solar panels during the day. The diagram of the solar power supply system of the compact hydraulic group can be found in fig. 1. This contains the photovoltaic energy harvesting part with 2 photovoltaic panels, the battery for energy storage and the inverter for converting the DC voltage from the battery into single-phase AC voltage of 230 V for powering the electric motor. The 2 photovoltaic panels are connected by means of a DC fuse disconnector to MPPT charger, and the output from the charger is connected to a 12 V / 220 Ah lead battery. The inverter is supplied with DC voltage from the battery and the alternating current output is connected to a soft starter through a thermal-magnetic circuit breaker and a fuse switch disconnector. The electric motor is powered by a soft starter to have a smooth start and not to overload the inverter at start-up. The overload at start-up is explained by the fact that upon initial energization of the electric motor, the rotor remains stationary, causing a current flow equal to the current in blocked state (inrush current). This current gradually decreases as the motor gains speed and generates a back electromotive force (EMF) in opposition to the power source. AC induction motors operate as a transformer with the secondary winding short-circuited until the rotor initiates motion, whereas brushed motors primarily exhibit winding resistance. Minimizing the load on the motor until it reaches a certain speed can shorten the duration of the initial transient phase. This is done by starting the hydraulic group with the flow switched to the tank (minimum hydraulic pressure) until the electric motor reaches the nominal speed.

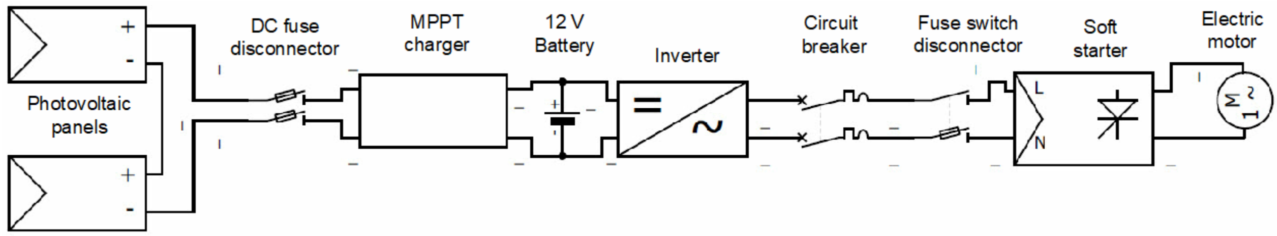

Fig. 1. The solar power supply system for hydraulic power unit

The electrical equipment of the photovoltaic system and the compact hydraulic group are placed in an enclosure protected against the penetration of water and dust. The electrical equipment consists of: electrical cabinet with electrical accessories, MPPT solar charger, 12 V battery and a shunt for monitoring the charging current and the current consumed. The electrical cabinet comprises: disconnectors, circuit breaker, soft starter, battery status monitor, a controller for adjusting the MPPT charger, signal lights and control buttons.
The solar charge controller has functions such as MPPT - fast Maximum Power Point Tracking, short circuit protection, reverse polarity, and high temperature.
The MPPT controller used is from the Victron Energy company and allows to find out information about the status of the solar charge controller and to set certain parameters. On the screen of this monitoring system, users can see information about the state of charge of the battery, the battery voltage, the load current and the amount of energy available from the photovoltaic panels. The device ensures uninterrupted and professional monitoring of information related to the photovoltaic system.
MPPT Controller Features and Functions can be seen in the Table 1.

Table 1: MPPT Controler Features

Feature / Function	Value
Displays the status of parameters in real time	panel power, battery voltage, charging current, output current.
The archive of information for the values recorded	last 30 days
Settings for the MPPT controller	battery voltage and type, max. current, bulk time, absorption voltage/time, float voltage, temp. compensation, et al.
Input voltage range	6.5 - 95VDC (battery) 5VDC (via VE.Direct cable)
Own consumption	< 4mA
Operating temperature range	-20 degrees C - +50 degrees C

Battery status monitor has the main function of calculating power consumption and battery charge status. The consumption in ampere-hours is calculated by integrating the electric current entering or leaving the battery. The equipment used is type BMV-702 from Victron Energy.
Monitored parameters of the battery:
- Battery voltage (V)
- Load level (%)

- Battery charge/discharge current (A)
- Ampere-hours consumed (Ah)
- The time until the discharge level is reached
- Visual and audible alarm: over and under voltage and/or low battery
- Programmable alarm relay.

The support on which the 2 solar panels are installed is placed next to the enclosure with the equipment (fig. 2).

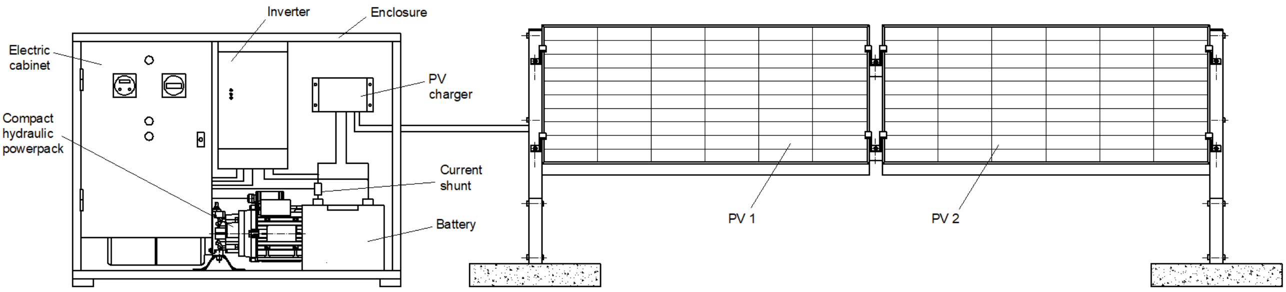

Fig. 2. Photovoltaic panels and enclosure with equipment

The technical characteristics of the photovoltaic system are:
- Number of photovoltaic panels: 2 pcs
- Installed power (peak power): 600 W
- Voltage at maximum power: 65 V
- Current drawn at maximum power: 9.38 A
- Overall dimensions of PV panels group: 2500 x 2000 x 800 mm.

Figure 3 shows the recordings during a battery charging with the group of 2 PV panels on a day in March.

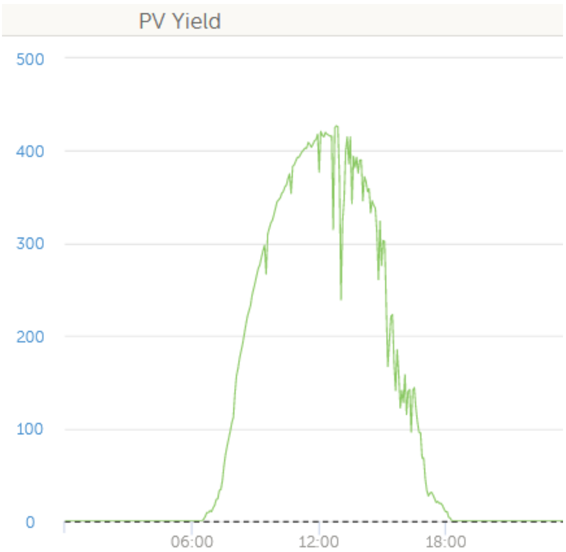

a) PV Yield

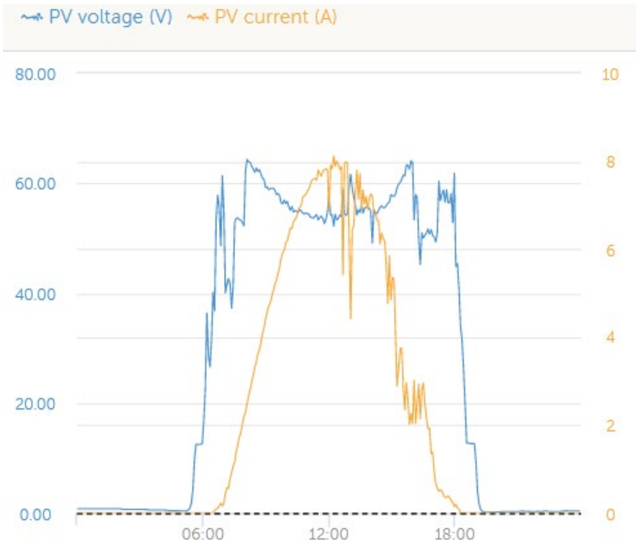

b) PV voltage and current

Fig. 3. Recordings during battery charging

3. The compact hydraulic power unit

The pumping unit is the main component of a hydraulic drive system. In the present case, a 1500 W pumping group is used, which is mounted in the enclosure next to the electrical equipment. The hydraulic group [7] receives electrical energy from the photovoltaic system and transforms it into hydraulic energy, which it sends to the linear hydraulic motor, which transforms it into the mechanical energy required to actuate the mechanism of an equipment such as: irrigation canal gate, valve, compaction press, etc. The hydraulic diagram of the pumping group (fig. 4) contains two directional valves with manual control, one for connecting / disconnecting the hydraulics and one for controlling the hydraulic motor connected to the system by means of 2 quick couplings.

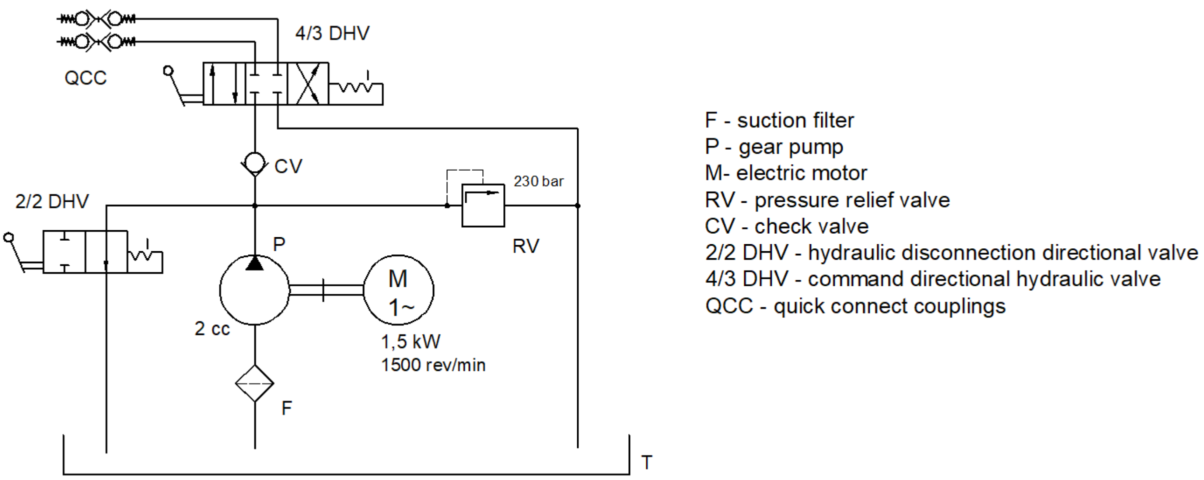

Fig. 4. Diagram of the hydraulic power unit

The hydraulic directional valves can be replaced with ones with electric control for a version of the system with remote control.
For remote control, the system must be completed with a controller through which the pumping group can be started and the hydraulic controls can be activated. Also, the system must be provided with a telemetry system that provides information about the SoC (state of charge) of the battery and the confirmation of the accomplishment of commands sent from a remote location [8]. To this end, a general purpose programmable logic controller, ESP32 microcontroller module [9], Arduino platform, etc. can be used.
Characteristics of the hydraulic group:

- Power of the pumping group: 1.5 kW
- Supply voltage: 230 Vac
- Maximum pressure: 250 bar
- Maximum flowrate: 3 l/min
- Manual operated 2/2 directional valve size 6 for disconnection of the hydraulics
- Manual operated 4/3 directional valve size 6 for hydraulic motor command.

In fig. 5, the hydraulic group can be seen during the testing and adjustment of the relief valve performed in the laboratory.

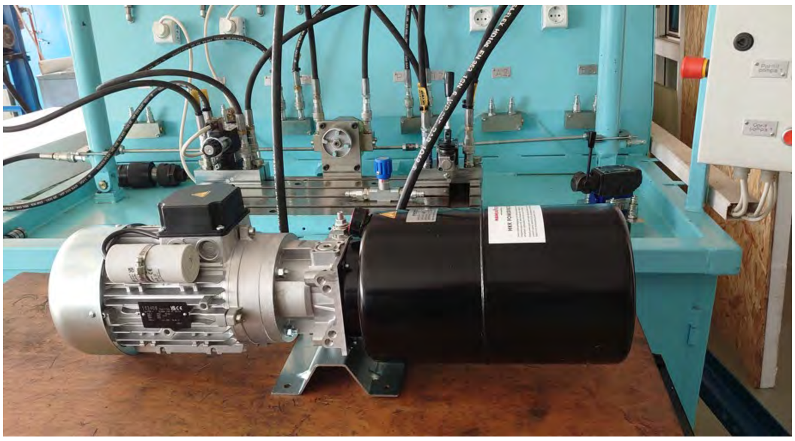

Fig. 5. Hydraulic power unit during laboratory testing

4. Conclusions

Examples of the use of solar photovoltaic energy, produced locally in areas that do not have access to the electrical grid are for: irrigation systems that use solar pumps, hydraulic actuation systems for irrigation canal gates, hydraulic drive for knife gate valve for the mining industry, etc.
The use of electrical energy obtained through the conversion of solar energy directly contributes to the reduction of noxious pollution, when it replaces energy that would otherwise come from burning fuels (e.g., in hybrid mobile machines); in isolated places, electricity from solar energy is the only solution to facilitate human activity.
Indirectly, local energy production contributes to reducing pollution; waste compactors of various sizes can be mentioned here. The local compaction of waste, which becomes possible even where there is no common electricity network, reduces the volume of waste, decreases the fuel consumption required for their transportation, and the application of "smart" solutions, such as the transmission of information about the state of the compaction equipment, contributes even more to reducing pollution.

Acknowledgement

This work was carried out through the Core Program within the National Research Development and Innovation Plan 2022-2027, carried out with the support of MCID, project no. PN 23 05.

References

[1] Farooq, M., A. Hussain, S. Hashim, L. Yang, and M. Ali. "Automated Irrigation System based on irrigation gates using fuzzy logic." Paper presented at the 2020 International Conference on Internet of Things and Intelligent Applications (ITIA), Zhenjiang, China, November 27-29, 2020.
[2] Kumsa, Teshome, and Yohannis Admasu Shimekit. “Design of Solar Powered Mini Hydraulic Crane for Light Weight the Case of Mettu Area.” *Journal of Offshore Structure and Technology* 8, no. 3 (2021): 65-70.
[3] Gevorkov, Levon, José Luis Dominguez-Garcia, and Lluis Trilla Romero. “Review on Solar Photovoltaic-Powered Pumping Systems.” *Energies* 16, no. 1 (2023): 94.
[4] Sanjula, W. A. K. L., K. T. W. Kavinda, M. A. K. Malintha, W. M. D. L. Wijesuriya, S. Lokuliyana, and R. de Silva. "Automated Water-Gate Controlling System for Paddy Fields." Paper presented at the 2020 2nd International Conference on Advancements in Computing (ICAC), Malabe, Sri Lanka, December 10-11, 2020.
[5] PrimeHyd. “Remote monitoring and hydraulic systems control“. Accessed March 18, 2024. https://www.primehyd.com.au/page/9/solar-solutions.
[6] Shafer Valve – Emerson Company. “HPUs - Solar powered HPU“, p. 5. Accessed March 18, 2024. https://www.emerson.com/documents/automation/brochure-hydraulic-power-unit-shafer-en-83890.pdf.
[7] Hansa Flex “Hydraulic Power Packs”. Accessed March 18, 2024. https://shop.hansa-flex.de/en_GB/hydraulic-components/hydraulic-power-packs/compact-power packs/c/webcat_HF_HKO_0450_0100 .
[8] Velichko, M., Yu Gladkikh, and I. Kostina. “The Development of Solar-Powered Gas Metering Units Equipped with Radio or 3G Based Telemetry Systems.” *IOP Conference Series: Materials Science and Engineering* 791 (2020): 012060.
[9] Ayala-Chauvin, Manuel, Pedro Escudero, Patricio Lara-Alvarez, and Carles Domènech-Mestres. “IoT Monitoring for Real-Time Control of Industrial Processes.” Paper presented at the 8th International Conference, CITI 2022, Guayaquil, Ecuador, November 14–17, 2022.

Assessing Flood Severity and Risk to Residents in Bosque Chapultepec

Ing. **Itai NAVA-ROMERO**[1,*], M.I. **José Avidán BRAVO-JÁCOME**[2], M.I. **Margarita Elizabeth PRECIADO-JIMÉNEZ**[2]

[1] Departamento de ingeniería en irrigación, Universidad Autónoma Chapingo, Estado de México, México

[2] Instituto Mexicano de Tecnología del Agua, Morelos, México

* itai580@hotmail.com

Abstract: *This paper aims to study storm events that lead to urban flooding and their after-effects in Bosque Chapultepec, an urban forest located in Mexico City. Considering Bosque Chapultepec's landscape configuration and composition, along with micro-watersheds that drain into the four-sectioned study area, the water depths and velocities were estimated through hydrodynamic models in Iber derived from design storms for different return periods between 2 and 10,000 years. Risk to human safety assessment due to flooding was determined in terms of flow depth and velocity using the Dorrigo classification; and vulnerable zones prone to endanger people to be dragged by the flow were determined and classified following approach proposed by Milanesi, Pilotti, and Ranzi which has an inherent relationship not only to topographic data – since is one of the main data input in hydrodynamic simulations to create flood depth and velocity rasters – but also to human body conceptual model of human stability in a flow. 100-year return period storm events showed that more than 60% of area affected by flooding would not cause damages to light structures, vehicle instability nor reduce people's ability for wading; and more than 90% on area where people were at risk of being washed away corresponded to very low levels, meaning that people passing by the forest only need to be cautious. Furthermore, in light of the latter, recommendations were proposed to prevent flooding in Bosque Chapultepec and to reduce both flood severity and risk to residents to being washed away.*

Keywords: *Bosque Chapultepec, Mexico City, flooding, risk, Dorrigo, Milanesi, Iber*

1. Introduction

Hydrodynamic processes occurring within the hydrological cycle are inherently intricate and marked by considerable uncertainty, lacking a singular theory that comprehensively integrates all aspects of hydrology and hydraulics. Nonetheless, in recent decades, computer programs development has facilitated the generation of simulations using numerical models. These simulations serve not only to estimate water availability within a given region but also to emulate its behaviour—whether above or underground—including factors such as flow, velocity, depth, and disturbed extension. Primary objective is to facilitate preventive measures or problem-solving assessments, addressing various issues, including social concerns.

Regarding damages inflicted by water excess in Mexico over the past three decades, approximately 67% of natural disaster-related deaths are attributable to storms and floods. These events have been responsible for up to 40% of the national disaster damage recorded at 2018 year. [1, 2].

Additionally, in Mexico, the National Centre for Disaster Prevention (CENAPRED, by its acronym in Spanish) monitors and evaluates flood hazard, its incidence through the quantification and parameterization of the factors involved in it for it then to be expressed as a hazard [3]. Some of these parameters are water depth and velocity, toppling or slipping [3], which for hydro meteorological effects phenomena studies done in Mexico are applied in following criteria:

The Federal Emergency Management Agency (FEMA) and the Federal Office of the Economy of Water (OFEE, by its acronym in French) link the maximum water depth and velocity values to be expected and thus characterise the flood into three hazard categories (low, medium, and high) to describe whether buildings will be affected or if people are vulnerable both outside and inside these structures. Nanía and Témez's criteria characterises flooding as dangerous or non-dangerous based on the impact that water depth and velocity has on human stability to slipping [3].

The Mexican Institute of Water Technology (IMTA, by its acronym in Spanish) characterises risk of flooding by classifying it in four hazard levels, also due to toppling and slipping, as well as

characterises the risk associated to affectations to family homes and the loss of property within them [3, 4]. On the other hand, method used in Dorrigo, Australia, defines five flood severity levels (from very low to very high) based on an expected maximum water depth and velocity value, in which it is evaluated vehicle instability, adult people's ability for wading as well as possible structural damage of light structures [3, 5].
In this paper, it is determined water amount entering to the Bosque Chapultepec's land by rainfall for different design storms, focussing the analysis not only on the behaviour of the surface runoff but on the events that cause flooding as well. In this analysis, Dorrigo approach [6] is applied to determine flood severity; level and methodology proposed by Milanesi, Pilotti & Ranzi [7] is also applied to define areas where people are in risk of being dragged and classify its vulnerability level. Latter method is based on the assessment of the destabilising effect of local slope on a regional population to slipping and toppling. Required data on inflow, water depths and velocities for both methodologies are estimated using the software Iber [8], ArcGIS [9], and HEC-HMS [10].
The use of these two methodologies further allows appreciating measures for safeguarding citizens within the Bosque Chapultepec and surrounding areas, reducing runoff that could generate damages, and for water usage resources.

2. Materials and methods

2.1 Study area

This paper presents a study focused on Bosque Chapultepec, which is categorised as an urban forest, and is broken down into three sections that are located in Miguel Hidalgo borough, in Mexico City, Mexico; to which Military Base 1-F is also annexed as fourth section in Álvaro Obregón borough a field that belongs to the Ministry of National Defence (SEDENA, by its acronym in Spanish). Bosque Chapultepec is geographically located between parallels 19°23'40" and 19°25'45" N, and between meridians 99°10'40" and 99°14'15" W, at an altitude between 2250 and 2340 masl, in foothills of Sierra de Las Cruces' volcanic mountain.

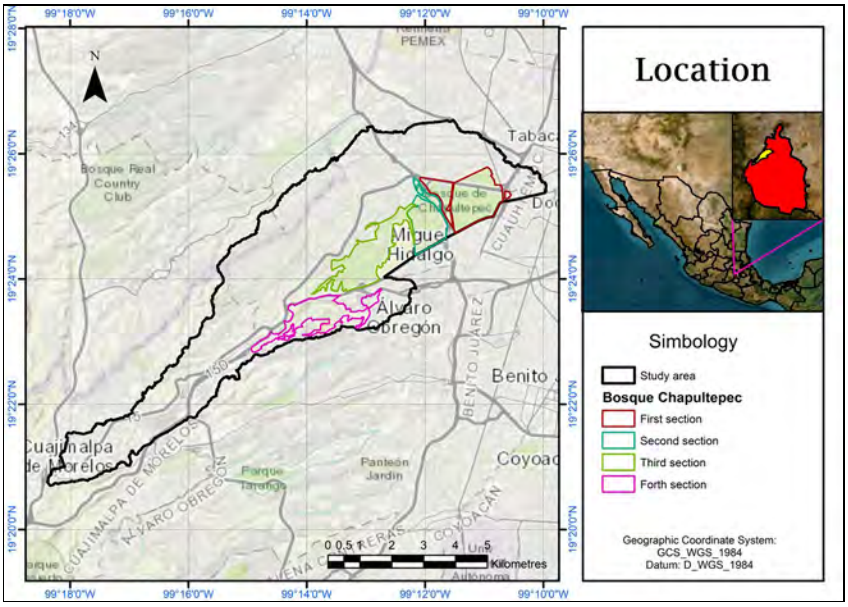

Fig. 1. Study area

Currently, a total 274,086 hectares area is covered by First Section, 168,032 hectares by Second Section 168,032 hectares, and 243,904 hectares by Third Section, while Fourth Section spans a 152,214 hectares area. Within study area, micro-watersheds contributing runoff to urban forest are also considered, resulting in a total area of study of 4420,697 hectares (Figure 1). This entire area is located between parallels 19°20'42" and 19°26'32" N, and between meridians 99°9'57" and 99°18'23" W, at an altitude between 2250 and 2225 masl, according to LIDAR terrain model, with a 5 x 5 metres horizontal resolution [11].

2.2 Physio-hydrological characterisation

Major soil types in study area are Feozem Luvic and Petrocalcium [12]. It was resumed at digital land and vegetation use representation created by IMTA, 2022, based on satellite images and aerial photographs, which considers several classifications such as forest, street, canal, stream, water body, residential, scrubland, grassland, dam, bare land and urban built; residential, street, and urban built land use cover study area 74.95%, followed by forest that covers 11.41%.

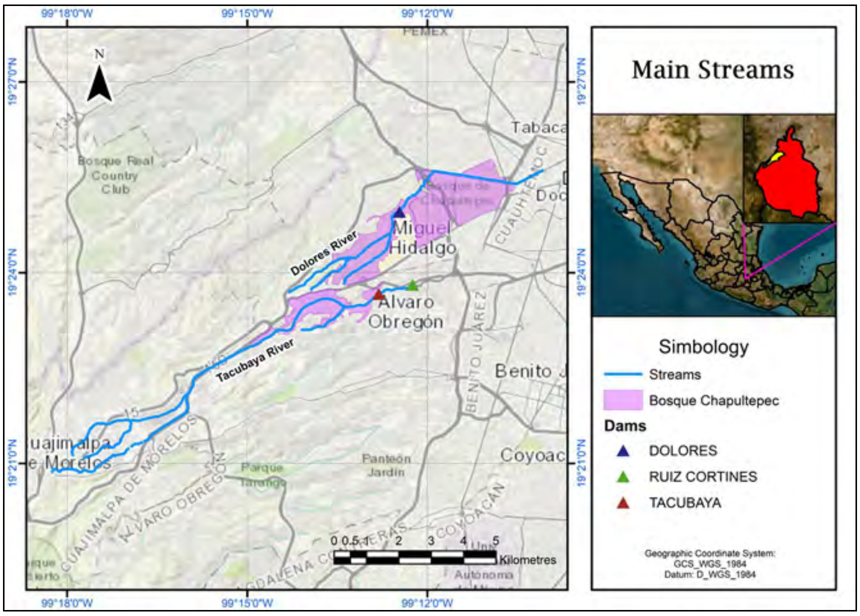

Fig. 2. Main streams located in the study area. (Source: [13, 14])

Within study area, two main intermittent streams are located: Tacubaya and Dolores. Likewise, there are two dams for flood control, each one situated on two aforementioned streams: Dolores and Tacubaya (Figure 2). Other water bodies additionally located in Bosque Chapultepec are artificial lakes Mayor and Menor (excavated in the late 19th century), which are divided between first and second sections of the urban forest. Next meteorological and hydrological studies were obtained from the General Report, first stage, carried out by IMTA [15]: " DIAGNÓSTICO Y PROPUESTAS PARA LA GESTIÓN DE LOS RECURSOS HÍDRICOS EN LAS CUATRO SECCIONES DEL BOSQUE DE CHAPULTEPEC " and are described below.

2.3 Meteorological study

In Table 1, it is shown the maximum precipitation depth in 24 hours for selected return periods from 2 to 10,000 years, which was obtained by calculating the influence area using Thiessen polygon method, for maximum precipitation values estimated from Double Gumbel Probability Distribution Function for each climatological station.

Table 1: Maximum precipitation depth in 24 hours for different return periods.

T	hp	T	hp
years	*mm*	*years*	*mm*
2	42.645	200	91.321
5	58.320	500	96.072
10	67.687	1000	99.240
20	74.924	2000	102.117
50	82.443	5000	105.547
100	87.183	10000	107.896

Figure 3 shows a unit hyetograph in orange that corresponds to mean value of all the storms analysed from the Synoptic Weather Station Tacubaya, while it also shows a unit hyetograph in blue that represents the mean value of the storms that reached 80% of the precipitation before 10 a.m. Since the latter hyetograph represents the worst-case scenario, it was used to define the 24-hour temporal distribution of the design storms, for each return period, in the hydrologic model and the two-dimensional hydraulic model.

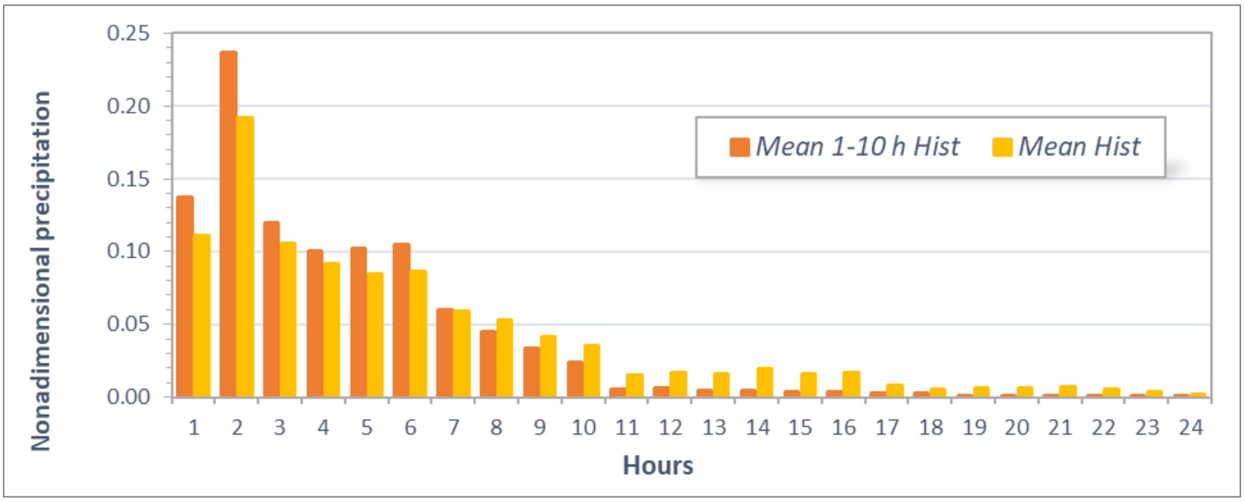

Fig. 3. Unit hyetograph. (Source: [15])

2.4 Hydrological study

Table 2: Micro-watersheds characterisation that comprises study area.

Micro-watershed	Area	Length of main channel	Elevation difference	S (Channel slope)	CN	Tc	tr
	km²	*km*	*m*			*hours*	*hours*
Dolores	4.14	4.21	165.47	0.01525	82.73	1.06	0.63
Tacubaya	9.66	12.45	492.5	0.01631	88.08	1.64	0.99

Main physiographic micro-basins characteristics contributing runoff into Bosque Chapultepec, Dolores and Tacubaya, are shown in Table 2: main channels slope was computed by Taylor Schwarz's method, curve number CN, the mean Tc value estimated by Kirpich, Rowe, SCS and Chow's methods; and the tr computed with Chow's equation. This information was introduced into the software HEC-HMS 4.2.1 for hydrological modelling; the following results were obtained:

Table 3: Runoff computed in HEC-HMS of contributing micro-basins.

Micro-basin	Peak discharge, in m^3/s, for each return period (*years*)											
	2	5	10	20	50	100	200	500	1000	2000	5000	10000
Dolores	2.5	4.5	5.8	6.8	7.9	8.5	9.3	9.8	10.3	10.7	11.2	11.5
Tacubaya	5.1	8.5	10.5	12.1	13.8	14.9	16	16.8	17.6	18.2	19	19.5

2.5 Two-dimensional modelling in Iber

To carry out hydraulic simulations using Iber, the study area was divided into four models that contain the following sections of Bosque Chapultepec in the next order: the first and second sections, the third section, the fourth section, and the upper Tacubaya basin; in order to optimise the simulation processing since it was necessary to represent the hydraulic infrastructure in greater detail, and it was not possible to model the five areas as a whole. The geometry of each model included:

a. Boundary conditions and outlet boundaries: The boundary condition was assigned as an output with a supercritical/critical regime for the main boundary of each model. For the model containing the first and second sections of the urban forest, an inlet boundary was assigned as an upstream boundary condition to the entrance of the Dolores dam where it was introduced hydrographs obtained from simulation of the forest’s third section modelling for each return period, with a critical/subcritical regime, as the total inflow in the inlet. For the model of the fourth section of the forest, an inlet was assigned as a boundary condition in the upper area introducing the hydrographs obtained from previous simulation of Tacubaya micro-basin, assigned as total inflow for each return period, with a critical/subcritical regime.
b. Initial conditions: non-existent flow condition (without previous rainfall) was established as a water depth equal to zero in the entire area to be modelled except in the four artificial lakes to which a depth of 0.3 meters was assigned.
c. Design Storm Hyetograph: Total rainfall input to model by return period from meteorological study.
d. Roughness coefficient: Manning's coefficient was assigned based on land use map created by IMTA [15] and based on values suggested by Ven Te Chow [16], combined as well with values specified by default in the software Iber.
e. Infrastructure: Circular and rectangular culverts were put where bridges crossing channels were detected, with a Manning roughness coefficient of 0.02. Sinks were added to represent the storm drains connected to the storm sewer of Mexico City.
f. Generation of unstructured triangled meshes, entering element sizes of 2, 4, 5 and 6 meters.
g. Digital elevation model: To set elevation on unstructured meshes, DEM generated from a 5-meter LIDAR was used, merged with a 1-meter LIDAR DEM just in certain places where the Mayor and Menor artificial lakes are located.

In total, 36 hydraulic models were generated which correspond to four sections and twelve return periods.

2.6 Flood severity, applying Dorrigo approach

To estimate flood severity level or flood hazard in buildings after storm events, the National Water Commission (CONAGUA, by its acronym in Spanish) for the National Program Against Hydraulic Contingencies (PRONACCH, by its acronym in Spanish) used Dorrigo criterion [6] by adapting its Flood Hazard Diagram, which also making hazard maps associated to flood events for a particular study region (Figure 4). Only water depth and velocity rasters obtained from *Iber* simulation were used as inputs, each one extracted per hour as time step for return periods of 2 to 10 000 years; and that were processed through the ArcGIS tool Model Builder. Flood severity index classified for map generation are described in Table 4, where green represents areas with no critical damage while red represents areas with potential severe or critical damage.

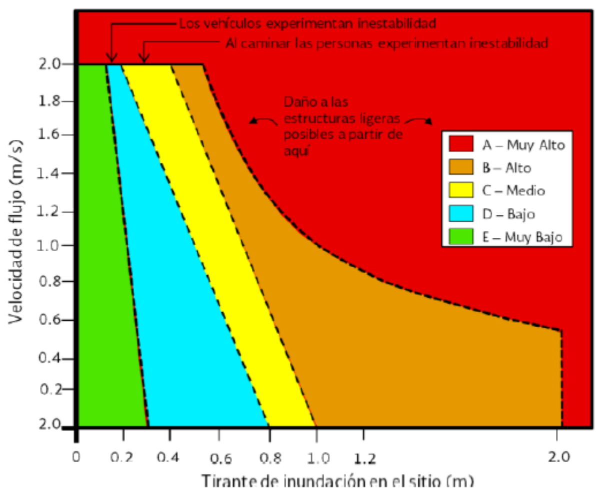

Fig. 4. Flood severity indexes according to the Dorrigo approach. (Source: [6, 17])

Table 4: Colour coding for creating flood severity maps.

N°	Letter	Index	Colour	Constraints	
				Depth (*m*)	Velocity (*m/s*)
5	A	Very high	(red)	Y > 2	V > 2
4	B	High	(orange)	1 < Y ≤ 2	V ≤ 2
3	C	Medium	(yellow)	0.8 < Y ≤ 1	V ≤ 2
2	D	Low	(cyan)	0.3 < Y ≤ 0.8	V ≤ 2
1	E	Very low	(green)	Y ≤ 0.3	V ≤ 2

2.7 Dragging people risk

Milanesi, Pilotti & Ranzi [7] propose a model related, physically and quantitatively, to slipping, toppling, and drowning of a human body into flow field, where human body is conceptualised as a set of cylinders whose stability to slipping and toppling is analysed according to equilibrium forces and moments for different environments. Moreover, model takes into account the destabilizing effect of local slope and fluid density; that is why it allows a graded classification of hydraulic risk (Figure 5).

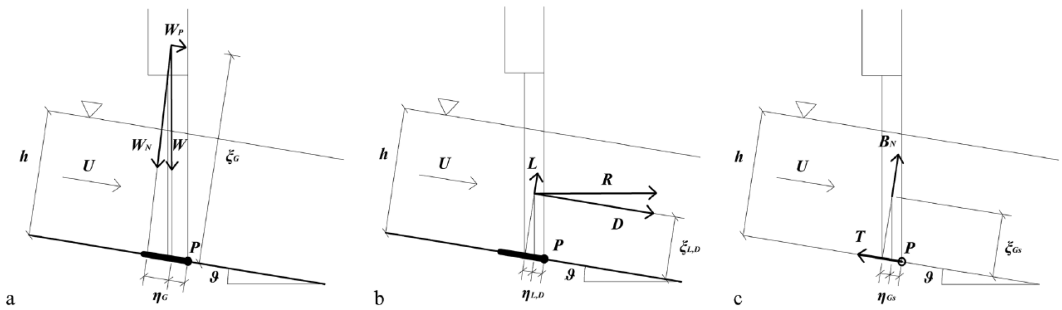

Fig. 5. Acting forces and their application points. (Source: [7])
W = body weight; W_N = normal component; W_P = parallel component, to the slope; R = fluid dynamic force; D = dynamic and parallel dragging force; L = dynamic and orthogonal lifting force; B_N = buoyancy force; T = friction; η_G y ξ_G = coordinates of the centre of mass of the body; $\eta_{L,D}$ y $\xi_{L,D}$ = coordinates of dragging and lifting forces applied on the submerged human body; h = water depth; U = mean water velocity.

Soriano [18], in turn, based on this criterion [7], further develops mathematical concepts to determine the dragging people risk index by applying Equation (1), valued between 0 and 1; in Table 5, Soriano [18] defines a hazard levels classification relating to values obtained from Equation (1).

Table 5: Flood hazard to people. (Source: [18]).

Value (HR)	Classification – Description
HR = 0	Secure (dry)
0 ≤ HR < 0.30	Very low hazard – be cautious
0.30 ≤ HR < 0.60	Low hazard – Includes people with disabilities
0.60 ≤ HR < 1.0	Medium hazard – Includes most of the population
HR ≥ 1.0 or hf ≥ hd	High – Includes everybody

HR = Flood hazard to people index; hd = drowning water depth threshold; hf = water depth.

$$HR = \min\left(1, \frac{U}{\min\left(U_{der}, U_{des}\right)}\right) \quad (1)$$

In which: HR = flood hazard to people index; Udes y Uder = critical velocities for instability due to friction, and destabilizing moments, in (m/s) respectively; U = water velocity, in (m/s), obtained from the hydrological-hydrodynamic simulation. Critical toppling velocity calculation Uder (in meters per second) and critical slipping velocity Udes (in meters per second) is calculated by using following equations:

$$U_{der} = \sqrt{\frac{4\left[WX_G - \rho g V_s\left(X_G + \frac{1}{2}Y_G sen2\vartheta\right)\right]}{C_C \rho A_s\left[hcos\vartheta + x_{G_s} sen2\vartheta\right]}} \quad (2)$$

Where: Uder = critical toppling velocity, in (m/s); CC = drag coefficient of a circular cylinder measured for uniform flow profile orthogonal to the body frontal area; W = bodyweight, in (kg_f); g = gravity acceleration, in (m/s^2); ρ = flow density, in (kg/m^3); As = wetted frontal area, in (m^2); Vs = submerged volume of the body, in (m^3); X_G = X coordinate of the body's centre of gravity, in (m); Y_G = Y coordinate of the body's centre of gravity, in (m); x_{Gs} = X coordinate of the centre of gravity of the submerged volume, in (m).

$$U_{des} = \sqrt{\frac{2\left(-Wtan\vartheta + W\mu - \mu g \rho V_s\right)}{C_C A_s \rho\left(cos^2\vartheta + \frac{1}{2}\mu sen2\vartheta\right)}} \quad (3)$$

Where: Udes = critical slipping velocity, in (m/s); CC = drag coefficient of a circular cylinder measured for uniform flow profile orthogonal to the body frontal area; W = bodyweight, in (kg_f); g = gravity acceleration, in (m/s^2); ρ = flow density, in (kg/m^3); As = wetted frontal area, in (m^2); Vs = submerged volume of the body, in (m^3); μ = friction coefficient, (adim).
Other parameters related to physical population characteristics of the study area were defined for an average Mexican adult, which are described in Table 6. To estimate dragging people risk exerted by the flow, it was necessary to use ArcGIS Model Builder tool to process rasters derived from simulation in Iber of water depth and velocity, extracted by one-hour time step intervals for return periods of 2 to 10,000 years, with corresponding DEM in tandem. For dragging people risk map generation, risk indexes were plotted according to Table 6 and Table 7.

Table 6: Average Mexican adult people physical characteristics. [19]

	Height (Y)	**Weight (m)**	**Torso diameter (D)**	**Leg diameter (d)**
	m	*kg*	*m*	*m*
Men	1.64	74.8		
Women	1.50	68.7		
Mean value	1.61	71.75	0.311	0.155

Table 7: Colour coding for creating dragging people risk maps.

N°	**Letter**	**Risk index**	**Colour**
5	A	High	
4	B	Medium	
3	C	Low	
2	D	Very low	
1	E	Safe	

Figure 6 describes processing performed and how are they linked in Model Builder once requested input parameters are entered: water depth raster and water velocity raster for a return period *i*, and a time step *j*, where each cell is evaluated to obtain the flood severity index. In steps II and III, for each velocity value per cell, four corresponding virtual water depths (y1, y2, y3 and y4) are calculated, where y1 corresponds to the boundary between the very low and low severity zones, y2 corresponds to boundary between low and medium severity zones, y3 corresponds to boundary between medium and high severity zones, and y4 corresponds to boundary between high and very high severity zones, boundaries depicted in Figure 4. In step V, a conditional evaluation was performed to compare cell by cell whether real water depth *Yi* is greater, less than, or equal to temporarily stored water depths y1, y2, y3, and y4, in order to categorise water depth severity level *Yi*, according to index values described in Table 4. The resultant raster is a raster containing severity indexes for a return period *i*, and a time step *j*.
Finally, for each *T i*, it is evaluated whether a cell in a raster of time step *j* has a greater value than value of that same cell of previous raster *j - 1* and make a substitution on previous raster until all the arrays have been compared, resulting in an array with maximum values.

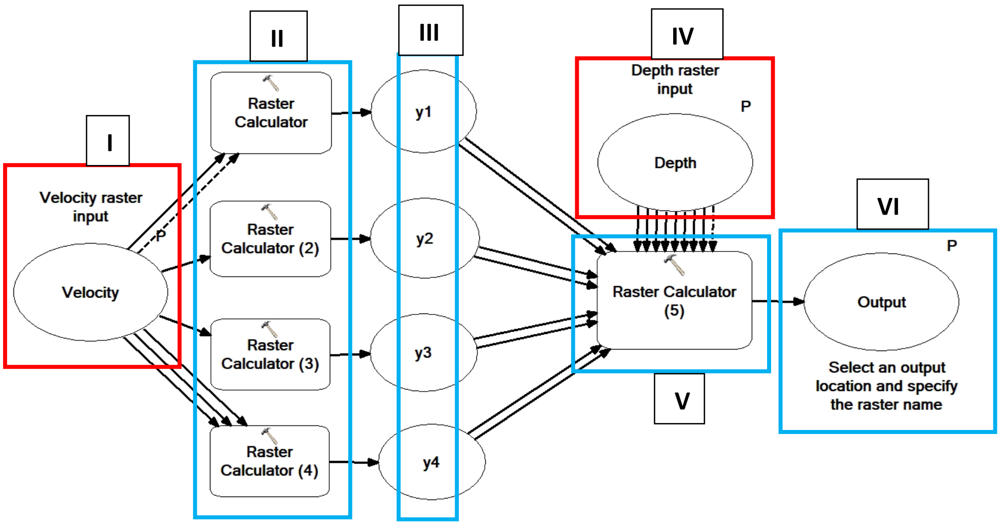

Fig. 6. Workflow diagram for flood severity index classification.

Similarly, to apply Milanesi criteria [7], Figure 7 describes processing performed and how are they linked in Model Builder once requested input parameters are introduced: water depth raster and the water velocity raster for a return period *i*, and a time step *j*, where each cell is evaluated to obtain people at risk index to being dragged by flooding, in tandem with a digital elevation model.
For step II, the variables related to the conceptualized representation of the human body such as the wetted frontal area and body submerged volume are calculated, defined as a function of human body height, torso diameter, legs diameter, and slope already determined from corresponding DEM. In step III, *Udes* and *Uder* (Equation 2 and 3, respectively) are estimated using a friction coefficient of 0.46 and a drag coefficient of 1; afterwards, both rasters with *Udes* and *Uder* values obtained are compared cell by cell to extract only minimum values, creating a third raster. In step IV, flood hazard to people index HR is obtained, which is equal to water velocity raster input divided by minimum critical toppling and slipping velocity; thus, values in a range of 0 to 1 are contained in resulting raster. In step V, all cells are reclassified according to Table 5 and Table 7 to obtain a final raster for a return period *i*, and a time step *j*.
This process is concluded by evaluating for each *T i* whether a cell in a raster of time step *j* has a greater value than value of that same cell on previous raster *j - 1* and make a substitution on previous raster until all arrays have been compared, resulting in an array with maximum values.

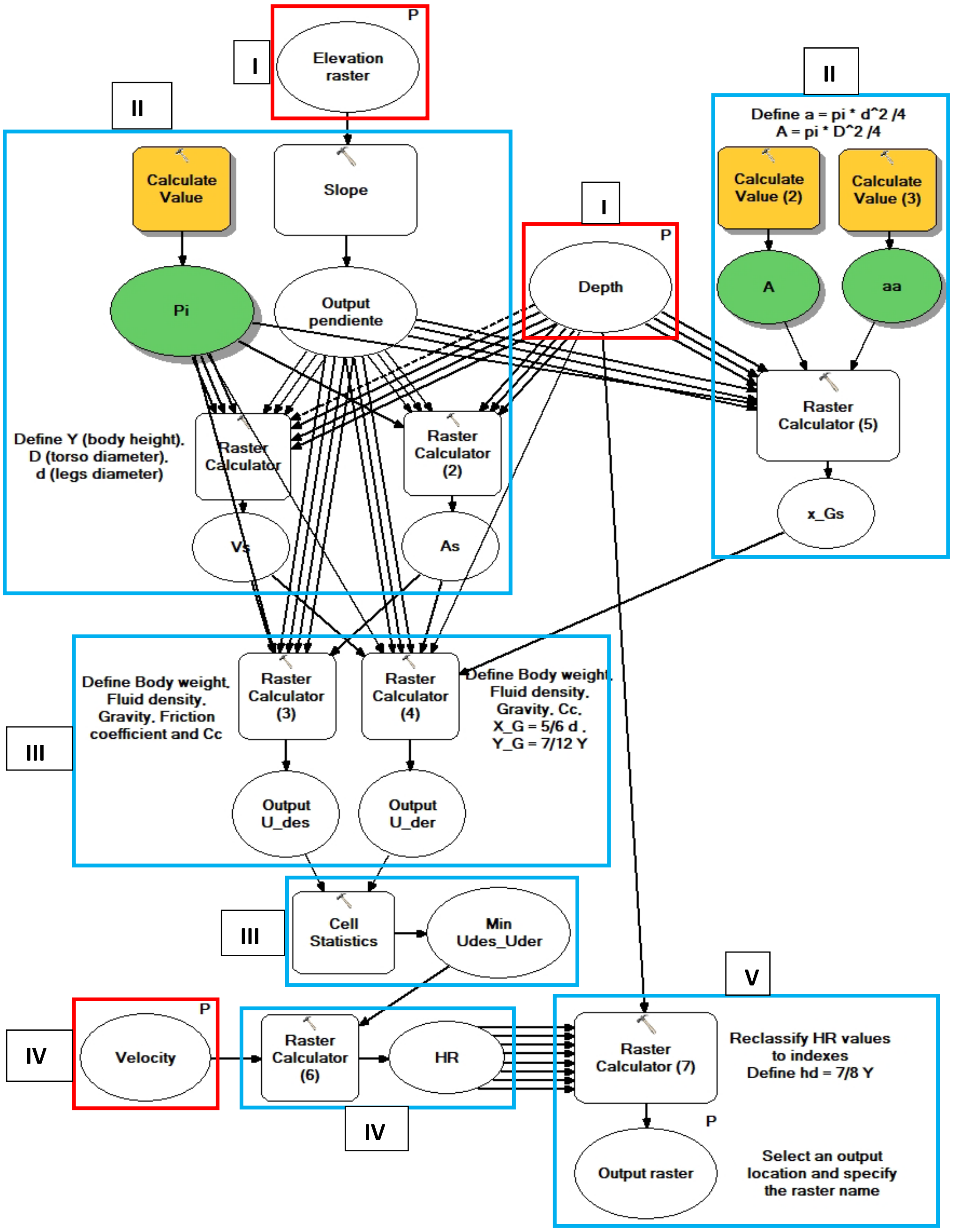

Fig. 7. Workflow diagram for the classification of the dragging people risk index.

3. Results and analysis

From Figure 8 to Figure 10 it is presented flood severity maps for a 100-year return period of Bosque Chapultepec's four sections; most of the area identified with flood severity within these four sections corresponds to hazard level E, which is described as a very low severity level (Table 4). In first and second sections of urban forest, for a return period of 100 years, about 83% of total affected area of approximately 1.39 km^2 corresponds to level E (Figure 8). For a *T* of 2 years and 10,000 years, approximately 82.78% and 80% correspond to severity level E respectively. On the other hand, for a 2-year *T*, 1.16% of affected areas is defined with a severity index A while for a 10,000-year *T* this index represents 1.11% of total affected area. Areas with a very high severity for a 100-year *T* are mostly visible in Miguel Hidalgo borough, on intersection of Cto. Interior Melchor Ocampo and Paseo de la Reforma Ave, on junction of Rubén Darío St, Calzada Chivatito and

Arquímedes St, and on Morvan St; also, in Cuauhtémoc borough on Lieja St, an underpass crossing Paseo de la Reforma Ave (Figure 8).

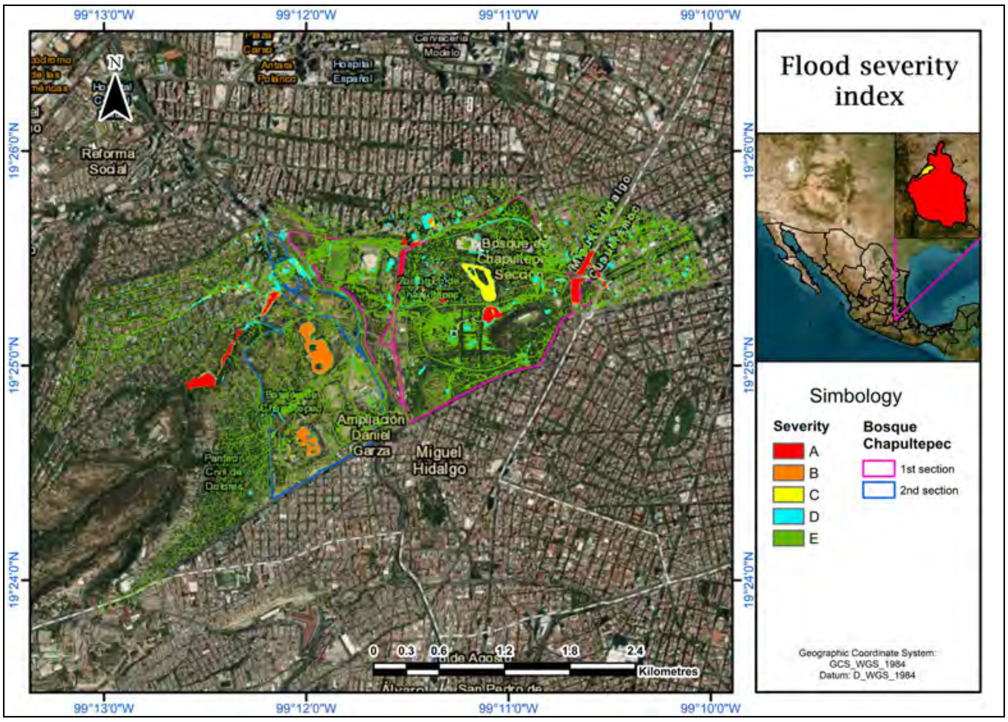

Fig. 8. Flood severity on 1st and 2nd sections of Bosque Chapultepec, for a 100-year return period.

In third section of Bosque Chapultepec, it was observed that for all return periods evaluated, about 70% of affected areas had a severity level E. Affected areas with a severity index A for a 2-year *T* accounted for 8.9% of the total, and for a 10,000-year *T* it increases by 2%. For a 100-year *T*, most of areas with very high severity correspond to Dolores dam and natural channels that discharge into it, in Miguel Hidalgo borough (Figure 9).

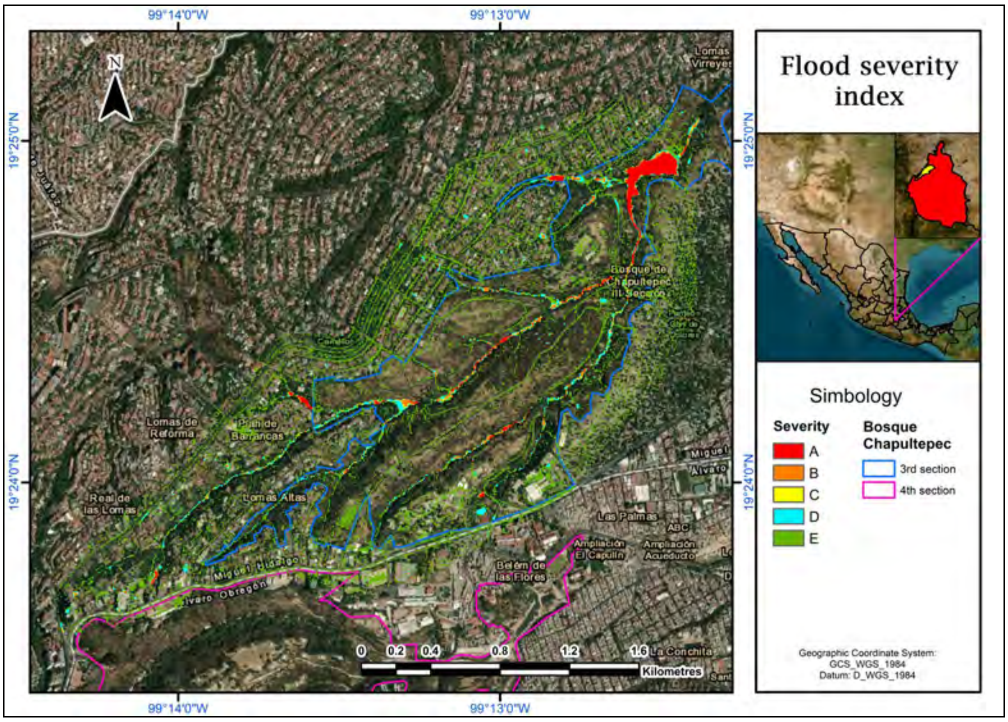

Fig. 9. Flood severity on 3rd section of Bosque Chapultepec, for a 100-year return period.

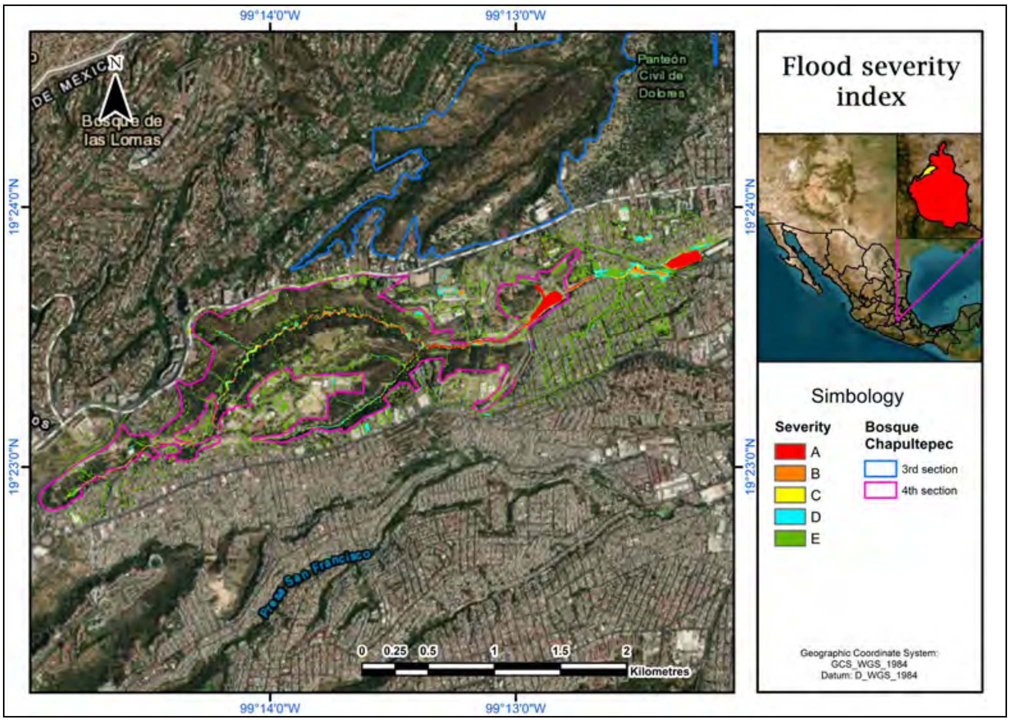

Fig. 10. Flood severity on 4th section of Bosque Chapultepec, for a 100-year return period.

In the fourth section it was observed that for a 100-year *T* there is a total affected area of 0.22 km^2, about 62.3% corresponds to severity level E (Figure 10); for a *T* of 2 and 10,000 years there is an affected area of 67.4% and 60.4% respectively with severity level E. For a 2-year Tr, 0.74% of the total area affected reaches a severity index A, and for a 10,000-year *T* it rises by 17%. These areas with a high severity are mainly displayed at Tacubaya dam, as well as its downstream subarea where the discharge water is conducted from the dam's outlet work to Mexico City drainage network plus, on Ruiz Cortines dam and into Tacubaya River, in Álvaro Obregón borough of (Figure 10). Figure 11 to Figure 13 show 100-year return dragging people risk maps for the four sections of bosque Chapultepec; most of area identified as people in risk of being washed away corresponds to dragging risk level D, which is described as a very low risk level, but caution should still be exercised (Table 5).

Particularly, in the forest's first and second sections, for a 100-year *T* of total area at risk which is about 1.92 km^2 (represented in Figure 11) approximately 95.26% corresponds to a risk level D. For a *T* of 2 years and 10,000 years, about 98.5% and 93.6% correspond to the risk level D respectively. Furthermore, for a 2-year *T*, 0.17% of affected areas are defined with a risk level A while for a 10,000-year *T* it represents 1.43% of total affected area. For a 100-year *T*, these areas with a high drag risk are mainly exhibited on Calz. Mahatma Gandhi continuing towards Parque de la Amistad and Calz. General Mariano Escobedo, on main access ramp to Chapultepec Castle in first section of the urban forest, also on Paseo de la Reforma Ave on north side of National Auditorium and military Marte Field, on Calz. Chivatito, and to west side of the former Feria de Chapultepec on De los Compositores Ave turning towards Rodolfo Neri Vela Ave; in Miguel Hidalgo borough (Figure 11).

It was observed in third section of urban forest that for a *T* of 100 years, 0.68 km^2 were affected, where a little more than 93.1% corresponds to risk level D (Figure 12). For a *T* of 2 years and 10,000 years, approximately 95% and 92% of total affected area correspond to a risk level D respectively. As for the risk index A, for a 2-year *T* affected areas correspond to 2.34% of total, and for a 10,000-year *T* correspond to 4.18%. For a 100-year *T*, most of the areas with a high dragging people risk were primarily in natural channels that discharge into the Dolores Dam, as well as at the entrance of the dam and in its discharged downstream, in Miguel Hidalgo borough (Figure 12).

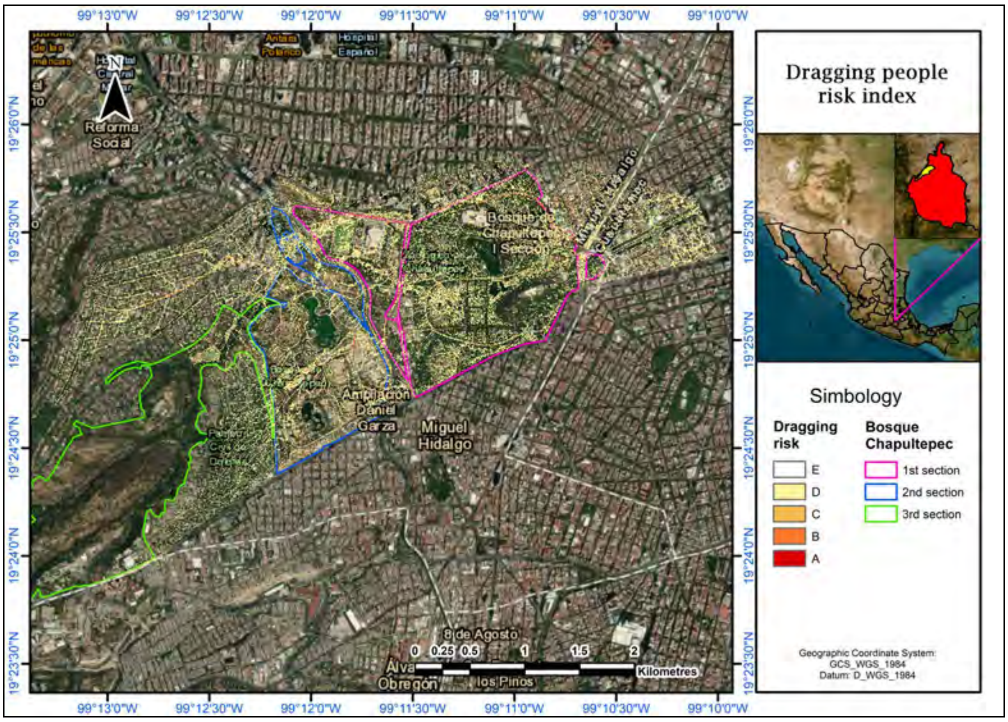

Fig. 11. Dragging people risk on 1st and 2nd sections of Bosque Chapultepec, for a 100-year return period.

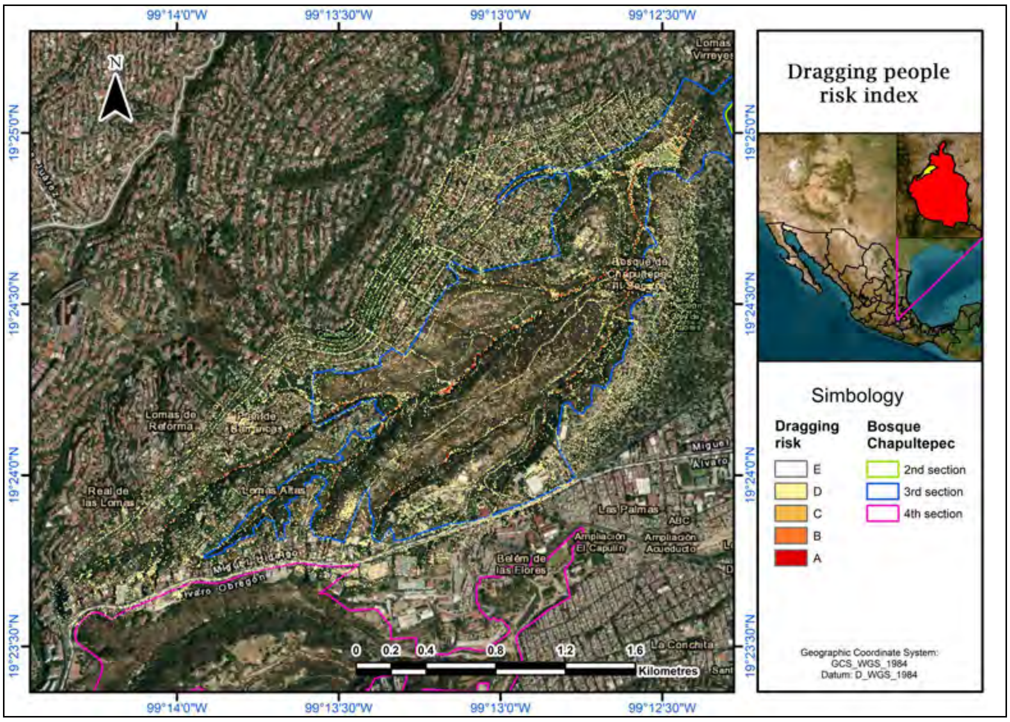

Fig. 12. Dragging people risk on 3rd section of Bosque Chapultepec, for a 100-year return period.

Lastly, in the fourth section of Bosque Chapultepec, a total affected area of 0.58 km^2 was obtained for a 100-year *T*, and about 90.6% of it relate to a drag risk level D (Figure 13); for a *T* of 2 and 10,000 years there is an affected area of 92.1% and 90% respectively displaying this same level of risk. However, at risk level A, affected areas for a 2-year *T* accounted for 6.76% of the total, and for a 10,000-year *T* accounted for 9.62%. These zones with high drag risk are mainly located at various points along Tacubaya River, which discharges into Tacubaya Dam, and these zones continue in superficial runoff towards to Ruiz Cortines Dam despite the fact that Tacubaya Dam discharges through an outlet structure downstream connected to Mexico City drainage network; similarly, on Río Santo Domingo and Presidente Juárez streets, in Álvaro Obregón borough (Figure 13).

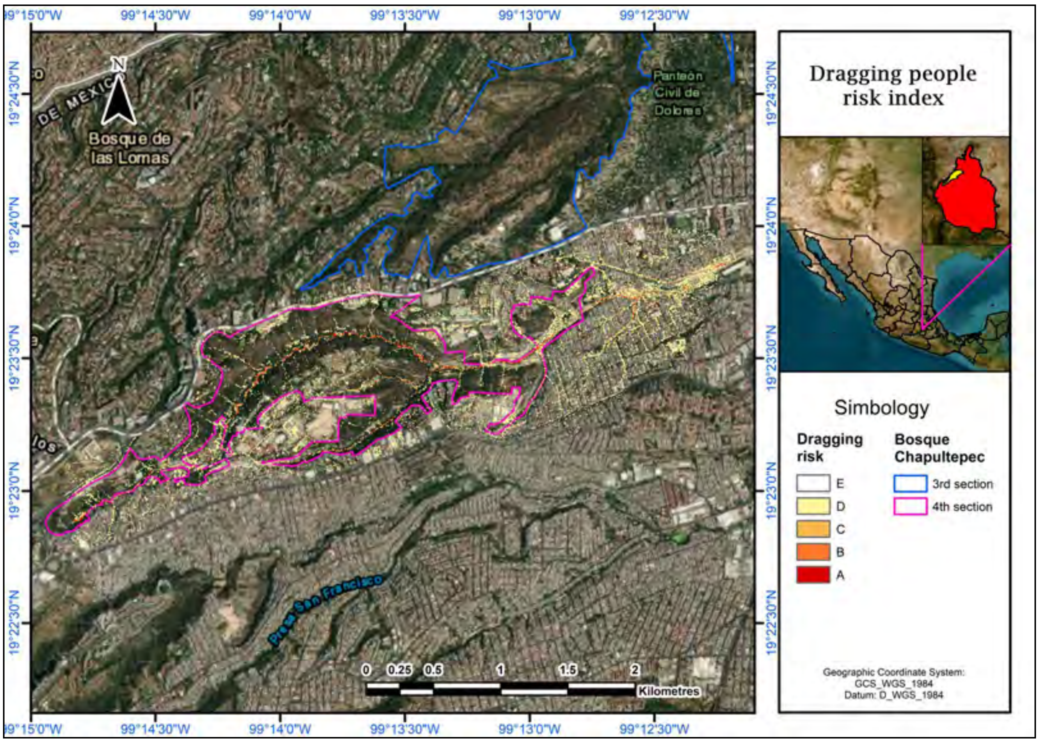

Fig. 13. Dragging people risk on 4th section of Bosque Chapultepec, for a 100-year return period.

4. Discussion

A medium to high level of people risk to being washed away was mainly presented in natural channels, especially in 3rd and 4th sections, and on some streets and footpaths within 1st and 2nd sections, indicating that most of the population would be vulnerable during a storm event.
In case of 3rd and 4th sections, both are micro-basins with runoff generating on roads but quickly concentrating into rivers that discharge to Dolores Dam and Tacubaya Dam. Nonetheless, 1st and 2nd sections have more streets that reduce surface runoff volume entering permanent water bodies, where flow direction is determined by its slope itself, concentrating to local runoff towards areas with steepest slopes. From a variation analysis of drag risk and flood severity levels throughout all areas affected obtained by both methods, it was observed that change in percentage in distribution of each level of severity and risk of people being dragged changed minimally. For example, areas with severity or drag risk type A remain almost the same for a 10,000-year *T* compared to the 2-year *T*, there is a proportional expansion between return periods; in other words, between the 2-year and 10,000-year *T*, there is practically the same level of flood risks for the same area.

5. Conclusions

The software Iber facilitated hydrodynamic models generation to study the runoff process during and after a storm event (for return periods of 2 to 10,000 years) in Chapultepec's four sections. The ArcGIS Model Builder tool made it easy to integrate data from extracted rasters plus the MDE to significantly reduce the processing time required for generating flood severity and dragging people risk maps.
This paper utilized two methodologies focusing on population risk (Milanesi's criterion) and considering infrastructure and vehicles (Dorrigo's criterion). By applying Dorrigo criterion for each pixel with a depth and velocity value, a flood severity index is obtained. A medium to high severity

occurred especially where there were bodies of water, natural channels, or underpasses. When implementing Milanesi criteria, defining population’s anthropometric characteristics is an important factor to characterise aftereffects on our study area; hence, population physical parameters were specified in accordance with average values of the central region of the country, which was only information available for the past 10 years. Furthermore, slipping or toppling velocities are dependent on runoff depth and terrain slope, which in comparison to applying Dorrigo approach for processing water depth and velocity rasters, a value of slipping or toppling velocity is not obtained in all cells of these rasters; therefore, not all runoff results in people being dragged, but it may cause drowning which severity maps can identify.

Finally, it is recommended to plan road closures and create evacuation routes within recreational areas of Bosque Chapultepec in case of emergency due to storms and/or flooding, which show to visitors the way to the nearest pre-assigned meeting locations inside or outside the immediate area, as well as the nearest exits of the forest. It should be noted the possibility of expanding social programs for garbage collection in surrounding areas to this urban forest, which frequently obstruct Mexico City‘s drainage system both at entrance to drainage and in conduction system, and to make visitors aware to use garbage deposits properly and continuously since there are several commercial areas that increase proliferation of inorganic garbage within the forest.

Acknowledgements

Authors would like to thank the Fondo Institucional para el Desarrollo Científico, Tecnológico y de Innovación FORDECYT-PRONACES from the Comisión Nacional de Ciencia y Tecnología.

References

[1] National Civil Protection Coordination / Coordinación Nacional de Protección Civil (CNPC). “Floods in Mexico” / “Inundaciones en México”, May 2018. Gobierno de México. Accessed September 8, 2020. from https://www.gob.mx/cms/uploads/attachment/file/336984/1._180503_SRI_Inundaciones.pdf.
[2] Notimex. “Hurricanes and Floods Cause 40% of Disaster Damage in Mexico: AMIS.” / “Huracanes e Inundaciones Causan el 40% de Daños por Desastres en México: AMIS.” *El Economista,* June 17, 2019. Accessed February 15, 2024. https://www.eleconomista.com.mx/politica/Huracanes-e-inundaciones-causan-el-40-de-danos-por-desastres-en-Mexico-AMIS-20190617-0055.html.
[3] National Water Commission / Comisión Nacional del Agua (CONAGUA). *Drinking Water, Sewage and Sanitation Manual: Book 19* / *Manual de Agua Potable, Alcantarillado y Saneamiento: Libro 19*. Mexico City, Mexico: Comisión Nacional del Agua, 2019.
[4] Alcocer-Yamanaka, V. H., J. M. Rodríguez-Varela, V. J. Bourguett-Ortiz, O. J. Llaguno-Guilberto, and P. M. Albornoz-Góngora. “Methodology for generating flood risk maps in urban areas.” / “Metodología para la generación de mapas de riesgo por inundación en zonas urbanas.” *Tecnología y ciencias del agua* 7, no. 5 (2016): 33-55.
[5] Paterson Consultants Pty Ltd. *Dorrigo Flood Study*. New South Wales, Australia, Bellingen Shire Council, 2007.
[6] National Water Commission / Comisión Nacional del Agua (CONAGUA). *National Program for the Prevention of Hydraulic Contingencies* / *Programa Nacional de Prevención Contra Contingencias Hidráulicas (PRONACCH)*, 2013.
[7] Milanesi, L., M. Pilotti, and R. Ranzi. “A Conceptual Model of People’s Vulnerability to Floods.” *Water Resources Research Journal* 51, no. 1 (2015): 182–197.
[8] Iber. *Hydraulic Reference Manual* / *Manual de Referencia Hidráulico*, September 19, 2014. https://iberaula.es/space/54/downloads.
[9] Environmental Systems Research Institute. “ArcGIS Desktop”, 2014. https://desktop.arcgis.com/es/desktop/index.html.
[10] US Army Corps Engineers & Hydrologic Engineering Center. *HEC-HMS*. (n.d.). Accessed March 25, 2021. from https://www.hec.usace.army.mil/software/hec-hms/.
[11] National Institute of Statistics, Geography and Informatics, Mexico / Instituto Nacional de Estadística, Geografía e Informática, México - INEGI. LIDAR Terrain Model / Modelo de terreno LIDAR, 5 x 5 m horizontal resolution, 2010.
[12] National Commission for the Knowledge and Use of Biodiversity, Mexico / Comisión Nacional para el Conocimiento y Uso de la Biodiversidad, México – CONABIO. Edaphology. Scale 1:250,000 / Edafología. Escala 1:250,000. *Portal de Geoinformación 2024*. Accessed October 21, 2020. http://www.conabio.gob.mx/informacion/gis/.
[13] National Water Commission / Comisión Nacional del Agua (CONAGUA). “Dam Safety System” /

"Sistema de Seguridad de Presas". Accessed September 27, 2020. https://presas.conagua.gob.mx/inventario/hnombre_presa.aspx.

[14] National Institute of Statistics, Geography and Informatics, Mexico / Instituto Nacional de Estadística, Geografía e Informática, México - INEGI. Hydrographic network. Scale 1:50,000. Edition 2.0., Lake Texcoco and Zumpango, Cuenca R. Moctezuma, RH Pánuco (RH26Dp) / Red hidrográfica. Escala 1:50,000. Edición 2.0., Lago de Texcoco y Zumpango, Cuenca R. Moctezuma, RH Pánuco (RH26Dp), 2010. Accessed November 29, 2020. https://www.inegi.org.mx/temas/hidrografia/.

[15] Mexican Institute of Water Technology / Instituto Mexicano de Tecnología del Agua (IMTA). National Council for Science and Technology / Consejo Nacional de Ciencia y Tecnología (CONACYT). *Diagnosis and proposals for the management of water resources in the four sections of the Chapultepec forest* / *Diagnóstico y propuestas para la gestión de los recursos hídricos en las cuatro secciones del bosque de Chapultepec*, 2022.

[16] Chow, V. T. *Open Channel Hydraulics* / *Hidráulica de Canales Abiertos*. Bogotá, Colombia, McGRAW-HILL INTERAMERICANA, 2004.

[17] National Water Commission / Comisión Nacional del Agua (CONAGUA). Mexican Institute of Water Technology / Instituto Mexicano de Tecnología del Agua (IMTA). *Programs against hydraulic contingencies by river basin organizations and for the country's main cities (Stage 1)* / *Programas contra contingencias hidráulicas por organismos de cuenca y para las principales ciudades del país (Etapa 1)*, 2015.

[18] Soriano, J. C. *Evaluation of Criteria for Dragging People due to Floods in Urban Areas* / *Evaluación de los Criterios de Arrastre de Personas por Inundaciones en Zonas Urbanas*. Master thesis. National Autonomous University of Mexico, Mexico City, Mexico, 2018.

[19] EFE. "The Average Mexican Measures 1.64 Meters and Weighs 74 Kilos: Study." / "El Mexicano Promedio Mide 1.64 Metros y Pesa 74 Kilos: Estudio." *El Universal*, March 7, 2012. Accessed April 21, 2021. https://archivo.eluniversal.com.mx/notas/828544.html.

Simulation Study of a Double-Acting Hydraulic Cylinder with Shock Absorber

Dr. eng. **Tiberiu AXINTE**[1,*], Dipl. Eng. **Lidia CALANCEA**[1], Dr. mat. **Elena CURCA**[1], Dipl. Eng. **Mihai DIACONU**[1], Dipl. Eng. **Camelia PASCU**[1]

[1] Research Center for Navy, Romania

*tibi_axinte@yahoo.com

Abstract: *This paper focuses on the efficiency of the double-acting hydraulic cylinders with shock absorber at stroke end. In the present work, the simulation of two hydraulic circuits and an electro-hydraulic circuit with double-acting cylinders with shock absorber is studied. Thus, the first hydraulic circuit is made of the following components: tank, throttle check valve, 4/2-way hand lever valve with spring, filter, fixed displacement pump, and double-acting cylinder with shock absorber at stroke end (Dacs 1-1). The second hydraulic scheme has the following devices: pump unit, throttle valve, 4/3-way hand lever valve, and two double-acting cylinders with shock absorber at stroke end (Dacs 2-1 and Dacs 2-2). The third circuit studied is an electro-hydraulic scheme. The last scheme is made of the following components: tank, 4/3-way solenoid valve, nozzle, relay, valve solenoid, lamp, capacitive proximity switch, and double-acting cylinder with shock absorber (Dacs 3-1).*

Keywords: *Hydraulic, cylinder, shock, stroke, tank*

1. Introduction

Some hydraulic systems are equipped with double-acting cylinder with shock absorber at stroke end. Such systems are used in various fields of activity: telescopic hydraulic cylinders at trucks, metallurgical equipment, mining industry, military grade hydraulic cylinders, marine and shipyard use [1].
A double-acting hydraulic cylinder is built in two versions:

a) Without shock absorber.
b) With shock absorber.

Although the second option is more expensive, the quality is much better than the first option.
In the hydraulic actuator, the piston of the cylinder is controlled by the connected pressure loads. Also, the shock absorber can be adjusted by means of two adjustment screws [2].
Usually, a double-acting cylinder with shock absorber at stroke end used to stop a moving load smoothly and slowly. Such a model of hydraulic cylinder (OEM 48511-26040) was used at telescopic shock absorber for car (e.g. Toyota HiAce), Fig. 1.

Fig. 1. A double-acting cylinder with shock absorber

In these manuscript, the parameters of the hydraulic cylinders are presented in Table 1.

Table 1: The components from first scheme

Parameters	Value	Unit
Piston diameter	0.5	m
Piston rod diameter	0.4	m
Piston position	0.8	m
Coulomb friction force	5000	N
Break-away force	5000	N
Moving mass	10	kg
Damping length	0.05	m

In the design of hydraulic circuits, a double-acting cylinder with shock absorber at stroke end has a specific symbol, Fig. 2.

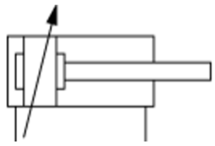

Fig. 2. Symbol of a double-acting cylinder with shock absorber

2. Simulation of a double-acting cylinder with shock absorber

The operation of a hydraulic and electro-hydraulic working circuit involves a continuous flow agent (oil) transported by the pump at certain values of the working pressure [3].
The layout of the circuits that have the double-acting cylinders with shock absorber at stroke end gives the hydraulic system high energy efficiency. Therefore, these schemes improve the internal instability of traditional hydraulic circuits [4].
First, hydraulic circuit made in this paper is designed as a simple scheme using only one double-acting cylinder with shock absorber at stroke end, Fig. 3.

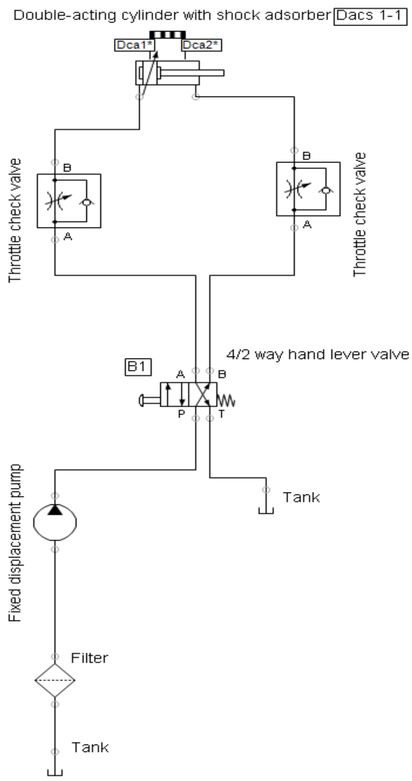

Fig. 3. Hydraulic circuit with a double-acting cylinder (Dacs 1-1)

In the first hydraulic circuit, operator must press the B1 button belonging to the 4/2-way hand lever valve with spring. Then, the piston rod moves from point Dca*1 to point Dca*2, Fig. 4.
After operator stops pressing the B1 button, the piston rod returns, because the 4/2-way hand lever valve has a spring, Fig. 4.

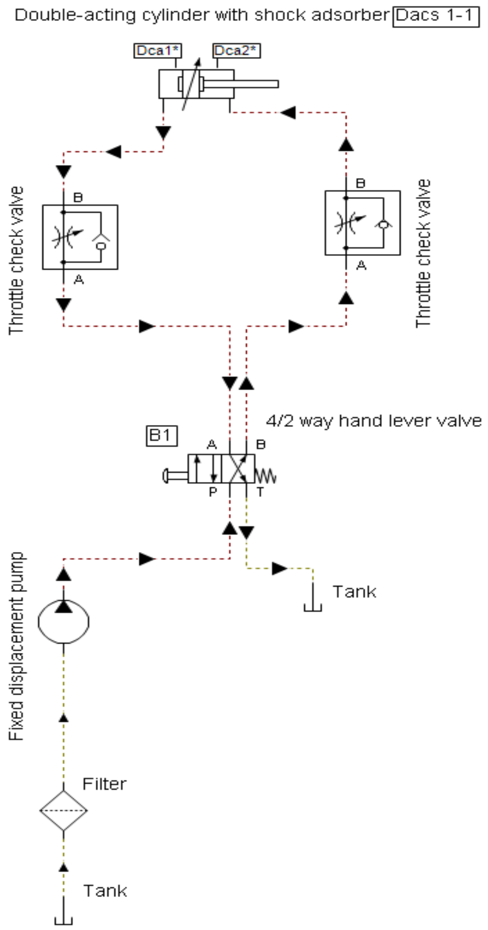

Fig. 4. Hydraulic circuit with a double-acting cylinder (Dacs 1-1). Simulation

The components which belong to the first hydraulic circuit are presented in the table below.

Table 2: The components from first scheme

Description	Number of components
Tank	2
Throttle check valve	2
Double-acting cylinder with shock absorber (Dacs 1-1)	1
4/2 way hand lever valve with spring	1
Filter	1
Fixed displacement pump	1

The diagrams show variation of the operating parameters of the double-acting cylinder with shock absorber at stroke end (Dacs 1-1). These operating parameters are: distance, velocity, and acceleration, Fig. 5.

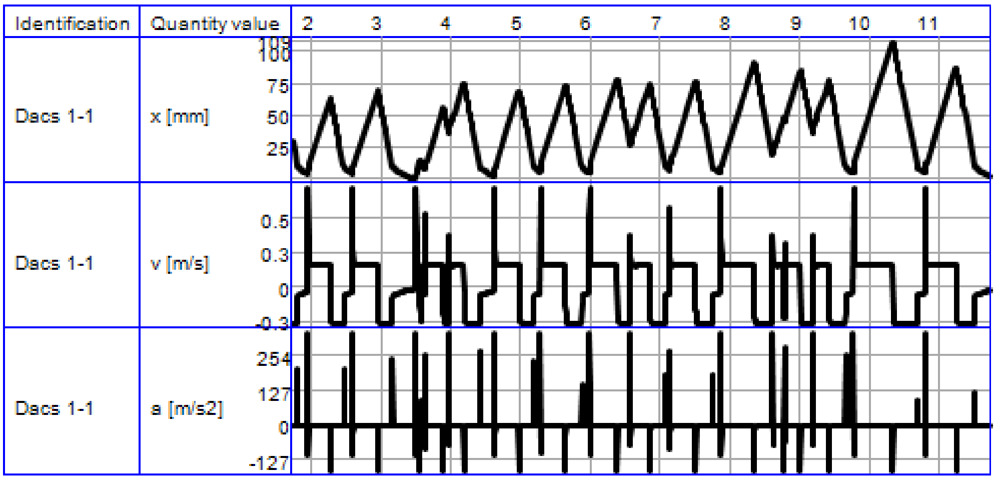

Fig. 5. Diagrams of the double-acting cylinder (Dacs 1-1)

Likewise, the second hydraulic circuit has two double-acting cylinders with shock absorber at stroke end (Dacs 2-1 and Dacs 2-2), Fig. 6.

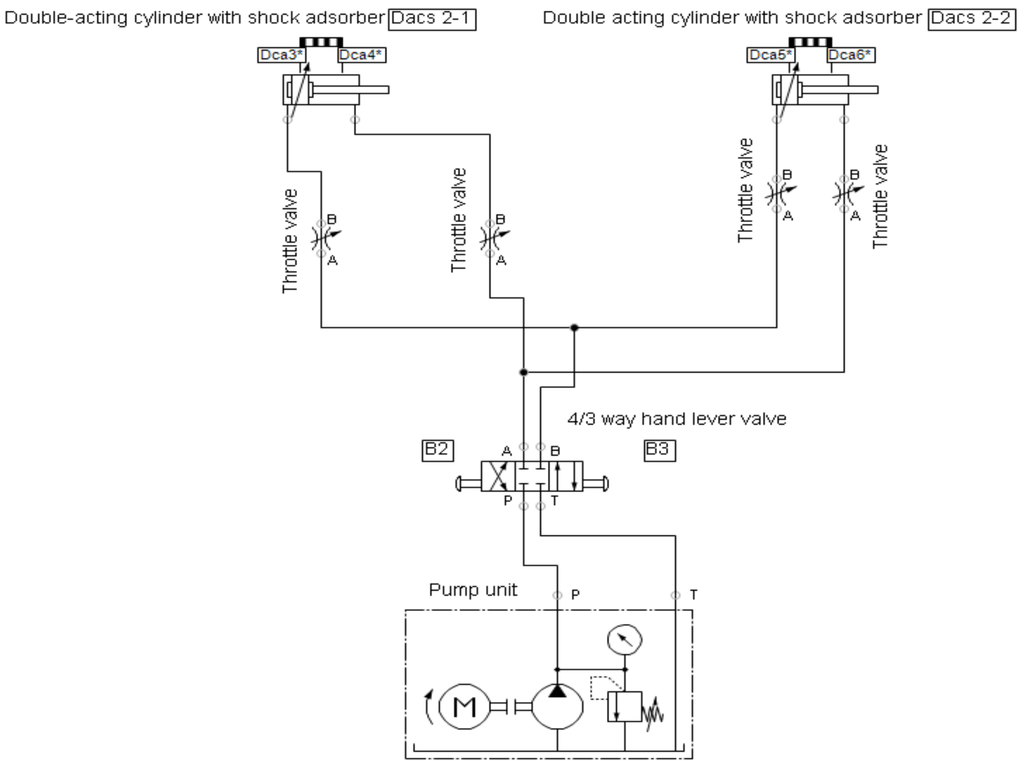

Fig. 6. Hydraulic circuit with double-acting cylinders (Dacs 2-1 and Dacs 2-2)

If operator presses the B2 button, then both piston rods of the double-acting cylinders (Dacs 2-1 and Dacs 2-2) move at the same; namely, the piston rod of the double-acting cylinder (Dacs 2-1) moves from point Dca3* to point Dca4*, and respectively the piston rod of the double-acting cylinder (Dacs 2-2) moves from point Dca5* to point Dca6*, Fig. 7.

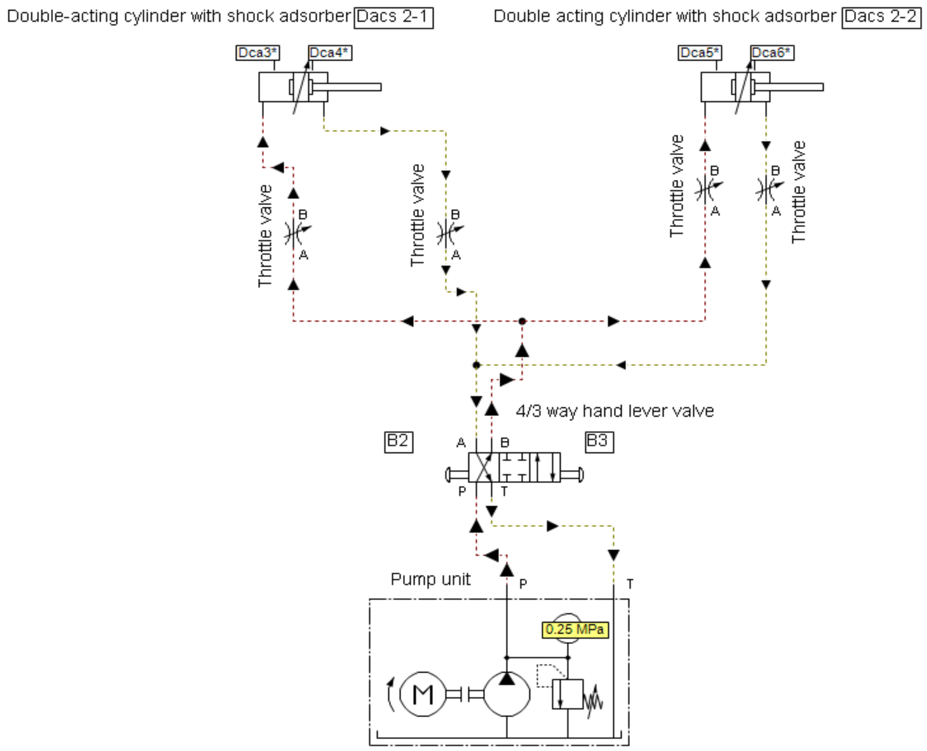

Fig. 7. Hydraulic circuit with double-acting cylinders. Simulation 1

But, if operator presses the B3 button, the piston rod of the double-acting cylinder with shock absorber (Dacs 2-1) returns from Dca4* to point Dca3*. Simultaneously, the piston rod of the double-acting cylinder with shock absorber (Dacs 2-2) returns from Dca6* to point Dca5*, as in second simulation, Fig. 8.

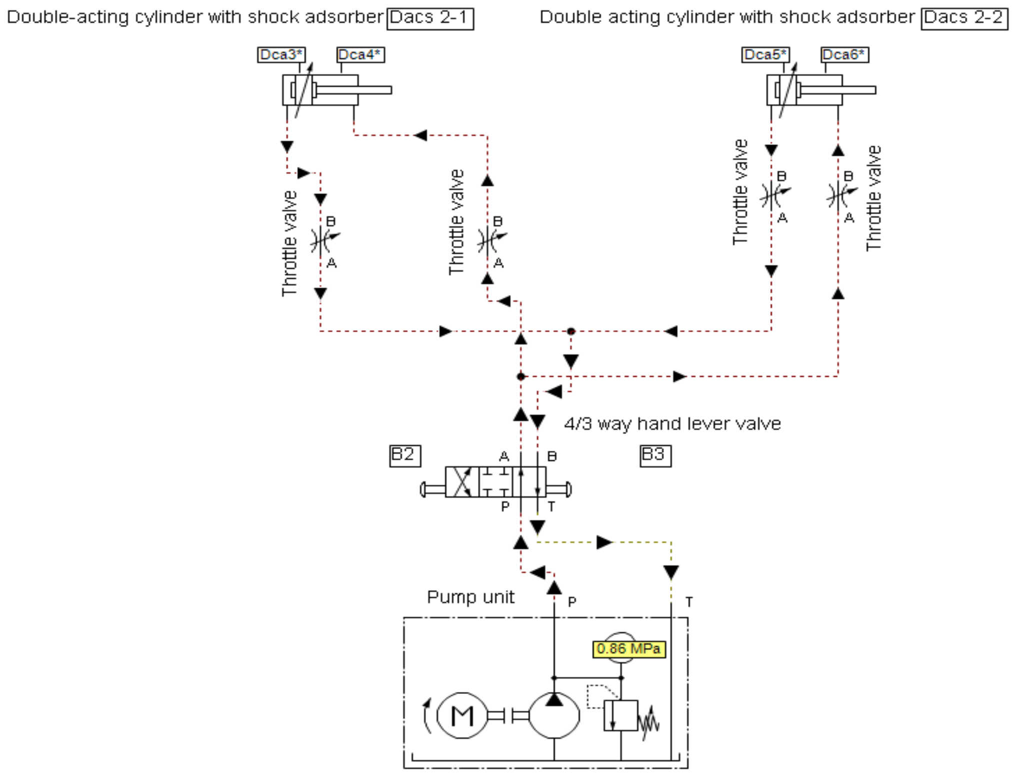

Fig. 8. Hydraulic circuit with double-acting cylinders. Simulation 2

Table 3 below shows six component devices used in the hydraulic scheme.

Table 3: The components from second scheme

Description	Number of components
Pump unit	1
Throttle valve	2
Double-acting cylinder with shock absorber (Dacs 2-1and Dacs 2-2)	2
4/3 way hand lever valve	1

Finally, an electro-hydraulic scheme that has a double-acting cylinder with shock absorber at stroke end is presented, Fig. 9.

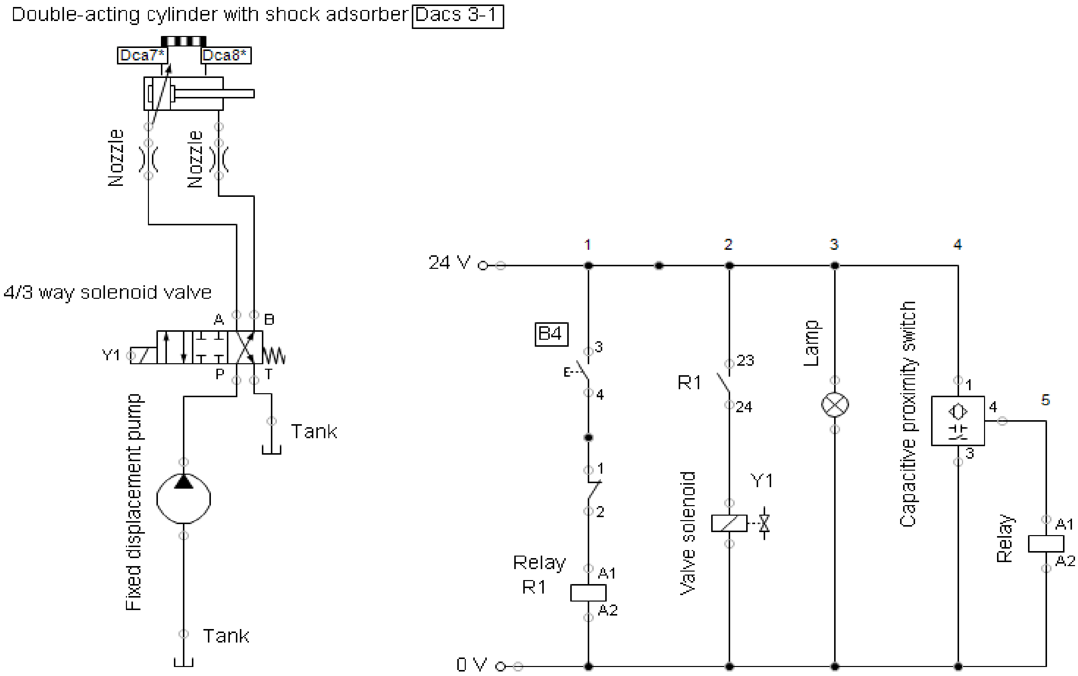

Fig. 9. Electro-hydraulic circuit with a double-acting cylinder

Table 4 below shows twelve component devices used in the hydraulic scheme, [5].

Table 4: The components from third scheme

Description	Number of components
Tank	2
Fixed displacement pump	1
Double-acting cylinder with shock absorber (Dacs 3-1)	1
4/3-way solenoid valve	1
Nozzle	2
Relay	2
Valve solenoid	1
Lamp	1
Capacitive proximity switch	1

Further, when operator presses the B4 button, the piston rod from double-acting cylinder with shock absorber (Dacs 3-1) moves from point Dca7* to point Dca8*.
In addition, a lamp shows a blue signal, Fig. 10.

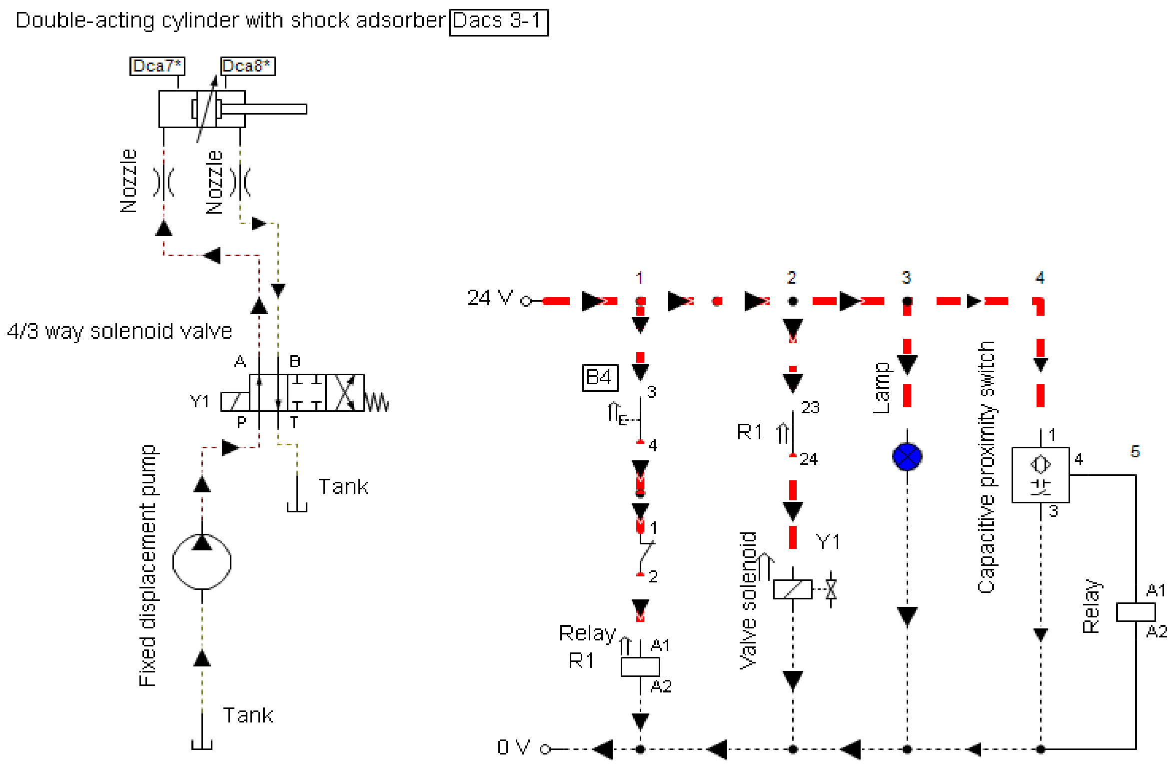

Fig. 10. Electro-hydraulic circuit with a double-acting cylinder. Simulation

The most commonly used actuators for pneumatic drives are cylinders (single acting and double acting). There are many applications that require a turning or twisting movement of up to 360 degrees. Only semi-rotary drives can be used for these pneumatic applications.

3. Conclusions

In fact, the double-acting cylinders with shock absorber at stroke end are actuators that are used in simulation of hydraulic and also electro-hydraulic installations.
Some benefits of the double-acting cylinder with shock absorber at stroke end:

- Safety in operation of double-acting cylinder.
- Faster reaction than hydraulic cylinders without shock absorber.
- Suitable for repetitive actions in a short time.
- Applies greater push and pull forces than a single-cylinder.

However, the double-acting cylinders with shock absorber at stroke end are often use for:

- Repetitive actions (e.g. jack and crib applications).
- When very long hoses are required.
- A controlled retraction time.
- Strong pushing and pulling uses.

In the future, we plan to develop electro-hydraulic schemes using double-acting cylinders with shock absorber at stroke end for research and education.

Acknowledgements

We wish to thank Professor dr. eng. Panaitescu Viorel of the Constanta Maritime University, for his unwavering guidance and support in the preparation of this paper.

References

[1] Blejan, Marian, Iulian Dutu, Ioana Ilie, Petrin Drumea, and Mircea Comes. “Electronic intelligent module for a hydraulic briquetting press.” Paper presented at the 31st International Spring Seminar on Electronics Technology ISSE 2008, Budapest, Hungary, May 7-11, 2008.
[2] Bârsan, Ghiță, Vasile Năstăsescu, and Vlad-Andrei Bârsan. “Simulation and gamification in e-learning technical courses.” Paper presented at the 23rd International Scientific Conference – The Knowledge-Based Organization (KBO), Sibiu, Romania, June 15-17, 2017.
[3] Voicu, Ionuț, L. G. Dumitrescu, Viorel Fănel Panaitescu, and Mariana Panaitescu. “Studies on the oil spillage near shorline.” *IOP Conference Series: Materials Science and Engineering* 227 (2017): 012135.
[4] Dumitrache, Constantin Luois, and Dumitru Deleanu. “Water centrifugal pump, design and fluid analysis.” *International Journal of Modern Manufacturing Technologies* 14, no. 3 (2022): 56-61.
[5] Dragan, Cristian, and Costel Stanca. “Development on quality management concepts.” *Constanta Maritime University Annals* 16, no. 2 (2011): 29-32.

ISSN 1453 – 7303 "HIDRAULICA" (No. 1/2024)
Magazine *of Hydraulics, Pneumatics, Tribology, Ecology, Sensorics, Mechatronics*

PWM Drive Method Considerations for Proportional Pneumo-Hydraulic Solenoid Valves

PhD. stud. Eng. **Robert BLEJAN**[1,2,*], PhD.Eng. **Marian BLEJAN**[1],
PhD. stud. Eng. **Alexandru IONESCU**[3,4]

[1] National Institute of Research & Development for Optoelectronics/INOE 2000, Subsidiary Hydraulics and Pneumatics Research Institute/IHP / Romania

[2] National University of Science and Technology Politehnica Bucharest, Doctoral School of Power Engineering / Romania

[3] National Institute of Research and Development for Machinery and Installations for Agriculture and Food Industry – INMA Bucharest / Romania

[4] National University of Science and Technology Politehnica Bucharest, Doctoral School of Biotechnical Systems Engineering / Romania

* robertblejan.ihp@fluidas.ro

Abstract: *The evolution of programmable controllers, PLCs, has allowed the digital approach to hydraulic and pneumatic applications made with proportional devices. Thus, the presence of built-in PWM (Pulse Width Modulation) blocks in most PLCs allows the direct control of the valve coils, using a simple electrical circuit to adapt the digital output of the PLC to the solenoid of the proportional device. This paper presents the calculus of the parameters for PWM drive according to the parameters of the proportional solenoid valve. An original method of increasing the native resolution of the PWM block is also presented.*

Keywords: *PWM drive, proportional solenoid valve, PWM resolution, PLC*

1. Introduction

Pulse width modulation, or PWM, is a way to digitally manipulate the power supplied to a solenoid or other device to increase efficiency. This is done by reducing the amount of power supplied during the portions of the operating cycle that do not require the full supply voltage – fig. 1 [1], [2].
While the solenoid is pushing or pulling a load, the power requirement peaks. The energy required to overcome the inertia of the load is much higher than what is required to hold the load after the plunger is fully seated. When using standard power supply the voltage is constant, so the voltage applied must match the peak power requirement. This means that the full voltage is also being applied through the full operating cycle of the device. PWM allows for the manipulation of power so that the supply can be reduced while the plunger is fully seated.
The PWM circuit modulates power by switching it off and on according to a specified duty cycle at a high frequency. The duty cycle is the ratio of on and off time. This ratio of on and off time creates an average output voltage, which becomes the input voltage for the device. The frequency this cycle is repeated fast enough so that the device does not respond to the on/off switching and instead only responds to the average.

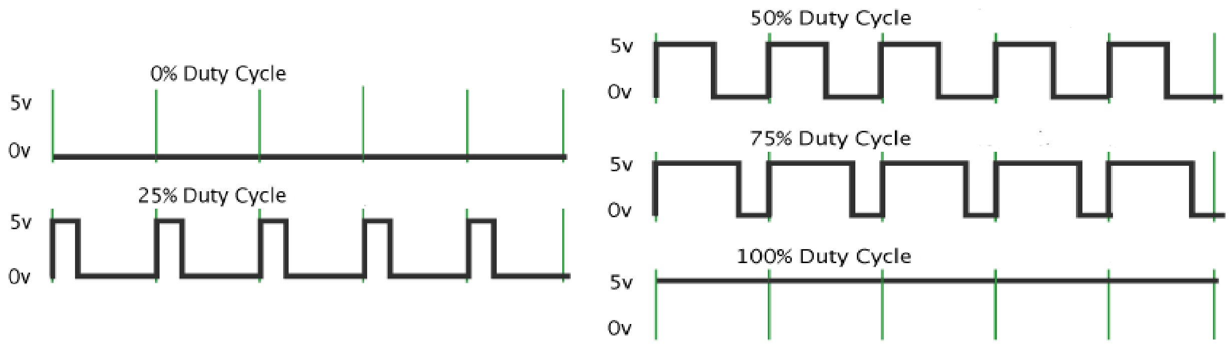

Fig. 1. Waveforms for pulse width modulation

2. Calculus of the parameters for PWM drive

As an example, a proportional relief valve, RZME-A-010 [3] with the following catalog parameters value was chosen:

Coil code	→	option /6, drivers with power supply 12 V_{DC}
Coil resistance at 20^0C	→	2Ω
Maximum solenoid current	→	2.75A
Maximum power	→	30W
Response time 0-100% step signal	→	150ms

The power value dissipated by the coil resistance through the Joule heating is

$$P_{Rmax} = RI_{max}^2 = 2 * 2.75^2 \cong 15W \quad (1)$$

The maximum value of the reactive power that actuates the poppet of the proportional relief valve is

$$P_{max} - P_{Rmax} = 30 - 15 = 15W \quad (2)$$

The maximum value of the magnetic field energy is

$$\frac{1}{2}LI^2 = \frac{1}{2}L2.75^2 \cong 3.8L \quad (3)$$

where L is inductance of the valve solenoid in henry. This magnetic field energy is mainly used to drive the valve poppet.

The maximum value of the power actuating the valve poppet is when valve executes the full pressure step response

$$3.8L/0.15 = 15 \;\Longrightarrow L \cong 0.6H \quad (4)$$

Fig. 2 shows the electrical diagram of the signal conditioner between the digital output of the PLC and the solenoid of the hydraulic device. This circuit was simulated in Ltspice® [4] to validate the calculation of the PWM parameters.

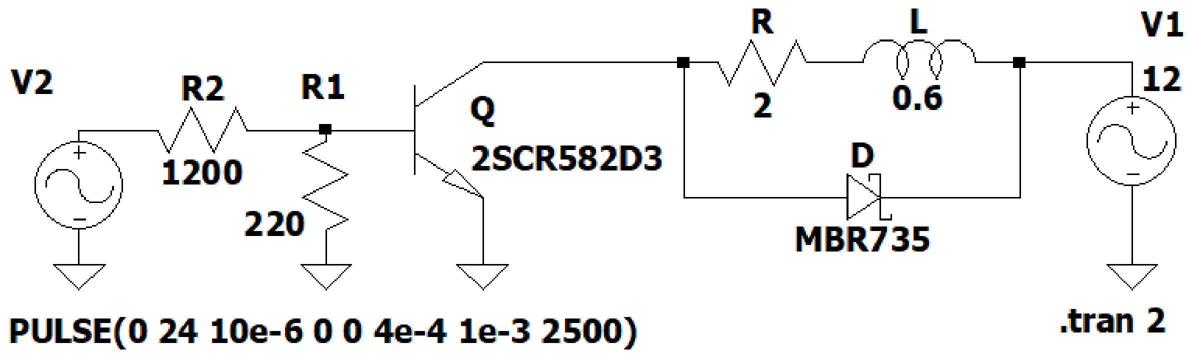

Fig. 2. SPICE model for signal conditioner

The voltage drop equation for the conduction interval T_{on} of the transistor is

$$V1 = RI + L\frac{\Delta I}{T_{on}} \quad (5)$$

Similarly for the blocking interval $T - T_{on}$ of the transistor following results

$$RI = L\frac{\Delta I}{T - T_{on}} \quad (6)$$

From equations (5) and (6) the current ripple value can be calculated

$$V1 = L\frac{\Delta I}{T - T_{on}} + L\frac{\Delta I}{T_{on}} \Leftrightarrow L\frac{\Delta I}{T_{on}} = V1\frac{T - T_{on}}{T} \quad (7)$$

From equations (5) and (7) the current value can also be calculated

$$V1 = RI + V1\frac{T-T_{on}}{T} \Leftrightarrow RI = V1\frac{T_{on}}{T} \tag{8}$$

where $T = 1ms$ is the value of PWM signal period and $V_1 = 12V$.
The values of current and current ripple is

$$\Rightarrow I = \frac{V1}{R}\frac{T_{on}}{T}, dI = V1\frac{T_{on}}{L}\left(1 - \frac{T_{on}}{T}\right) \tag{9}$$

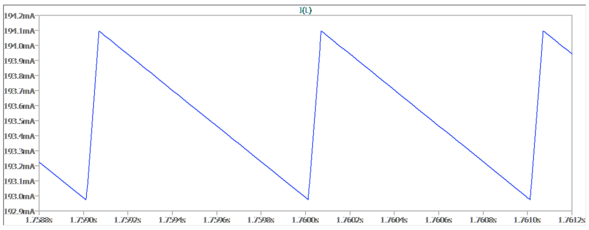

$\frac{T_{on}}{T} = 5\% \Rightarrow dI = 0.95mA\ ;\ I = 0.3A$

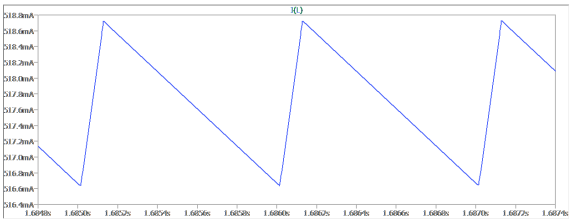

$\frac{T_{on}}{T} = 10\% \Rightarrow dI = 1.8mA\ ;\ I = 0.6A$

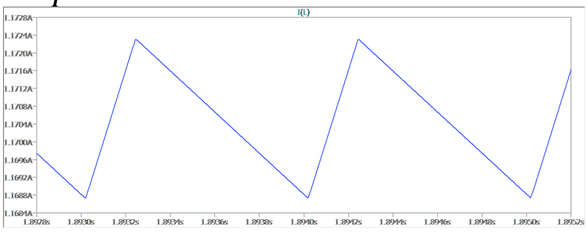

$\frac{T_{on}}{T} = 20\% \Rightarrow dI = 3.2mA\ ;\ I = 1.2A$

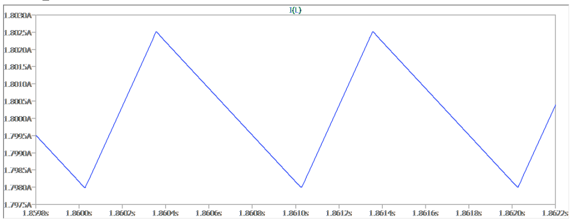

$\frac{T_{on}}{T} = 30\% \Rightarrow dI = 4.2mA\ ;\ I = 1.8A$

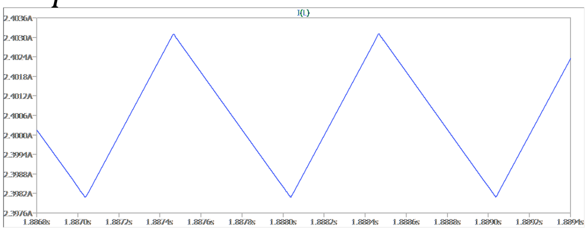

$\frac{T_{on}}{T} = 40\% \Rightarrow dI = 4.8mA\ ;\ I = 2.4A$

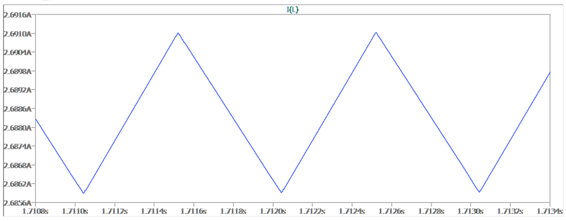

$\frac{T_{on}}{T} = 45\% \Rightarrow dI = 4.95mA\ ;\ I = 2.7A$

Fig. 3. The solenoid valve waveforms of current

Fig. 3 shows the simulated coil current waveforms and the calculated current and current ripple values according to (9).

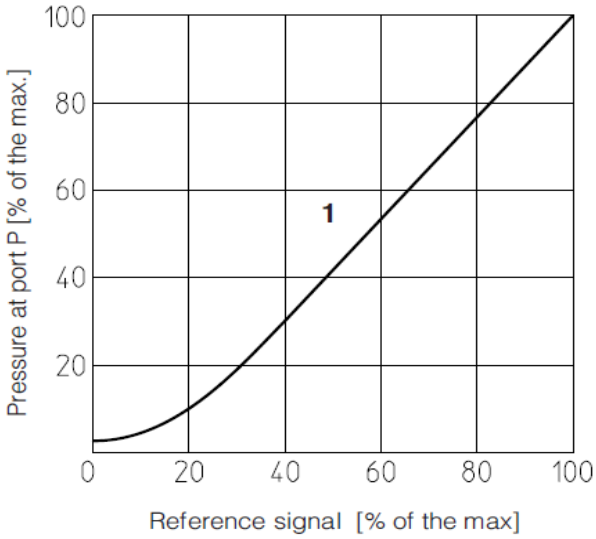

Fig. 4. Proportional relief valve regulation diagram at flow rate Q = 1 l/min

Fig. 4 shows the adjustment diagram for proportional relief valve, RZME-A-010 [3].
It is noted that the variation range of the PWM duty factor must be in the range of 10%...45% to fall within the linear regulation area, fig. 3. This corresponds to the range 20%...100% of the reference signal, fig. 4.

3. Increasing the native resolution of the PWM

A case study will be presented for the previously considered proportional valve RZME-A-010 controlled with a TM221C24T PLC with PNP transistor output [5].
The assumptions are:

- PWM output resolution value for PLC is 1% [Modicon M221 Logic Controller Advanced Functions Library Guide, chapter Pulse Width Modulation (%PWM) at [5]].
- The variation range of the PWM duty factor in the range of 10%...45% to fall within the linear regulation area, see fig. 3 and fig. 4.

Consequently, the PWM resolution is only 45% - 10% = 35 steps of pressure values for the linear control range. In industrial applications, this resolution value is often insufficient. The idea of increasing the PWM resolution is to average multiple periods of the PWM signal, periods that have duty factor values two successive steps from the native resolution values.
For example, the duty factor value of 20.3%, if one wants to increase ten times the 1% native resolution value of the PWM block, it is necessary to produce ten periods, respectively three periods with a duty factor value of 21% and seven periods with a duty factor value of 20%.
Thus, the period of pulses required for averaging the current in the controlled coil will be multiplied ten times. This signal processing is very similar to that of the digital decimation filter [6].

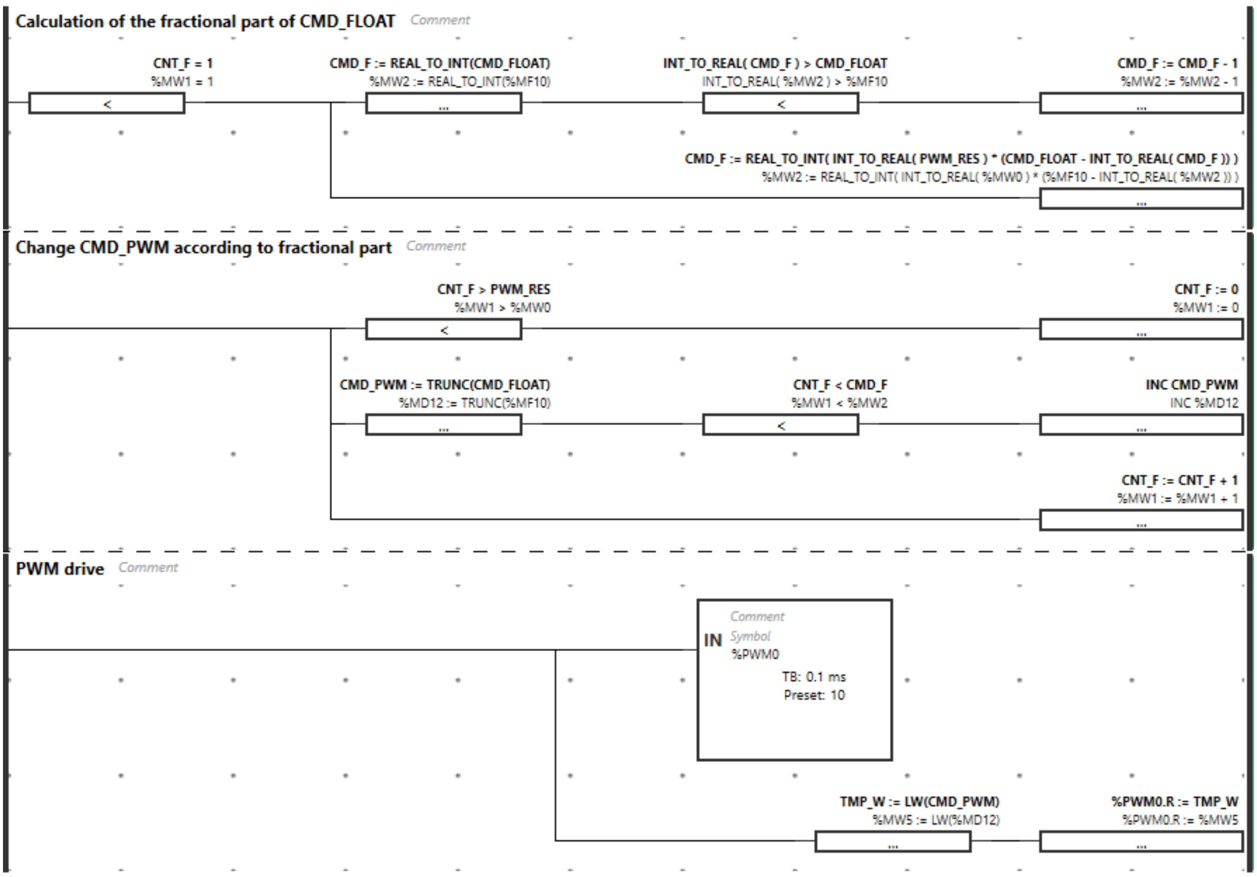

Fig. 5. Increasing the native resolution of the PWM – ladder diagram implementation

Fig. 5 shows the program, in ladder diagram language, that implements the PWM resolution increasing sequence.

4. Conclusion

To achieve adequate electrical control of proportional pneumo-hydraulic devices, a systemic approach is required. Thus, the method of calculating the parameters of the electronic control block based on the catalog parameters of the proportional device has been presented.
Also, if the native resolution of the built-in PWM block in the PLC is too small, a method to increase its original resolution has been proposed.

Acknowledgments

This work was carried out through the Core Program within the National Research Development and Innovation Plan 2022-2027, carried out with the support of the Romanian Ministry of Research, Innovation and Digitalization (MCID), project no. PN 23 05. The research was financially supported by a project funded by MCID through Programme 1 – Development of the national research & development system, Sub-programme 1.2–Institutional performance–Projects financing the R&D&I excellence, Financial Agreement no. 18PFE/30.12.2021.

References

[1] Magnet-Schultz of America. Accessed March 3, 2024. https://magnet-schultzamerica.com/.
[2] Sun, Jian. "Pulse-Width Modulation." In: Vasca, F., and L. Iannelli (eds.). *Dynamics and Control of Switched Electronic Systems*. *Advances in Industrial Control*. London, Springer, 2012.
[3] Atos S.P.A. Accessed March 3, 2024. https://www.atos.com.
[4] Analog Devices, Inc. Accessed March 3, 2024. https://www.analog.com/en/resources/design-tools-and-calculators/ltspice-simulator.html
[5] Schneider Electric. Accessed March 3, 2024. https://www.se.com.
[6] National Instruments Corp. "Decimation (Digital Filter Design Toolkit)". *LabVIEW Digital Filter Design Toolkit API Reference*, March 14, 2023. Accessed March 3, 2024. https://www.ni.com/docs/en-US/bundle/labview-digital-filter-design-toolkit-api-ref/page/lvdfdtconcepts/dfd_decimation.html.

Environmental Risk Assessment and Analysis for Nuntaşi Hydrographic Basin

Dr. Eng. **Mariana PANAITESCU**[1,*], Dr. Eng. **Fănel-Viorel PANAITESCU**[1],
Senior Lecturer Dr. Eng. **Ionuț VOICU**[1], PhD student Eng. **Aurelia-Florentina VASILICA**[2]

[1] Constanta Maritime University, Faculty of Naval Electro-Mechanics, Romania

[2] Doctoral School of Energy Engineering, National University of Science and Technology POLITEHNICA, Bucharest, Romania

* panaitescumariana1@gmail.com

Abstract: *The way of approaching the flood hazard in the Dobrogea Hydrographic Area consists in a first phase in the grouping of registered water courses on three levels of detail according to the frequency of floods in recent years, their amplitude, the form of manifestation, the degree of equipping with works of defence against floods, social or economic objectives subject to flood hazard. The causes of these floods were the amounts of precipitation from torrential rains recorded in a certain period of time. Due to the flood waves, the danger levels were exceeded, some sectors of the permanently flowing watercourses were flooded. In Nuntași, between 02.09-04.09.1999, the flood produced on the Nuntaşi river destroyed houses, cultures, lives, etc. The assessment of the water resources in this basin consists in the assessment of the hydrographic and hydrogeological basins, which together form the reception basin. surface, shape, hypsometric curve and average altitude of the basin, average slope, vegetation cover, hydrogeological basin, hydrograph, rainfall hyetogram, etc.) The risk analysis of the NUNTAȘI hydrographic space consists in the measurement and quantification of 4 parameters using the RkFMEA method (RisK Failure Mode Evaluation Analysis): vulnerability (exposure) (R), probability (P), the effect of the existence of a control instrument/measure/control/action (N) and the efficiency indicator of a new measure (F). The simple risk level (RPN factor) and the efficiency factor F (complex risk level, RPNF) were automatically calculated. The conclusion of the risk analysis was: the NUNTAȘI bed falls under "low risk with serious prevention measure without any urgent implementation with RPNF values between (1...150)".*

Keywords: *Risk, environment, assessment, analysis, basin, vulnerability, probability, control, level, measure*

1. Introduction

The risk factors for the NUNTAȘI hydrological basin are floods and anthropogenic pollution.
One of the risk factors is *flooding.* The way of approaching the flood hazard in the Dobrogea Hydrographic Area consists in a first phase in the grouping of registered water courses on three levels of detail according to the frequency of floods in recent years, their amplitude, the form of manifestation, the degree of equipping with works of defence against floods, social or economic objectives subject to flood hazards, etc. (Fig. 1) [1]: level A – very detailed; level B – detailed; level C. The Nuntași Basin - Nuntași locality, the Nuntași Basin - Fântanele locality were analysed. From the point of view of the structural measures, costs are imposed regarding the regularization of the bed on the urban section Nuntași-Fântanele and costs for the regularization of the bed on the urban section Nuntași-Nuntaşi Basin, which have as their final goal the avoidance of loss of human life [2]. The causes of these floods were the amounts of precipitation from torrential rains recorded in a certain period of time. Due to the flood waves, the danger levels were exceeded, some sectors of the permanently flowing watercourses were flooded (Fig. 2) [3]. In Nuntași, between 02.09-04.09.1999, the flood produced on the Nuntaşi river destroyed houses, cultures, lives, etc.
Another risk factor is *anthropogenic pollution*. Human activities lead to alterations in the riverbed morphology and dynamics to change its hydraulics. Aspects should be considered amending the short term (dams, bridges, erosion, etc.) and long term (changes generated by the embodiment Management work) [3].

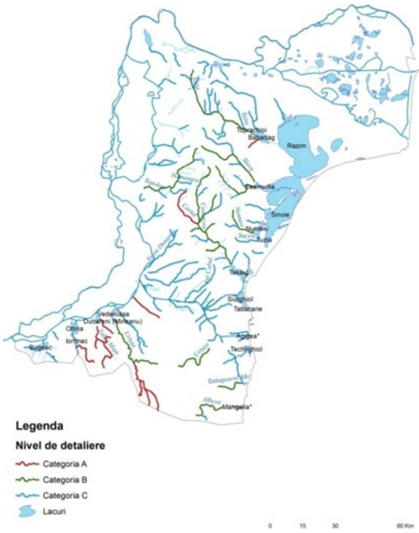

Fig. 1. Map of the hydrographic network Dobrogea Water Basin Administration [2]

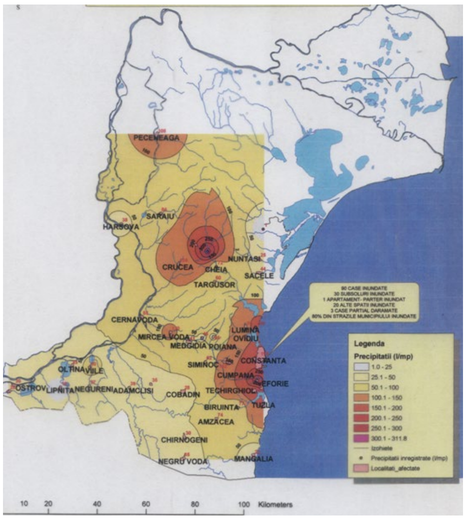

Fig. 2. Map with isohyets resulting from the hydro meteorological phenomena of August 2004 [3]

Due to the flood waves, the danger levels were exceeded, some sectors of the permanently flowing watercourses were flooded.

2. Material and methods

In this work we propose to present the flood produced on the Nuntași river and risk analysis for this case study (Fig. 3) [2].

Fig. 3. Flood bed Nuntași [2]

Considering the flood risk situation, in order to overcome the damage caused by the overflowing of the river, it was considered that the most suitable option, for the Nuntași Basin area - Fântanele locality (Fig. 4) [2] is the execution of a covered trapezoidal section, because this option offers a high degree of naturalness and integration of the works in the environment compared to the possibility of channelling the water course on urban land.

Fig. 4. Nuntași Basin - Fântanele locality [2]

This option implies a slight increase in the occupied area, in an area subject to intense human pressure, and a dramatic process of regression of natural values.
For the Nuntași Basin area - Nuntași locality (Fig. 5) [2], the flow of the river increases dramatically as a consequence of torrential rains. As a result of this circumstance, floods occur that cover large areas on both banks, because the size of the current water course does not have enough capacity to evacuate the maximum flow that comes along the course. This fact causes the water to flow to the areas adjacent to the channel, leading to overflow and flooding (flood), causing damage to agriculture, urban and industrial areas and people's lives. To overcome the damage caused by the overflowing of the river, the execution of a covered trapezoidal section was considered as the most suitable option [4], [1].

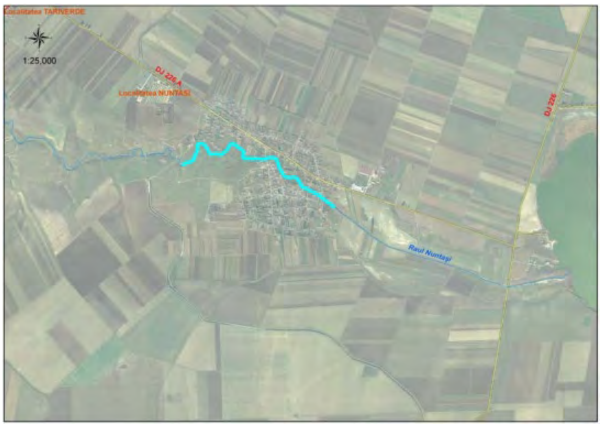

Fig. 5. Nuntaşi Basin - Nuntași locality [2]

From the point of view of the structural measures, costs are imposed regarding the regularization of the bed on the urban section Nuntași-Fântanele and costs for the regularization of the bed on the urban section Nuntași-Nuntaşi Basin, which have as their final goal the avoidance of loss of human life [3].
Human activities lead to the alteration of the morphology of the bed, as well as to the modification of its hydraulic dynamics. Both short-term and long-term change aspects must be considered. Among the short-term aspects, we mention: changes in local sections as a result of constructions in the riverbed (dykes, bridges, etc.), or major changes generated by materials resulting from erosion, transported by currents and randomly deposited. Among the long-term aspects, we

mention the changes generated by the way the landscaping works are carried out. The flood on the Nuntași river either destroyed human settlements, cultures, or bypassed the damming works upstream and spilled over the road, the situations being repeatable (in 2004 and 2007).

2.1 The assessment of the water resources in Nuntași basin

2.1.1. Catchment

In the case of Nuntași Basin, it includes the Nuntaşi River and Nuntași Lake (Fig. 6) [5,6].

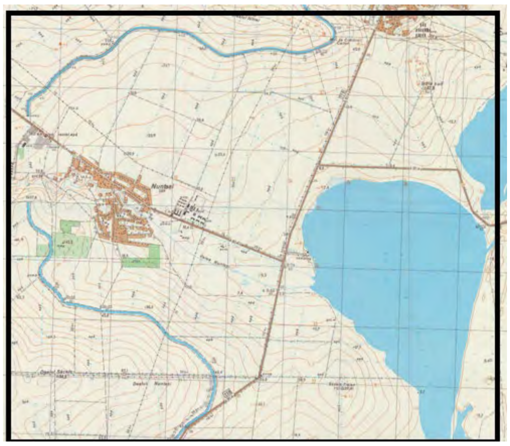

Fig. 6. The hydrographic basin-delimitation on the map

- *Catchment area*

Catchment area is expressed in km^2 or ha. Nuntaşi Basin has an area F = 145 km^2.

- *Form of the basin*

It can be stated with some approximations in a regular geometric shape and quantified by (Fig. 7) [5]:

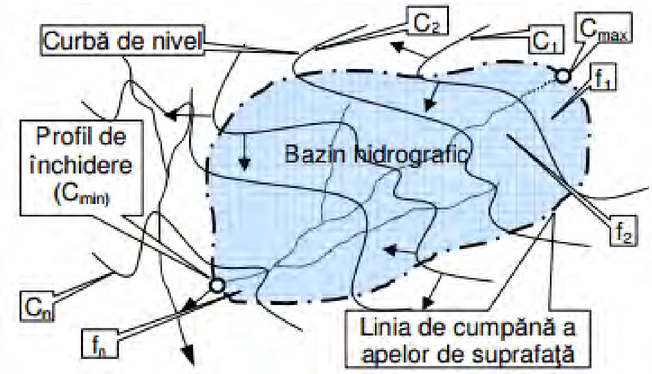

Fig. 7. The hydrographic basin-delimitation on the map

- average width of the river basin B (eq. 1) is B = 10,357 km;

$$B = F / \lambda \tag{1}$$

- basin shape coefficient (β) (deviation from circular shape) (eq. 2) is β = 0.364,

$$2\,\beta = 4\pi\, F / L^2 \tag{2}$$

Where L- the total length of the surface water balance line that delimits the watershed.

- hypsometric curve and average altitude basin (Fig. 8) [6].

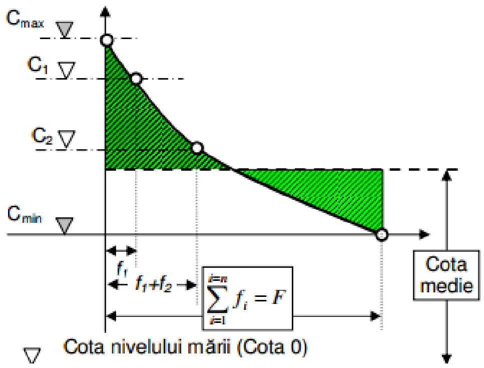

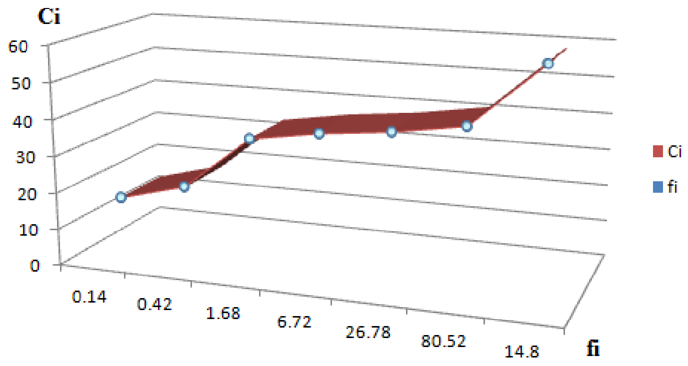

Fig. 8. Hypsometric curve of Nuntaşi basin

Hypsometric curve allows rapid assessment of the average river basin and areas that are above or below certain levels.

- *The average slope of the basin*

Average slope of the basin (i) is estimated based on the slope between each two consecutive contours (eq. 3) and is:

$$\bar{i} = \frac{\sum_{k=1}^{k=n} i_k \cdot f_k}{F} = \frac{\sum_{k=1}^{k=n} \frac{C_k - C_{k-1}}{b_k} \cdot f_k}{F} \tag{3}$$

where C_k - elevation of the k level curve; b_k - the average width between the level curves C_k and C_{k-1}; f_k - the surface of the hydrographic basin between the level curves C_k and C_{k-1}; F - total area of the hydrographic basin. So,

i_{med} = (0.028+0.100+0.080+0.214+0.966+1.00)/145=0.0165.

- *The coating plant of the river basin*

Is expressed through afforestation (α_p) of the river basin (eq. 4)

$$\alpha_p = \frac{F_p}{F} \tag{4}$$

and equals α_p = 0.1.

2.1.2. Hydrogeological basin

The hydrogeological basin represents the aquifer domain (underground), simple or complex, in which groundwater flows to the same surface drainage element, which can be a water course or a line of springs. The correct assessment of the flow regime of water courses is mainly determined by the knowledge of two categories of information:

- morphometry of the hydrographic network;
- hydrometry of the hydrographic network.

The morphometric characteristics of the hydrographic network are expressed by:

- the transverse profile of the bed (Fig. 9) [3, 6];
- the longitudinal profile of the bed (Fig. 10) [3, 6];
- the density of the hydrographic network (Table 1).

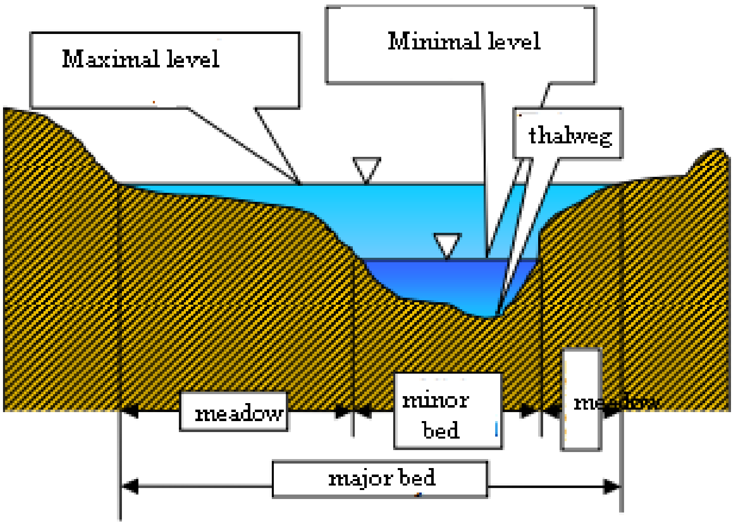

Fig. 9. Transverse profile through the bed of a river

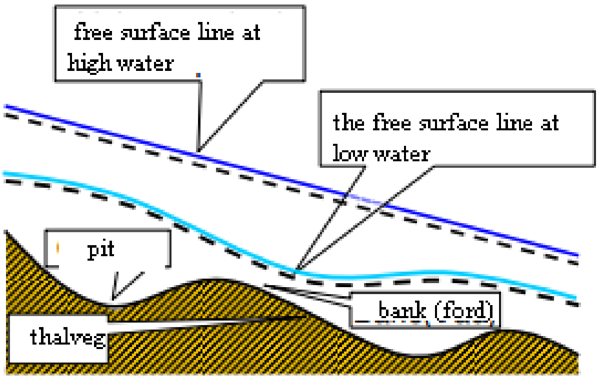

Fig. 10. Longitudinal profile through the bed of a river

Table 1: The characteristics of the Nuntași basin [7]

River	L (km)	Total Volume (mil.m3)	S (km2)	Alt (mdM)	Q_{medma} (m3/s)	$Q_{minlmedma\ asig}$ 80% (m3/s)	$Q_{minlmedma}$ asig 90% (m3/s)	$Q_{minlmedma}$ asig 95% (m3/s)	Q^{min}/Q_{max*}
Nuntași	14	9.3	145	10	0.473	0.280	0.200	0.140	1/2250

2.2 The Nuntași Hydrography Basin

- *Unitary hydrograph*

The unit hydrograph can be defined as the flood hydrograph produced by an excess of precipitation equal to 1 mm, precipitation reaching the drain, or more briefly is the direct runoff hydrograph resulting from an effective (net) rainfall of a unit layer produced on a basin homogeneously in a given time. In order to determine the characteristic elements of a unitary hydrograph, several methods have been developed: the Snyder method, the US Soil Protection Service method, the Gray method [8].
For the construction of the hydrograph, a 14-hour rainfall forecast was received from 28.06.2007 on the Nuntași hydrographic basin (Fig. 11, Table 2) [3, 9, 10].

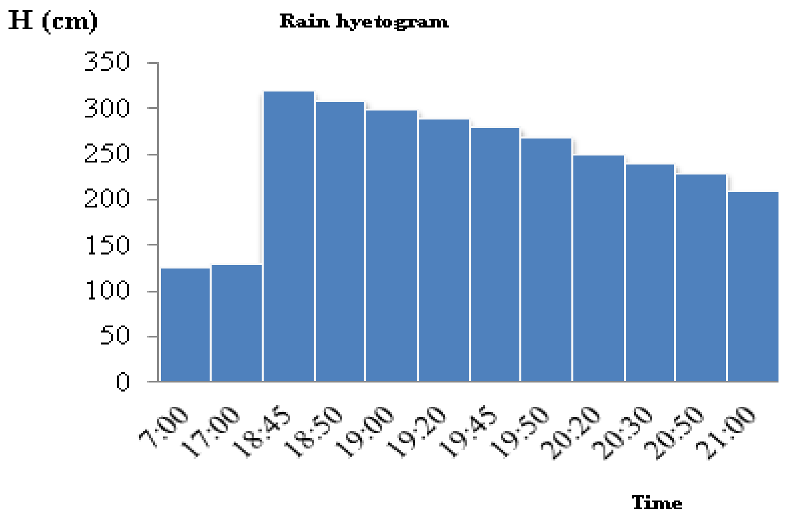

Fig. 11. Hyetogram of precipitation from the Nuntași basin

Table 2: Rainfall intensity in the Nuntași basin [2]

Date	Time	H (m)
27/ 06/ 2007	17:00	1.26
28/ 06/ 2007	7:00	1.26
28/ 06/ 2007	17:00	1.30
28/ 06/ 2007	18:45	3.20
28/ 06/ 2007	18:50	3.10
28/ 06/ 2007	19:00	3.00
28/ 06/ 2007	19:20	2.90
28/ 06/ 2007	19:45	2.80
28.06.2007	19:50	2.70
28/ 06/ 2007	20:20	2.50
28/ 06/ 2007	20:30	2.40
28/ 06/ 2007	20:50	2.30
28/ 06/ 2007	21:00	2.10

To analyze the hydrograph of the flow, the surface of the Nuntași hydrographic basin, F=148 km^2, and the maximum flows shown in the following table are taken into account (Table 3).

Table 3: Flood wave for the NUNTAȘI basin

Date	Time	Q (m3/s)
27/ 06/ 2007	17:00	0.05
28/ 06/ 2007	7:00	0.05
28/ 06/ 2007	17:00	0.08
28/ 06/ 2007	18:45	17

Date	Time	Q (m3/s)
28/ 06/ 2007	18:50	15
28/ 06/ 2007	19:00	14

The flood wave hydrograph, as well as its separation into its basic components (quick runoff, hypodermic runoff, and base runoff) are plotted in Figures 12 and 13 [10].

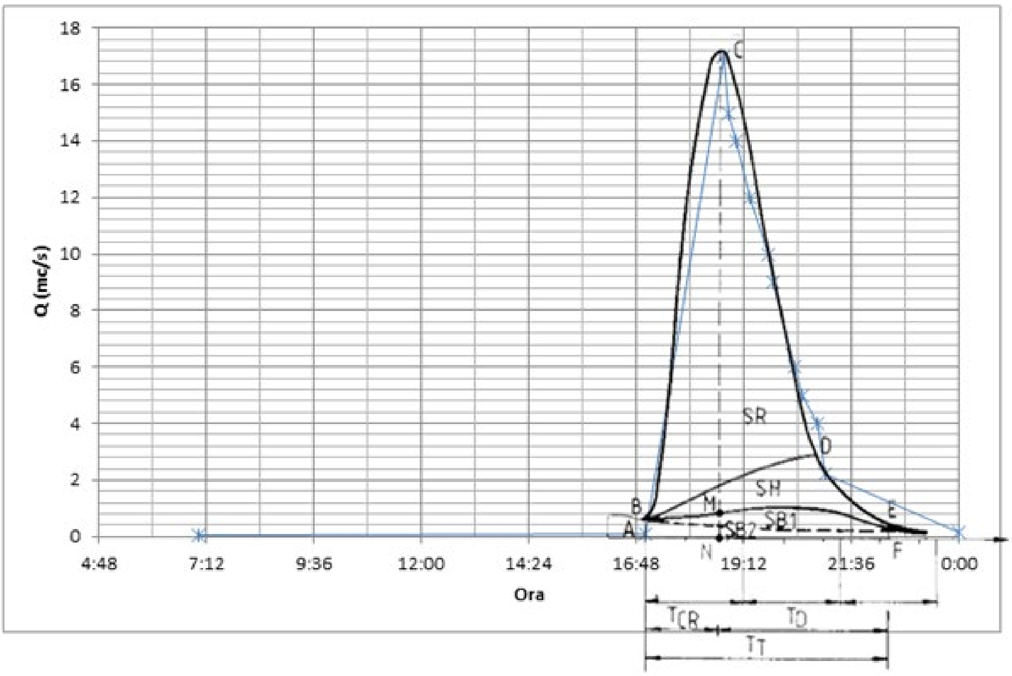

Fig. 12. The flood hydrograph for the NUNTAȘI basin

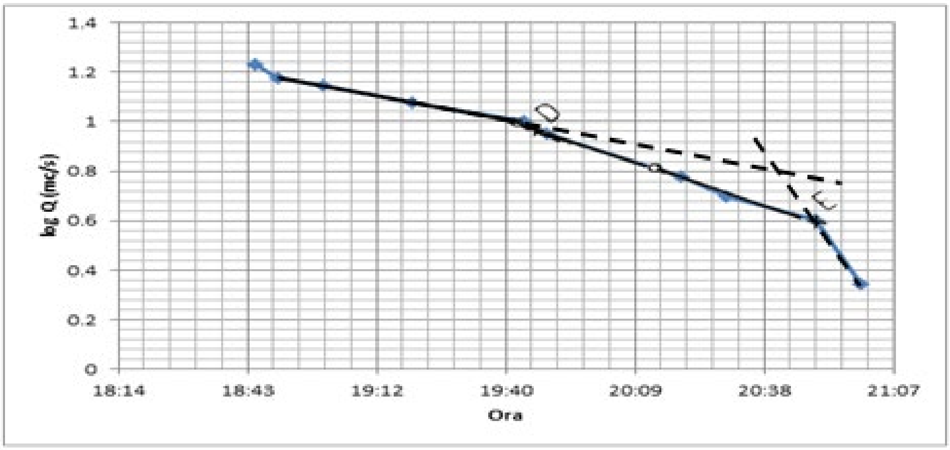

Fig. 13. Descending branch of the runoff hydrograph

The same hydrograph can be constructed with the MIKE 11 program (Figure 14) [3].

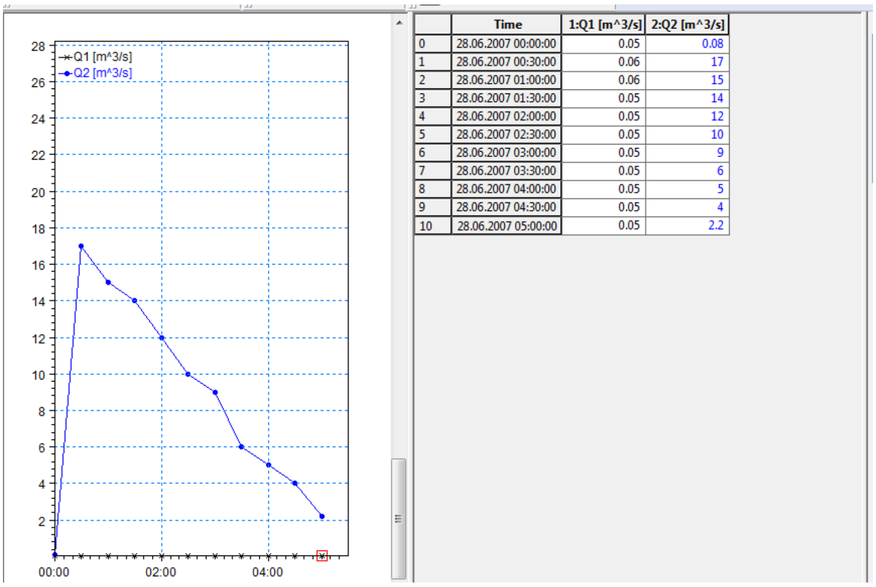

	Time	1:Q1 [m^3/s]	2:Q2 [m^3/s]
0	28.06.2007 00:00:00	0.05	0.08
1	28.06.2007 00:30:00	0.06	17
2	28.06.2007 01:00:00	0.06	15
3	28.06.2007 01:30:00	0.05	14
4	28.06.2007 02:00:00	0.05	12
5	28.06.2007 02:30:00	0.05	10
6	28.06.2007 03:00:00	0.05	9
7	28.06.2007 03:30:00	0.05	6
8	28.06.2007 04:00:00	0.05	5
9	28.06.2007 04:30:00	0.05	4
10	28.06.2007 05:00:00	0.05	2.2

Fig. 14. Flow simulation for two discharge flows at the 2007 level

3. Risk analysis of hydrographic area NUNTAȘI

With the method of analysis of the possibilities of risk RFMEA (failure mode risk evaluation analysis) are measured and quantified four parameters [11], [12], [13], [14]:

- •vulnerability (exposure) (R)
- • the probability (P),
- • the effect of being an instrument of control / measurement / control / share (N)
- • efficiency indicator of a new measure (F).

Vulnerability characterize exposure to risk factors analyzed location. For probability, an event in a year can be classified with another likely in the coming year, when more accurate data are available. The same is true with other factors in the selection process. Next, will be described the means of prevention and protection present actions and active policies. These are defined mainly by preventing complex parameter-control measure (N). The level of risk can be simply determined (RPN), or determined by the efficiency factor F (complex level of risk, RPNF).
Automatic calculation of the level of risk (value RPN) is done by multiplying the three values.
The risk levels based on RPN values are chosen so:

- • High (marked in red) for RPN values> 250;
- • Intermediate (marked in yellow) є RPN values (41 .... 250);
- • Low (marked in green) for RPN values є (1 .... 40).

F factor is automatically calculated by simply comparing the estimate danger in Euro (years for recovery), with estimated budget (years to recover) the measure of prevention (Table 4).
For urban river engineering on the section Nuntași- Basin Fantanele we fit the "prevention budget is higher than the estimated expense" (€ 5,797,003.10 - budget considered and the benefit obtained, € 760.763) [15], so the rate damages / costs is prevention 1.01 (falling between 1 ... 5) and F = 4.
For urban river engineering on the section Nuntași Basin Nuntași- we fit the "prevention budget is higher than the estimated damage" (4.404.135.83 € - budget considered and the benefit obtained, € 698.420), so the rate damages / costs is prevention 1.03 (fall between 1 ... 5) and F = 4.
Complex risk factor values RPNF is set as follows: high risk with prevention measure values greater priority for 1500 (red) (Table 4); environmental risk prevention measure acceptable values between (151 .... 1500) (yellow); low risk prevention measure without any serious urgent deployment of between (1 ... 150) (green).
So we fit at low risk of serious preventive measure without any urgent deployment of between (1 ... 150) (green).

Table 4: Complex risk factor values RPNF

The economic efficiency factor F – costs for damage and prevention	Damage rate/prevention costs	F value
Very high – the estimated damage is considered higher than the prevention budget	>50 1	10
	>20 to 1	9
High – the estimated damage is considered much higher than the prevention budget	10 1	8
	5 to 1	7
Almost equal – the estimated damage is slightly above the prevention budget	2 to 1	6
Equal	1	5
The prevention budget is greater than the estimated damage	1 to 5	4
The prevention budget is considerably high compared to the estimated damage	1 to 20	3
	1 to 100	2
Extraordinarily high prevention costs compared to estimated damages	>1 to 1000	1
Extraordinarily high prevention costs compared to estimated damages	>1 to 1000	1

The analysis offers the possibility of proposing new preventive measures. For each of these, an RPNF is calculated. The highest calculated RPNF value related to a new prevention measure implies the urgent implementation of this proposed new measure.

3. Conclusions

For studying the flow in the Nuntași riverbed eroded with environmental risk were analyzed elements: location and description of the hydrographic area, data sources feeding the aquifer basin data sources feeding the aquifer basin balance flows to the hydrographic area Dobrogea for 1999, 2004, 2007 and 2010, reporting to the climatological normal catchment area Dobrogea; hydro meteorological regime for the guests catchment area reported at Constanta County; morphological and morphometric elements of the bed of the guests; Nuntași riverbed proper flow modeling; risk analysis in the event of floods.

Building the model accordingly to Nuntași basin riverbed assumed the existence of a stage modeling that was done with the program MIKE 11 situation of 2007, to a forecast of rainfall for a period of 14 hours, the hydrograph basin Nuntași, based on the rainfall hyetogram; then simulated the flow along the river, indicating the distribution of speeds of flood related natural hydrograph.

Environmental risk analysis appropriate basin bed Nuntași imposed through some stages of analytical calculation and construction of flood wave hydrograph and its separation into its basic components, and use the same program to raise MIKE 11 hydrographer. It was also required volume calculation flood through plane measuring the S surface hydrograph and surface its basic components and the use method RFMEA (risk failure mode evaluation analysis) to calculate vulnerability, probability, the effect of being an instrument of control / measurement / control / share and efficiency indicator of new measures, the level of risk simple (RPN) and the risk level complex (RPNF), according to F-efficiency factor.

The conclusion of the risk analysis was: Nuntași riverbed fits at "*low risk prevention measure without any serious urgent implementation RPNF with values between (1 ... 150)*".

Following theoretical and experimental findings about river conditions change in response to the liquid phase flows and sediments are:

- Current depth is directly proportional to fluid flow and inversely proportional to the flow of solid material dragged;
- limits the embankments of river bed varies in direct proportion to the flow of liquid and solid material;
- varying flow is directly proportional to the variation solid ratio width / depth;
- slope of the river bed varies in direct proportion to solid and grain alluvial flow and inversely proportional to fluid flow;
- river meanders rate is directly proportional to the variation in relief and inversely proportional to the solid flow.

References

[1] ***. *Plan for the prevention, protection and mitigation of floods effects in the Dobrogea-Seaside hydrographic space / Planul pentru prevenirea, protecţia şi diminuarea efectelor inundaţiilor în spaţiul hidrografic Dobrogea-Litoral*.

[2] http://www.rowater.ro/dadobrogea/Lists/Anunturi1/Attachments/61/PPPDEI-ABADL-ver3.pdf, pp.329-337.

[3] Panaitescu, Mariana. *Hydraulic modeling and evaluation of surface waters with environmental risk / Modelarea hidraulica si evaluarea apelor de suprafata cu risc de mediu*. Constanta, Nautica Publishing House, 2016.

[4] Dobrogea – Seaside Water Basin Administration / Administrația Bazinală de Apă Dobrogea – Litoral. “Flood risk management plan” / “Planul de management al riscului la inundatii”, pp.1-8, 2012. Accessed March 4, 2024. https://dobrogea-litoral.rowater.ro/wp-content/uploads/2021/02/11-PMRI-Dobrogea-Litoral.pdf.

[5] Scradeanu, D., and A. Gheorghe. *General Hydrogeology* - Chap. "Natural factors of groundwater supply and regime" / *Hidrogeologie generală* - Cap. “Factori naturali ai alimentării și regimului apelor subterane”, pp. 1-42. University of Bucharest, 2014.

[6] Archive of the Ministry of National Defense, Socialist Republic of Romania, Military Topographic Directorate / Arhiva M.A.N., R.S.R., Direcţia Topografică Militară, 1981.

[7] National Agency for Environmental Protection / Agenția Națională pentru Protecția Mediului. *Report on the state of the environment in Romania*, Chap. 3. Water / *Raport privind starea mediului în România*, Cap. 3. Apa.

[8] Pătrașcu, S. *Physical assessment of climate impacts on hydrological extremes / Evaluarea fizică a impactului climatic asupra extremelor hidrologice*. Doctoral Thesis Abstract. University of Bucharest, 2008.

[9] Enache, I.A. s*Modeling of the water runoff components from the Dobrogea- Seaside hydrographic basin / Modelarea componentelor scurgerii apelor din bazinul hidrografic Dobrogea-Litoral*. Bachelor thesis, Maritime University of Constanța, 2014.

[10] ***. Hydro-Informatics, Modelling tools MIKE 11, Part 1-Introduction, IHE 2001-2003.

[11] Kanev, V. *System and web application for risk assessment of oil spill in black sea and prevention management – covered hazards and risks, users’ response and further development*. Final Book of IUCRISKMAN project, pp. 22-39, 2015.

[12] *** Apl. Ref. 2.2.1.73194.264, “Creation of Interuniversity centre for risk management and assessment for prevention of ecological and technological risks in the Black Sea” (IUCRISKMAN), Training on RISK Monitoring & Database Software WEB Application for the RkFMEA System for Risk Assessment and Prevention Management. Guidebook and Application Manual, 2015.

[13] Manescu, M. *Hydraulics of bridges and floors / Hidraulica podurilor si podeţelor*. Timisoara, University Horizons Publishing House, 2002.

[14] *** *ANCOLD Guidelines on Risk Assessment*. Position paper on revised criteria for acceptable risk to life. A.N.C.O.L.D. Working Group on Risk Assessment, 1998.

[15] Inspectorate for Emergency Situations "Dobrogea" / Inspectoratul pentru Situații de Urgență “Dobrogea”. “Constanţa County's risk analysis and coverage plan” / “Planul de analiză şi acoperire a riscurilor al judeţului Constanţa”, pp.14-20/83, 2015. Accessed March 5, 2024. http://www.isudobrogea.ro/wp-content/uploads/2016/03/Planul-de-Analiz%C4%83-%C8%99i-Acoperire-a-Riscurilor-al-jude%C8%9Bului-CONSTAN%C5%A2A-2015.pdf.

FLUIDAS

NATIONAL PROFESSIONAL ASSOCIATION OF HYDRAULICS AND PNEUMATICS IN ROMANIA

fluidas@fluidas.ro